

Huygens' synchronization of dynamical systems : beyond pendulum clocks

Citation for published version (APA):

Pena, J. (2013). *Huygens' synchronization of dynamical systems : beyond pendulum clocks*. [Phd Thesis 1 (Research TU/e / Graduation TU/e), Mechanical Engineering]. Technische Universiteit Eindhoven. <https://doi.org/10.6100/IR748516>

DOI:

[10.6100/IR748516](https://doi.org/10.6100/IR748516)

Document status and date:

Published: 01/01/2013

Document Version:

Publisher's PDF, also known as Version of Record (includes final page, issue and volume numbers)

Please check the document version of this publication:

- A submitted manuscript is the version of the article upon submission and before peer-review. There can be important differences between the submitted version and the official published version of record. People interested in the research are advised to contact the author for the final version of the publication, or visit the DOI to the publisher's website.
- The final author version and the galley proof are versions of the publication after peer review.
- The final published version features the final layout of the paper including the volume, issue and page numbers.

[Link to publication](#)

General rights

Copyright and moral rights for the publications made accessible in the public portal are retained by the authors and/or other copyright owners and it is a condition of accessing publications that users recognise and abide by the legal requirements associated with these rights.

- Users may download and print one copy of any publication from the public portal for the purpose of private study or research.
- You may not further distribute the material or use it for any profit-making activity or commercial gain
- You may freely distribute the URL identifying the publication in the public portal.

If the publication is distributed under the terms of Article 25fa of the Dutch Copyright Act, indicated by the "Taverne" license above, please follow below link for the End User Agreement:

www.tue.nl/taverne

Take down policy

If you believe that this document breaches copyright please contact us at:

openaccess@tue.nl

providing details and we will investigate your claim.

Huygens' synchronization of dynamical systems: beyond pendulum clocks

Jonatán Peña Ramírez



The research reported in this thesis is part of the research program of the Dutch Institute of Systems and Control (DISC). The author has successfully completed the educational program of the Graduate School DISC.

This research was partially supported by the Mexican Council for Science and Technology (CONACYT).

Huygens' synchronization of dynamical systems: beyond pendulum clocks
by Jonatán Peña Ramírez – Eindhoven University of Technology, 2013 – PhD thesis.

A catalogue record is available from the Eindhoven University of Technology Library.
ISBN: 978-90-386-3325-1
NUR: 992

Cover Design: Oscar Peña Ramírez.
Reproduction: Ipskamp Drukkers B.V., Enschede, The Netherlands.

Copyright ©2013 by J. Peña Ramírez. All rights reserved.

Huygens' synchronization of dynamical systems: beyond pendulum clocks

PROEFSCHRIFT

ter verkrijging van de graad van doctor
aan de Technische Universiteit Eindhoven,
op gezag van de rector magnificus, prof.dr.ir. C.J. van Duijn,
voor een commissie aangewezen door het College voor Promoties
in het openbaar te verdedigen
op woensdag 6 februari 2013 om 16.00 uur

door

Jonatán Peña Ramírez

geboren te Tulancingo de Bravo, Hgo, Mexico

Dit proefschrift is goedgekeurd door de promotor:

prof.dr. H. Nijmeijer

Copromotor:
dr.ir. R.H.B. Fey

Dedicated to my parents:

Erasmo & Josefina

To my brothers and sister:

Aldo, Daniel, Oscar, and Zayin

To Ana

Contents

	Summary	ix
1	Introduction	1
	1.1 Synchronization: the most pervasive behaviour in nature	1
	1.2 Huygens' synchronization: the sympathy of pendulum clocks.	2
	1.3 Thesis overview	4
	1.4 Preliminaries	10
2	A generalized Huygens setup	15
	2.1 Introduction.	15
	2.2 Experimental setup and general model description	18
	2.3 The classical Huygens' clocks experiment	20
	2.4 Discussion	26
3	Synchronization of nonlinear oscillators with limitations	27
	3.1 Introduction.	27
	3.2 Synchronization of oscillators driven by a Hamiltonian escapement	31
	3.3 Synchronization of oscillators driven by a van der Pol term	40
	3.4 Experimental results.	43
	3.5 Discussion	49
4	Synchronization of nonlinear oscillators	51
	4.1 Introduction.	51
	4.2 Oscillators self-driven by a Hamiltonian escapement: revisited	53
	4.3 Oscillators self-driven by a van der Pol term: revisited.	59
	4.4 Oscillators self-driven by a discontinuous force	63
	4.5 Discussion	68
	4.6 The influence of the coupling strength	69

5	Controlled synchronization of chaotic oscillators with Huygens' coupling	71
5.1	Introduction	71
5.2	Synchronization of two chaotic Duffing oscillators	72
5.3	Synchronization of two chaotic van der Pol oscillators	79
5.4	Discussion	83
6	Synchronization of oscillators with time-delayed Huygens' coupling	85
6.1	Introduction	85
6.2	Preliminaries	86
6.3	Oscillators self-driven by a Hamiltonian escapement	88
6.4	Oscillators self-driven by a van der Pol term	93
6.5	Oscillators self-driven by a discontinuous force	96
6.6	Experimental validation	96
6.7	Discussion	99
7	Huygens' coupling: more than a rigid bar	105
7.1	Introduction	106
7.2	Modeling of the system	106
7.3	Numerical analysis	115
7.4	Key parameters for the onset of synchronization	120
7.5	Discussion	122
8	Conclusions and Recommendations	125
8.1	Conclusions	125
8.2	Recommendations	128
A	Proof of Theorem 1.1	133
B	Euler beam element matrices	143
C	Static analysis for the flexible coupling structure	145
	Bibliography	147
	Samenvatting	155
	Resumen	159
	Acknowledgements	163
	Curriculum Vitae	165

Summary

Huygens' synchronization of dynamical systems: beyond pendulum clocks

Synchronization is one of the most deeply rooted and pervasive behaviours in nature. It extends from human beings to unconscious entities. Some familiar examples include the fascinating motion of schools of fish, the simultaneous flashing of fireflies, a couple dancing in synchrony with the rhythm of the music, the synchronous firing of neurons and pacemaker cells, and the synchronized motion of pendulum clocks. In a first glimpse to these examples, the existence of self-synchronization in nature may seem almost miraculous. However, the main “secret” behind this phenomenon is that there exists a communication channel, called coupling, such that the entities/systems can influence each other. This coupling can be, for instance, in the form of a physical interconnection or a certain chemical process.

Although synchronization is a ubiquitous phenomenon among coupled oscillatory systems, its onset is not always obvious. Consequently, the following questions arise: How exactly do coupled oscillators synchronize themselves, and under what conditions? In some cases, obtaining answers for these questions is extremely challenging. Consider for instance, the famous example of Christiaan Huygens of two pendulum clocks exhibiting anti-phase or in-phase synchronized motion. Huygens did observe that there is a “medium” responsible for the synchronized motion, namely the bar to which the pendula are attached. However, despite the remarkably correct observation of Huygens, even today a complete rigorous mathematical explanation of this phenomenon, using proper models for pendula and *flexible* coupling bar, is still missing.

The purpose of this thesis is to further pursue the nature of the synchronized

motion occurring in coupled oscillators. The first part, addresses the problem of natural synchronization of arbitrary self-sustained oscillators with Huygens coupling. This means that in the analysis, the original setup of Huygens' clocks is slightly modified in the sense that each pendulum clock is replaced by an arbitrary second order nonlinear oscillator and instead of the flexible wooden bar (called here *Huygens' coupling*), a rigid bar of one degree of freedom is considered. Each oscillator is provided with a control input in order to guarantee steady-state oscillations. This requirement of having a control input to sustain the oscillations can be linked to Huygens' pendulum clocks, where each pendulum is equipped with an escapement mechanism, which provides an impulsive force to the pendulum in order to keep the clocks running. Then, it is shown that the synchronized motion in the oscillators is independent of the kind of controller used to maintain the oscillations. Rather, the coupling bar, i.e. Huygens' coupling is considered as the key element in the occurrence of synchronization. In particular, it is shown that the mass of the coupling bar determines the eventual synchronized behaviour in the oscillators, namely in-phase and anti-phase synchronization. The Poincaré method is used in order to determine the existence and stability of these synchronous motions. This is feasible since in the system there exists a natural small parameter, namely the *coupling strength*, which value is determined by the mass of the coupling bar.

Next, the synchronization problem is addressed from a control point of view. First, the synchronization problem of two chaotic oscillators with Huygens' coupling is discussed. It is shown that by driving the coupling bar with an external periodic excitation, it is possible to trigger the onset of chaos in the oscillators. The mass of the coupling bar is considered as the bifurcation parameter. When the oscillators are in a chaotic state, the synchronization phenomenon will not occur naturally. Consequently, it is demonstrated that by using a master-slave configuration or a mutual synchronization scheme, it is possible to achieve (controlled) synchronization. Secondly, the effect of time delay in the synchronized motion of oscillators with Huygens' coupling is investigated. In this case, the wooden bar, is replaced by a representative dynamical system. This dynamical system generates a suitable control input for the oscillators such that in closed loop the system resembles a pair of oscillators with Huygens' coupling. Under this approach, the oscillators do not need to be at the same location and moreover, the dynamical system generating the control input should be implemented separately, using for instance a computer. Consequently, the possibility of having communication time-delays (either in the oscillators or in the applied control input) comes into play. Then, the onset of in-phase and anti-phase synchronization in the coupled/controlled oscillators is studied as a function of the coupling strength and the time delay.

In addition to computer simulations, the (natural and controlled) synchronized motion of the oscillators is validated by means of experiments. These experiments are performed in an experimental platform consisting of an elastically supported

(controllable) rigid bar (in Huygens' example the wooden bar) and two (controllable) mass-spring-damper oscillators (the pendulum clocks in Huygens' case). A key feature of this platform is that its dynamical behaviour can be adjusted. This is possible due to the fact that the oscillators and the coupling bar can be actuated independently, then by using feedback, specific desirable oscillators' dynamics are enforced and likewise the behaviour of the coupling bar is modified. This feature is exploited in order to experimentally study synchronous behaviour in a wide variety of dynamical systems.

Another question considered in this thesis is related to the modeling of the real Huygens experiment. The models used in the first part of this thesis and the ones reported in the literature are simplifications of the real model: the coupling bar has been considered as a rigid body of one degree of freedom. However, in the real Huygens experiment, the bar to which the clocks are attached is indeed an infinite dimensional system for which a rigorous study of the in-phase and anti-phase synchronized motion of the two pendula is, as far as is known, still never addressed in the literature. The third part of the thesis focuses on this. A Finite Element Modelling technique is used in order to derive a model consisting of a (finite) set of ordinary differential equations. Numerical results illustrating all the possible stationary solutions of the "true" infinite dimensional Huygens problem are included.

In summary, the results contained in the thesis in fact reveal that the synchronized motion observed by Huygens extends beyond pendulum clocks.

Chapter **I**

Introduction

The energy of the mind is the essence of life.

Aristotéles (384 B.C.E. - 322 B.C.E)

Abstract This chapter introduces the phenomenon of synchronization and presents an historical account of Huygens' synchronization. The chapter also presents the motivation, objectives, contributions, and outline of this thesis. Additionally, some definitions and mathematical tools, used later on this thesis, are presented.

1.1 Synchronization: the most pervasive behaviour in nature

One of the most ubiquitous forms of motion in the universe is oscillatory motion. Some examples that are common in everyday life are: the periodic motion of the Earth, the alternating electric current necessary for the functioning of home, office, and industrial devices, the ups and downs in economy, the swinging of the pendulum of a clock, or the reader may start to generate numerous other examples. When the oscillatory motion of a system is influenced by the oscillations of (an)other oscillatory system(s), then the interacting systems may experience a striking phenomenon called *synchronization*.

Synchronization, or as the Oxford advanced dictionary defines it, “agreement in time” or “happening at the same time” [1], is one of the most deeply rooted and pervasive behaviours in nature. It extends from human beings to unconscious entities. Referring to synchronization in human beings we can mention, for instance,

a couple dancing in synchrony with the rhythm of the music, synchronized swimmers, or the violinists in an orchestra playing in unison. On the other hand, synchronization of a starling flock in flight, the graceful motion of a school of fish or the striking synchronized attack of killer whales, synchronous firing of neurons and pacemaker cells, or synchronous rupturing of earthquake faults are some examples of subconscious and unconscious synchronization. These examples - amongst others - are nicely described in [63, 64, 74, 78, 79]. From a careful analysis of these examples, it is possible to notice that synchronization of oscillating objects or bodies seems to happen in a natural way, i.e. if the bodies are programmed in such way that a weak interaction between them will result in an adjustment of their rhythms. In fact, it is not surprising that the synchronization phenomenon is often perceived as miraculous, surprising, or fairly difficult to understand.

Hence, the natural question is, how exactly do coupled oscillators synchronize themselves, and under what conditions? In some cases, obtaining answers for these questions is extremely challenging. Notwithstanding this, something should be clear: the main ‘secret’ behind this phenomenon is that there exists a medium (for instance a physical interconnection or a certain chemical process), called coupling, such that the entities/systems can influence each other.

1.2 Huygens’ synchronization: the sympathy of pendulum clocks

Probably the earliest writing on inanimate synchronization is due to the Dutch scientist Christiaan Huygens (1629-1695), who discovered that two pendulum clocks hanging from a common support (a wooden bar supported by two chairs, see Figure 1.1), kept in pace relative to each other such that the two pendulums always swung together (in opposite motion) and never varied. By Huygens this was called “sympathy of two clocks”. After some systematic experiments he found the source of the “sympathy”: the imperceptible motion of the bar to which the pendulum clocks were attached, cf. [30, 37, 63]. Nowadays, the phenomenon described by Huygens (pendulums approaching and receding in opposite motions) is called anti-phase synchronization for obvious reasons. Note that the explanation given by Huygens is on the one hand correct and on the other hand is amazingly simple. He did manage to explain correctly the phenomenon even when he did not have at hand the necessary mathematical tools for performing the analysis - at that time differential calculus did not exist yet.

Half a century after Huygens’ observations, John Ellicott [18, 19] carried out similar experiments with pendulum clocks. In a manuscript submitted to the Royal

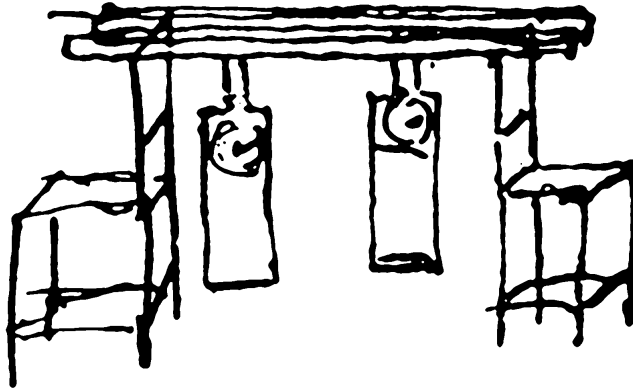


Figure 1.1 Original Huygens drawing cf. [30].

Society of London, he describes an ‘odd’ phenomenon: when two pendulums were placed sideways to one another, one of them was always found to stop working after 2 hours. He did conclude that the two pendulum clocks mutually did affect each other.

In 1873, the sympathetic behaviour described by Huygens ‘struck’ again. This time at the Royal Observatory of Greenwich. According to the observations of Williams Ellis [20], two pendulum clocks placed on a wooden stand did show sympathetic behaviour: during 9 consecutive days the times indicated by the clocks did remain constant, day after day and moreover, the pendulum of one clock swung to the left, whereas the other went to the right, i.e. they were synchronized in anti-phase. Additionally, Ellis placed 9 pendulum clocks on the wooden stand and in this case he did notice that the previous agreement in the pendulums did disappear and instead, the rate of the clocks showed great variations. He also did suspect that the clocks were communicating via the wooden stand.

Later, in the beginning of the 20th century, D.J. Korteweg did provide the first theoretical explanation of the Huygens’ observations by using an undamped and undriven three degrees of freedom model [37]. With this model he was able to conclude that anti-phase motion is the most dominant mode.

After the work of Korteweg, there is a void space in the literature (at least to the knowledge of the author) regarding Huygens’ synchronization.

However, by the end of the 20th century, the Huygens synchronization phenomenon was revisited by I.I. Blekhman [7]. In his analysis, similar to Korteweg, he did use a three degrees of freedom model but he did include the effect of damping. Additionally, this model takes into account the clock escapements, which are modelled

by using a van der Pol term. Blekhman drew the conclusion that two synchronization states can occur, namely in-phase and anti-phase synchronization, and that they depend on the initial conditions of the system.

During the last decade, the study of Huygens' synchronization has regained attention. Several authors have contributed towards the study of the intriguing Huygens' synchronization problem. We can distinguish two approaches: the theoretical approach and the one oriented to obtain insight by experimental analysis. Some works related to the theoretical approach are presented in [16, 17, 29, 31, 32, 33, 34, 52, 75, 86]. For the second approach several experimental setups have been created by researchers in order to reproduce the observations made by Huygens and find mathematical arguments for the synchronized motion of the clocks. Some of these experimental setups are presented in [5, 54, 55]. All of them have a common characteristic: the pendulum clocks are replaced by metronomes and the supporting bar is free to oscillate. In these cases, besides the synchronized motion, other kinds of motion have been reported, as for example, beating death (where one of the metronomes stops its oscillations, whereas the other one keeps oscillating, just as reported by Ellicott) [5] and intermediate synchronization (metronomes synchronize with constant phase difference but different amplitude) [54].

Besides the aforementioned attempts to better understand the true mechanism behind the sympathy of pendulum clocks, nowadays there exist works where the study of Huygens' synchronization has been extended to the case of arbitrary second order oscillators [59, 60, 70]. In such works, the pendulum clocks have been replaced by arbitrary nonlinear oscillators.

Finally, it should be emphasized that even today the study of Huygens' synchronization is an open research problem. A further motivation for the study of this exciting phenomenon is provided in the next section.

1.3 Thesis overview

This section presents a general overview of the thesis. First, a motivation for the study of Huygens' synchronization is provided. Then, the objectives of the project are discussed and finally, the contributions and outline of the thesis are given.

1.3.1 Motivation

Nowadays, there exists a large number of studies addressing the phenomenon of synchronization in several fields like biology, chemistry, physics, and engineering. However, further understanding of the complex synchronization phenomenon occurring in pairs of arbitrary oscillators (not necessarily pendulum clocks) with Huygens' coupling is still necessary. This may be motivated by the fact that the Huygens system has a certain degree of similarity with other systems (not necessarily mechanical).

Consider for instance the case of two driven unbalanced rotors (a familiar example of this kind of devices is a washing machine) mounted on an elastic support, i.e. coupled through Huygens' coupling. It has been found that, under certain conditions, the rotors may synchronize either in-phase or in anti-phase [8]. Note that the onset of anti-phase synchronization in this example is highly desirable, since this will reduce or even eliminate the vibrations of the common support during the operation of the rotors. However, the onset of in-phase synchronization is not desired at all, since this will induce resonance and high amplitude vibrations of the support ultimately resulting in harmful and undesirable effects.

Something similar happens in living organism. For instance, inside the human body, there are several biological rhythms: respiration, heartbeat, and blood perfusion just to mention a few of them. It has been found that when some of these rhythms synchronize with each other the energy consumption is minimal. Hence, in this case the onset of synchronization is beneficial [45]. On the other hand, synchronization can also be dangerous or detrimental. It is widely accepted, that the process of seizure generation is closely associated with an abnormal synchronization of neurons, see e.g. [44].

Note that in both cases, either unbalanced rotors or biological rhythms in the human body, the synchronization phenomenon occurs naturally. Therefore, it is necessary to determine under which conditions (maybe related to the coupling structure) the synchronization phenomenon (in particular, in-phase or anti-phase) may occur. This suggests that perhaps the (theoretical and/or experimental) achievements in one area, say mechanics, can help to better understand the natural synchronization phenomena occurring in for instance biological rhythms, where a rigorous theoretical study is most of the time unfeasible because of the obvious lack of good mathematical models.

Moreover, Huygens' synchronization also finds interesting applications. For example, in [76], it has been shown that an analogous phenomenon happens in acoustics: two thermoacoustic engines are discussed, which have their cases rigidly welded

together for vibration cancellation. Likewise, Huygens' system may be used in determining the behaviour of coupled transmission lines, cf. [80].

The reader should be convinced at this point that the Huygens' setup of coupled pendulum clocks is an exciting and challenging nonlinear dynamical system, whose complex dynamical behaviour is far from being completely understood. Further studies of this system will lead to unveiling more details about the complex yet intriguing synchronization phenomenon.

1.3.2 Objectives

This thesis aims to provide new insights into the exciting field of synchronization by means of analytical, numerical, and experimental analyses. Especially, the purpose is to exploit the observations made by Huygens and to obtain explanations/results that are beyond the current understanding.

The general objective of the thesis is to provide answers to the following questions: given the Huygens system (two pendulum clocks coupled through a bar with an elastic support), is it possible to replace the pendulum clocks by another type of second order nonlinear oscillator and still to observe the synchronized motion? In particular, what happens when the pendulum clocks are replaced by two arbitrary nonlinear self-sustained oscillators or by a pair of chaotic oscillators? Additionally, which is/are the key parameter/parameters in the coupled system for the occurrence of synchronization?

One of the particular objectives is to *analyze* and to *explain* the onset of natural synchronization occurring in oscillators that interact via Huygens coupling. On the one hand, conditions under which the synchronized motion exists and whether it is stable should be provided. On the other hand, it is desired to perform an experimental analysis in order to illustrate the synchronized motion in real oscillators and validate theoretical results.

The second objective is to show that, for the case where the oscillators are not physically connected via the coupling bar, it is still possible to observe synchronized motion in the oscillators, provided that a suitable control input is designed, such that, in closed loop, the oscillators resemble a pair of oscillators with Huygens' coupling.

Last but not least, the third particular objective is related to the *modelling* and *analysis* of the true Huygens setup of pendulum clocks linked via a wooden bar. The goal is to show that, besides the 'sympathetic' behaviour observed by Huygens, there exist more limit (synchronizing) solutions in the system of coupled pendula.

It is desired to show that for a thorough understanding of Huygens' synchronization the coupling should be considered as a flexible structure. In the current models available in literature, the coupling bar is considered as a rigid body. Hence, the purpose is to construct a model, which incorporates the *flexibility* of the coupling bar, i.e. to consider it as an infinite dimensional system.

In order to achieve the aforementioned objectives one can distinguish two approaches, the one used by Huygens, i.e. observation and *experimentation* and on the other hand, a mathematical analysis related to the existence and stability of the synchronous solutions. Therefore, the thesis requires a combination of the world of physicians with the world of mathematicians, i.e. it requires the use of tools from the field of Dynamics and Control.

1.3.3 Contributions and outline

Contributions

The research conducted in this PhD project is summarized in the upcoming chapters and the contributions are highlighted at the end of each chapter.

In summary, it can be said that the results given here demonstrate that different pairs of (nearly) identical oscillators interacting via Huygens coupling can synchronize in a natural way, i.e. without the influence of a control signal. This is extensively illustrated by means of experiments which, to the knowledge of the author, are one of the first successful experiments reported in the literature regarding oscillators with Huygens' coupling not being metronomes and/or pendulum clocks. Additionally, conditions for the existence and stability of synchronous solutions are derived by means of the Poincaré perturbation method. The obtained theoretical results are supported by computer simulations and experimental results. Another contribution is that it is shown that the use of Huygens coupling can be extended to chaotic oscillators and likewise, to the case where there is a communication time delay between the oscillators. Additionally, by using a Finite Element modelling technique, a Huygens' model has been derived, which closely approximates Huygens' original experiments. This model incorporates the flexibility of the coupling bar. As a first step in the analysis, numerical results are obtained and these are compared/validated against current models where the bar is modelled as a rigid body.

The following list of publications summarizes the main results obtained during this PhD project:

Journal articles

- Pena Ramirez, J., Fey, R. H. B. and Nijmeijer, H. (2012). In-phase and anti-phase synchronization of oscillators with Huygens' coupling. *Cybernetics and Physics*, 1(1), 58-66. [60].
- Pena Ramirez, J., Fey, R. H. B. and Nijmeijer, H. (2012). An experimental study on synchronization of nonlinear oscillators with Huygens' coupling. *Nonlinear Theory and Its Applications, IEICE* 3(2), 128-142. [59].

Journal articles in preparation

- Pena Ramirez, J., Fey, R. H. B. and Nijmeijer, H. Synchronization of weakly nonlinear oscillators interacting via Huygens' coupling (Chapter 3).
- Pena Ramirez, J., Fey, R. H. B. and Nijmeijer, H. A new model for the classical experiment on synchronization of pendulum clocks: what Huygens did not see (Chapter 7).

Book chapters

- Pena Ramirez, J. and Nijmeijer, H. (2012). A study of the onset and stabilization of parametric roll by using an electro-mechanical device. In Fossen, T.I. and Nijmeijer, H. (Eds.), *Parametric resonance in dynamical systems*, (pp. 287-304). Springer, New York. [62].
- Pena Ramirez, J., Fey, R. H. B. and Nijmeijer, H. (2012). An introduction to parametric resonance. In Fossen, T.I. and Nijmeijer, H. (Eds.), *Parametric resonance in dynamical systems*, (pp. 1-13). Springer, New York. [61].
- Pena Ramirez, J., Fey, R. H. B. and Nijmeijer, H. Controlled synchronization of chaotic oscillators with Huygens' coupling. In *Chaos, CNN, Memristors and beyond*. In press. To appear on February, 2013.

Conference proceedings

- Pena Ramirez, J., Fey, R. H. B. and Nijmeijer, H. (2011). On phase synchronization of oscillators mounted on a movable support. *Proceedings of the 7th European Nonlinear Dynamics Conference (ENOC 2011)*, July 24 - July 29, 2011, Rome, Italy. [58].

- Pena Ramirez, J., Alvarez Aguirre, A., Fey, R. H. B. and Nijmeijer, H. (2012). Effects of time delay in the synchronized motion of oscillators with Huygens' coupling. 3rd IFAC Conference on Analysis and Control of Chaotic Systems (3rd IFAC CHAOS Conference), Cancún, México, June 20 – 22, 2012. [57].

Outline

This thesis is divided in three parts preceded by an introductory part. The introductory part consist of Chapters 1 and 2. In Chapter 1, some definitions and mathematical tools that are used later in this thesis are presented. In particular, this chapter introduces the mathematical apparatus that is used in order to determine the existence and stability of synchronous solutions in a particular class of systems of coupled oscillators. Next, in Chapter 2, an experimental setup, which can be seen as a modern and generalized version of the original Huygens system of pendulum clocks is introduced. The main features of the setup are described and it is explained how this experimental platform allows to further pursue the nature of the synchronized motion occurring in a wide variety of dynamical oscillators.

The first part addresses the problem of *natural* synchronization of nonlinear self-sustained oscillators interacting via Huygens coupling. First, in Chapter 3 the onset of synchronization in pairs of weakly nonlinear self-sustained oscillators is investigated. Sufficient conditions for the existence and stability of synchronous solutions are derived using the Poincaré method and the obtained results are supported by experimental results. Additionally, it is emphasized that the mechanism underlying the synchronized motion in the oscillators is the bar to which they are attached. It is demonstrated that the mass of the bar is one of the key parameters on the onset of (in-phase and anti-phase) synchronous behaviour. Then, in Chapter 4, a similar analysis is conducted for the case of strongly nonlinear oscillators. In this case, the Poincaré method cannot be applied in determining conditions for synchronization. Instead, some analytic conditions for the stability of the anti-phase synchronized motion are derived under the assumption of small oscillations in the system, i.e. by using linearization. Again, several experimental results illustrating the synchronized motion of the coupled oscillators are provided. Furthermore, a brief comparison between the results obtained in Chapter 3 and the ones obtained in Chapter 4 is presented.

Next, in the second part of the thesis, the synchronization problem is addressed from a control point of view. First, in Chapter 5, the synchronization problem of two chaotic oscillators with Huygens' coupling is discussed. It is shown that when the oscillators are in a chaotic state, the synchronization phenomenon will

not occur naturally. Consequently, it is demonstrated that by using a master-slave configuration it is possible to achieve (controlled) synchronization. Then, in Chapter 6, the effect of time delay in the synchronized motion of oscillators with Huygens' coupling is investigated. In the analysis, the Huygens coupling is replaced by a representative dynamical system, which generates a suitable control input for the oscillators such that in closed loop the system resembles a pair of oscillators with Huygens coupling. The onset of in-phase and anti-phase synchronization in the coupled oscillators is studied as a function of the coupling strength and the time delay.

Then, in the third part of this thesis, the classical Huygens setup of pendulum clocks is revisited. In Chapter 7, a Finite Element model of the original Huygens setup is presented. In this model, the coupling structure for the two clocks, which consists of two wooden chairs and a wooden bar, see Figure 1.1, is assumed to be flexible. The pendulum clocks are considered as local nonlinearities attached to the flexible structure. This model is an extension of the current models used in the literature, where the beam is assumed to be rigid and the chairs are approximated by a linear spring. The resulting coupled model consists of a (finite) set of ordinary differential equations. Numerical results illustrating all the possible stationary solutions (including in-phase and anti-phase synchronization) of the 'true' infinite dimensional Huygens problem are included.

Finally, general conclusions and recommendations are provided in Chapter 8.

1.4 Preliminaries

This section introduces some definitions on synchronization and introduces the mathematical machinery that is used later in Chapter 3 in order to determine the existence and stability of synchronous solutions in systems of coupled oscillators.

1.4.1 Definitions

Throughout this thesis, the words in-phase synchronization and anti-phase synchronization are mentioned several times. In consequence, it is worth to define a priori what is meant by these words. To this end, consider the system

$$\dot{x}(t) = f(x(t), z(t)), \quad (1.1)$$

$$\dot{y}(t) = f(y(t), z(t)), \quad (1.2)$$

$$\dot{z}(t) = g(x(t), y(t), z(t)), \quad (1.3)$$

where $x, y \in \mathbb{R}^n$, $z \in \mathbb{R}^m$ are state variables and the functions $f : \mathbb{R}^n \times \mathbb{R}^m \rightarrow \mathbb{R}^n$ and $g : \mathbb{R}^n \times \mathbb{R}^n \times \mathbb{R}^m \rightarrow \mathbb{R}^m$ are locally Lipschitz. Note that the system under consideration represents a pair of identical subsystems, described by (1.1) and (1.2), interacting via the dynamics of subsystem (1.3). Throughout this thesis it will be assumed that (1.1) and (1.2) describe the dynamics of two identical self-driven nonlinear oscillators and (1.3) will be referred to as Huygens' coupling. Moreover, the case $n = m = 2$ is considered, except in Chapter 7 where $m > n = 2$.

The following definitions have been derived [9].

Definition 1.1. *Subsystems (1.1)-(1.2) are said to be (asymptotically) synchronized in-phase if the solutions $x(t)$, $y(t)$ of (1.1)-(1.3) with initial conditions $x(0)$, $y(0)$, $z(0)$ satisfy*

$$\lim_{t \rightarrow \infty} e_{in}(t) := x(t) - y(t) = 0. \quad (1.4)$$

Definition 1.2. *System (1.1)-(1.3) is said to be (asymptotically) synchronized in anti-phase if the solutions $x(t)$, $y(t)$ and $z(t)$ with initial conditions $x(0)$, $y(0)$, $z(0)$ satisfy*

$$\begin{aligned} \lim_{t \rightarrow \infty} e_{an}(t) := x(t) + y(t) &= 0, \\ \lim_{t \rightarrow \infty} z(t) &= 0. \end{aligned} \quad (1.5)$$

In this thesis, the synchronization phenomenon is largely investigated by means of experiments. Since in practical applications it is impossible to have identical subsystems (1.1)-(1.2), it is not possible to fulfill (1.4) or (1.5). For such cases, it is convenient to introduce the concept of *practical synchronization* [9].

Definition 1.3. *Subsystems (1.1)-(1.2) are said to be practically synchronized in-phase if the solutions $x(t)$, $y(t)$ of (1.1)-(1.3) with initial conditions $x(0)$, $y(0)$, $z(0)$ satisfy*

$$\lim_{t \rightarrow \infty} |e_{in}(t)| = |x(t) - y(t)| \leq \epsilon, \quad (1.6)$$

for certain $\epsilon > 0$.

Definition 1.4. *System (1.1)-(1.3) is said to be practically synchronized in anti-phase if the solutions $x(t)$, $y(t)$ and $z(t)$ with initial conditions $x(0)$, $y(0)$, $z(0)$ satisfy*

$$\lim_{t \rightarrow \infty} |e_{an}(t)| = |x(t) + y(t)| \leq \epsilon_1, \quad (1.7)$$

$$\lim_{t \rightarrow \infty} |z(t)| \leq \epsilon_2,$$

for certain $\epsilon_1, \epsilon_2 > 0$.

1.4.2 Poincaré method for quasilinear systems

The result presented here is due to Blekhman [7]. It is based on the Poincaré perturbation method, cf. [4], and it provides conditions on the existence and stability of periodic solutions of systems of the form

$$\dot{x}_s = \sum_{j=1}^l a_{sj}x_j + \mu\Phi_s(x_1, \dots, x_l), \quad s = 1, \dots, l, \quad (1.8)$$

where a_{sj} are real constants and $\mu > 0$ is a “sufficiently small” real parameter.¹ The following assumption is made on system (1.8)

A-1 The functions $\Phi_s(x_1, \dots, x_l)$ are analytical functions in x_1, \dots, x_l , i.e. they can be expanded as a power series in x_1, \dots, x_l or they are polynomials.

When $\mu = 0$, system (1.8) can be written as a set of linear differential equations with constant coefficients, i.e.

$$\dot{x} = Ax, \quad x = [x_1, \dots, x_l]^T. \quad (1.9)$$

For the matrix A the following assumption is made

A-2 The characteristic equation associated to matrix A has an arbitrary number (different from zero) of purely imaginary roots of any multiplicity² and the remaining roots are assumed to be either real or complex but with negative real part.

Then, by using a nonsingular linear transformation, system (1.8) can be transformed to the canonical form

$$\dot{y}_s = \lambda_s y_s + \mu f_s(y_1, \dots, y_l) \quad s = 1, \dots, l, \quad (1.10)$$

Determining the transformation that leads to obtain the canonical form (1.10) is not difficult, because for $\mu = 0$, system (1.8) becomes a linear system with constant coefficients, see (1.9). Hereinafter, the analysis is centered around system (1.10). The *fundamental* or *generating* system, i.e. $\mu = 0$, associated to (1.10) is

$$\dot{y}_s = \lambda_s y_s, \quad s = 1, \dots, l, \quad (1.11)$$

¹Because μ is considered to be small, system (1.8) is often called *quasilinear* system.

²However, it is required that the algebraic multiplicity of these roots is equal to their geometric multiplicity.

which has the solution

$$y_s^0 = \alpha_s e^{\lambda_s t}, \quad s = 1, \dots, l, \quad (1.12)$$

where α_s , $s = 1, \dots, l$, are arbitrary parameters determining the amplitude of the solution.

A-3 In accordance with A-2, it is assumed that the *characteristic exponents* λ_s , $s = 1, \dots, l$, are categorized as follows

$$\lambda_s = \begin{cases} in_s \omega, & s = 1, \dots, k, \\ -a_s + ib_s, & s = k + 1, \dots, l, \end{cases} \quad (1.13)$$

where i is the imaginary unit, i.e. $i = \sqrt{-1}$, $a_s > 0$, n_s is a positive or negative integer, $\omega = \frac{2\pi}{T}$ is the oscillation frequency associated to system (1.11) and T is the period. It will also be assumed that only real solutions x_s of (1.8), are of interest (physical systems do not have complex solutions!). Therefore, the characteristic exponents with purely imaginary part appear as complex conjugate pairs and likewise the functions f_s appear as complex conjugate pairs. This implies that k is a positive even number.

From the above assumption it follows that system (1.11) will have periodic solutions of period T , i.e. (1.12) can be written as

$$y_s^0 = \begin{cases} \alpha_s e^{\lambda_s t} = \alpha_s e^{in_s \omega t} & s = 1, \dots, k, \\ 0 & s = k + 1, \dots, l. \end{cases} \quad (1.14)$$

The problem now is to determine the values of α_s , $s = 1, \dots, k$, such that the periodic solutions of (1.10) reduce, for $\mu = 0$, to the generating solutions (1.14) of period T . Moreover, the periodic solutions of (1.10) will have a period different from T , i.e. $T^*(\mu) = T + \tau_c(\mu)$. Therefore, it is also necessary to determine the ‘‘correction’’ $\tau_c(\mu)$ of the period. The following theorem addresses these issues and also provides conditions for the existence and stability of the periodic solutions of (1.10).

Theorem 1.1. *Periodic solutions (of period $T^*(\mu) = T + \tau_c(\mu)$) of the autonomous set of equations (1.10) becoming at $\mu = 0$ periodic (period T) solutions (1.14) of the fundamental system (1.11), can correspond only to such values of constants $\alpha_1, \dots, \alpha_{k-2}, \alpha_{k-1} = \alpha_k$, which satisfy equations*

$$Q_s(\alpha_1, \dots, \alpha_k) = \alpha_k n_k P_s - \alpha_s n_s P_k = 0, \quad s = 1, \dots, k-1, \quad (1.15)$$

where

$$P_s(\alpha_1, \dots, \alpha_k) = \int_0^T f_s(y_1^0, \dots, y_l^0) e^{-in_s \omega t} dt \quad (1.16)$$

$$= \int_0^T f_s(\alpha_1 e^{in_1 \omega t}, \dots, \alpha_k e^{in_k \omega t}, 0, \dots, 0) e^{-in_s \omega t} dt, \quad s = 1, \dots, k. \quad (1.17)$$

If for a certain set of constants $\alpha_1 = \alpha_1^*, \dots, \alpha_{k-2} = \alpha_{k-2}^*, \alpha_{k-1} = \alpha_k = \alpha_k^*$ which satisfies equations (1.15), the real parts of all roots χ of the following algebraic equation are negative³

$$\left| \frac{\partial Q_s}{\partial \alpha_j} - \alpha_k n_k \delta_{sj} \chi \right| = 0, \quad s, j = 1, \dots, k-1, \quad (1.18)$$

then, for sufficiently small μ , this set of constants will indeed correspond to a unique, analytical in relation to μ , stable periodic solution of the set (1.10) with period $T^*(\mu) = T + \tau_c(\mu)$. At $\mu = 0$, it becomes a periodic (period T) solution (1.14) of the fundamental system (1.11). If the real part of at least one root of equation (1.18) is positive, then the respective solution is unstable. With accuracy up to terms of order μ , the period correction $\tau_c(\mu)$ is determined by

$$\tau_c(\mu) = -\mu \frac{P_k(\alpha_1^*, \dots, \alpha_{k-2}^*, \alpha_{k-1}, \alpha_{k-1})}{\lambda_k \alpha_k^*}. \quad (1.19)$$

The proof of this theorem is sketched in [7](in Russian). To the knowledge of the author of this thesis, the proof of this theorem is not published in any reference in English. Hence, in order to make this thesis self-contained, the proof has been derived following [4], [7], and [41] and it is presented in Appendix A. Note that the proof is instrumental since it will facilitate the understanding of Theorem 1.1 and also of the results presented in Chapter 3.

³ δ_{sj} is the Kronecker delta defined by

$$\delta_{si} = \begin{cases} 1 & \text{for } s = i, \\ 0 & \text{for } s \neq i. \end{cases}$$

Chapter 2

A generalized Huygens setup

An experiment is a question which Science poses to Nature, and a measurement is the recording of Nature's answer.

Max Karl Ernst Ludwig Planck (1858–1947)

Abstract This chapter introduces an experimental setup, which can be seen as a modern and generalized version of the original Huygens system of pendulum clocks. The main features of the setup are described and it is explained how this experimental platform allows to further pursue the nature of the synchronized motion occurring in a wide variety of dynamical oscillators with Huygens' coupling.

2.1 Introduction

On a quiet day in late February 1665, the Dutch scientist Christiaan Huygens made a serendipitous discovery while being confined to his bedroom for several days due to an illness: two pendulum clocks hanging from a common support (a wooden bar supported by two chairs, see Figure 2.1(a) kept in pace relative to each other such that the two pendulums always swung together (in opposite motion) and never varied. It should be noted that not only the conditions, under which the discovery of the synchronization phenomenon took place, are striking but also the very particular characteristics of the setup, on which this phenomenon was discovered.

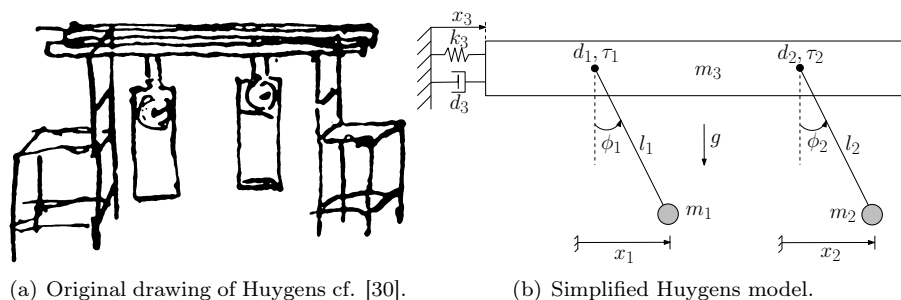
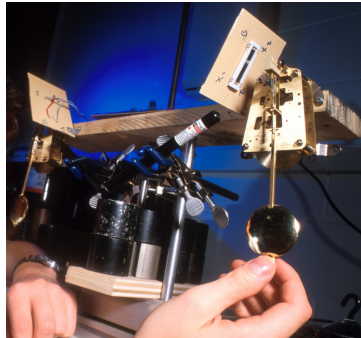


Figure 2.1 Huygens' original system of pendulum clocks and its simplification.

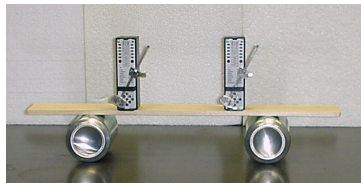
At first sight, the picture of Huygens' setup depicted in Figure 2.1(a) may seem very simple. However, even today, in an era where several modeling tools are at hand, a proper model of the original Huygens system has not been derived! Notwithstanding this fact, in the recent history, several authors have contributed towards the study of Huygens' synchronization by using simplified models. Consider, for example, the model depicted in Figure 2.1(b). Note that the wooden bar at the top of two chairs has been modelled by a single degree-of-freedom (dof) rigid bar, which is attached to the fixed world via a spring and a damper. The pendulum clocks have been replaced by two damped pendula, which are both driven.

In fact, the study of Huygens' synchronization has gone beyond deriving mathematical models. Several experimental setups mimicking the Huygens experiment have been reported, see e.g. [5], [54], and [55], all aiming at demonstrating that in-phase or anti-phase synchronization of a number of pendulum-like oscillators can be achieved. Moreover, these setups have a common characteristic: the pendulum clocks are replaced by metronomes and the supporting bar is free to oscillate, see Figure 2.2. Experimental results have shown that, besides the synchronized motion, other kinds of motion may exist. In [5], for example, beating death, where one of the metronomes stops its oscillations, whereas the other one keeps oscillating, is reported. Intermediate synchronization, which happens when the metronomes synchronize with constant phase difference but different amplitude, is found in [54].

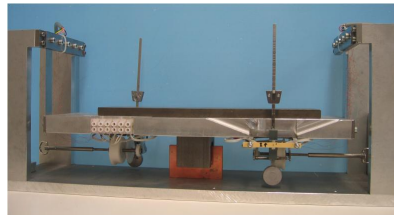
As mentioned in the introductory chapter, the purpose of the research reported in this thesis is to further pursue the nature of the synchronized motion occurring in *arbitrary* oscillators with Huygens' coupling not only from a theoretical point of view but also from an experimental point of view. Note that the importance of conducting an experimental analysis relies among others on the fact that in a real environment it is impossible to have two identical oscillators. Therefore, the experiments may reveal that the synchronous motion is robust against distur-



(a) Wiesenfeld's setup [5].



(b) Pantaleone's setup [55].



(c) Nijmeijer's setup [54].

Figure 2.2 Experimental setups that mimic Huygens' experiment.

bances and mismatches between the systems, just as in Huygens' case, where the clocks were far from being identical. Obviously, in order to create some freedom in performing experiments on synchronization, it is required to have a suitable, general experimental platform that allows to study synchronous behaviour in a wide variety of dynamical systems.

This experimental setup will be introduced in the next section.

2.2 Experimental setup and general model description

A generalized Huygens setup is presented. Here, generalized should be understood in the sense that in this setup, each pendulum clock can be replaced by an arbitrary second order oscillator. Only the main features of the system are discussed. For a complete description of the setup the interested reader is referred to [83].

The electro-mechanical setup used in this research is depicted in Figure 2.3. It consists of two oscillators mounted on an elastically supported rigid bar. The system has 3 dofs corresponding to the horizontal displacements of the two oscillators and the bar, respectively. Moreover, each dof is equipped with a voice coil actuator and with a linear variable differential transformer (LVDT) position sensor.¹

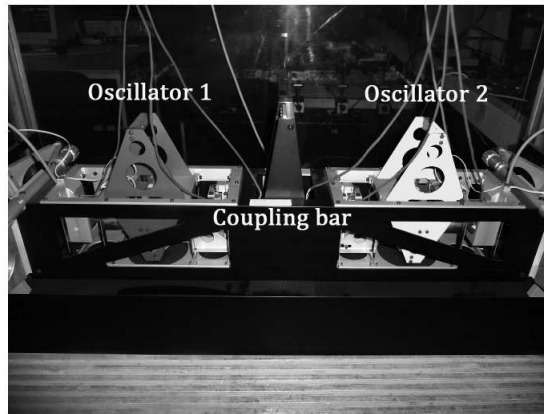


Figure 2.3 Photo of the experimental setup at the DCT lab at the TU/e.

Figure 2.4 shows a schematic representation of the experimental setup. The stiffness and damping characteristics present in the system are assumed to be linear with constant coefficients $\kappa_i, \beta_i \in \mathbb{R}^+$, $i = 1, 2, 3$, respectively. The 3 dofs of the system are indicated by $x_i \in \mathbb{R}$, $i = 1, 2, 3$, i.e. the absolute displacements of both oscillators and the coupling bar, respectively. The control inputs U_1 , U_2 of the two oscillators may be used to guarantee self-sustained oscillations and/or to modify the inherent dynamic properties of the oscillators, such as mass, stiffness, and damping properties, in a desired way. Likewise, the control input U_3 may be used to modify, if desired, the behaviour of the coupling bar. The masses corresponding to the oscillators are given by $m_i \in \mathbb{R}^+$, $i = 1, 2$, and the mass of the supporting bar is denoted by $m_3 \in \mathbb{R}^+$. The latter mass may be varied hardware

¹A video of this setup can be seen at <http://www.wtb.tue.nl/horaest/website/index.html>

wise in the range [4.1 - 41] [kg] by means of addition or removal of steel plates². Note that this feature allows for mechanical adjustment of the coupling strength. This feature is largely exploited through this research.

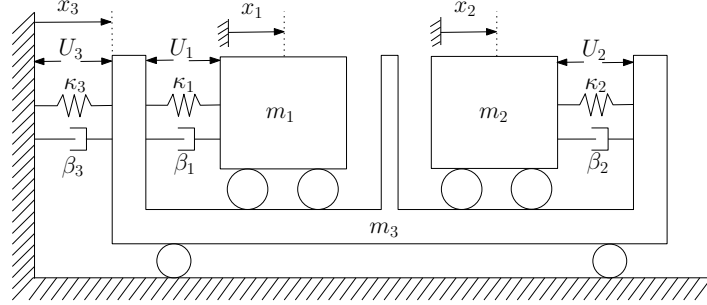


Figure 2.4 Schematic representation of the setup.

Note that the schematic model depicted in Figure 2.4 can be seen as a simplified though generalized version of Huygens' setup of Figure 2.1(a). In this model, the two pendulum clocks are now replaced by two (actuated) mass-spring-damper oscillators. The wooden bar supported by the two chairs is (again) modelled by a single dof suspended rigid bar. As may be noted, in this setup (and its model) *rotational* angles are replaced by *translational* displacements. It comes natural to relate the control inputs U_i , $i = 1, 2$ to the escapement mechanisms as used in the pendulum clocks.

Using Newton's 2nd law, it follows that the idealized - i.e. assuming that no friction is present - equations of motion of the system of Figure 2.4 are

$$\begin{aligned}\ddot{x}_1 &= -\omega_{1s}^2(x_1 - x_3) - 2\zeta_{1s}\omega_{1s}(\dot{x}_1 - \dot{x}_3) + U_1 \\ \ddot{x}_2 &= -\omega_{2s}^2(x_2 - x_3) - 2\zeta_{2s}\omega_{2s}(\dot{x}_2 - \dot{x}_3) + U_2 \\ \ddot{x}_3 &= \sum_{i=1}^2 \mu_i [\omega_{is}^2(x_i - x_3) + 2\zeta_{is}\omega_i(\dot{x}_i - \dot{x}_3) - U_i] \\ &\quad - \omega_{3s}^2 x_3 - 2\zeta_{3s}\omega_{3s}\dot{x}_3 + U_3,\end{aligned}\tag{2.1}$$

where³ $\omega_{is} = \sqrt{\frac{\kappa_i}{m_i}}$ [rad/sec], $\zeta_{is} = \frac{\beta_i}{2\omega_{is}m_i}$ [-] are respectively the angular eigenfrequency and dimensionless damping coefficient present in subsystem i , $i = 1, 2, 3$, and $\mu_i = \frac{m_i}{m_3}$ [-], $i = 1, 2$ are the coupling strengths. The electric actuation for subsystem i results in U_i [m/s²], $i = 1, 2, 3$. Since the actuators are not completely identical, the difference in actuator strength is compensated by multiplying the

²Actually, this mass may also be varied software wise by a suitable design of U_3 .

³The subindex s is used to indicate that the given parameter corresponds to a parameter of the model of the experimental *setup*.

outgoing signals with an appropriate gain. The LVDT displacement sensors are calibrated such that $1[V] = 5 [\text{mm}]$.

In [69], the parameter values of model (2.1) have been identified experimentally and these are provided in Table 2.1.

Table 2.1 Identified parameter values for model (2.1) of the experimental setup for $m_3 = 4.1 [\text{kg}]$.

Parameter	Oscillator 1	Oscillator 2	Coupling bar
$\omega_{is} [\text{rad/s}]$	12.5521	14.0337	9.7369
$\zeta_{is} [-]$	0.3362	0.4296	0.0409
$\mu_i [-]$	0.0411	0.0578	-

Note the differences in the properties of oscillators 1 and 2, whereas it was the intention to design identical ones [83].

The inputs U_i are generated as depicted in Figure 2.5. Each input consists of a feed forward part to cancel the original dynamics, plus compensation terms accounting for differences between the model and the real plant, plus the desired dynamics. The feed forward part is generated by using model (2.1) with parameter values as given in Table 2.1. Since in an experiment only positions are measured, the state vector is fully reconstructed by using a robust observer as presented in [71]. Next, the differences (due, for instance, to unmodelled dynamics, external disturbances and/or parameter uncertainties) between the real setup and its corresponding model (2.1) are estimated. According to [71], this can be achieved by filtering the discontinuous term $L\text{sign}(x - \hat{x})$, see Figure 2.5. Finally, by using the measured positions and the observed velocities (and, if appropriate, a coordinate transformation), it is possible to generate the desired system dynamics.

In an experiment mimicking Huygens' experiment the coupling bar is free to oscillate and, consequently, $U_3 = 0$. However, in cases where the dynamical behaviour of the coupling bar needs to be adjusted or controlled, then U_3 is generated either as described above or will correspond to an external signal, see e.g. Chapter 5.

2.3 The classical Huygens' clocks experiment

In this section, the capabilities of the experimental setup to conduct experiments with a wide variety of dynamical oscillators is illustrated by means of a specific experiment. The example at hand corresponds to the simplified Huygens' clocks model depicted in Figure 2.1(b). In this model, the wooden bar on two chairs

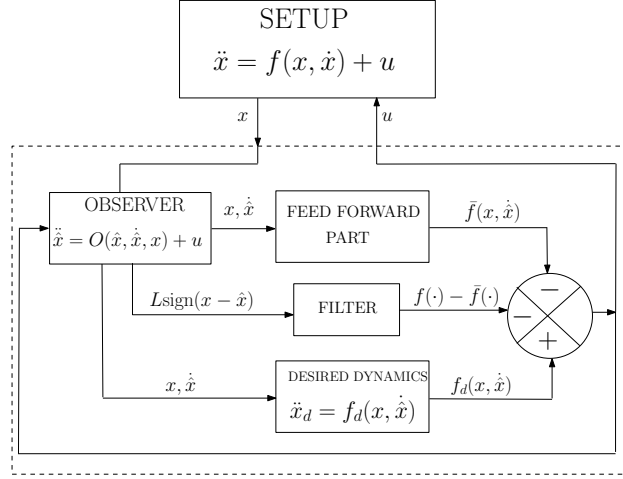


Figure 2.5 Adjustment of the dynamical properties of the setup.

has been replaced by a rigid bar of mass m_3 [kg], which is attached to the wall via a linear spring with elasticity k_3 [N/m] and a linear, viscous damper with damping constant d_3 [Ns/m]. The pendulum clocks in Huygens' experiment have been replaced by two identical pendula. Each pendulum is modelled by a point mass of mass $m = m_1 = m_2$ [kg] attached at the lower end of a massless bar of length $l = l_1 = l_2$ [m]. The damping in the pendula is also assumed to be viscous and linear with damping constant $d = d_1 = d_2$, [Nms/rad].

The idealized, i.e. it is assumed that no dry friction is present, equations of motion of the system are:

$$\begin{aligned} \ddot{\phi}_i &= -\frac{g}{l} \sin \phi_i - \frac{d}{ml^2} \dot{\phi}_i - \frac{\ddot{x}_3}{l} \cos \phi_i + \frac{\tau_i}{ml^2}, \quad i = 1, 2, \\ \ddot{x}_3 &= \frac{\sum_{i=1}^2 \left(\left(\frac{d}{l} \dot{\phi}_i + gm \sin \phi_i - \frac{\tau_i}{l} \right) \cos \phi_i + ml \sin \phi_i \dot{\phi}_i^2 \right) - d_3 \dot{x}_3 - k_3 x_3}{(m_3 + 2m - m \cos^2 \phi_1 - m \cos^2 \phi_2)}, \end{aligned} \quad (2.2)$$

where g [m/s²] is the gravitational acceleration, $\phi_i \in \mathcal{S}^1$, $i = 1, 2$, is the rotation angle of pendulum i in [rad], x_3 is the horizontal displacement of the bar in [m], and τ_i , $i = 1, 2$, represents the so-called escapement mechanism of pendulum i in [Nm].

Intermezzo

The limit behaviour of the uncontrolled system ($\tau_1 = \tau_2 = 0$) with undamped pendula ($d_1 = d_2 = 0$), can be analyzed as follows [66]. Consider the total energy of the system as a candidate Lyapunov function:

$$V = \frac{1}{2}m_3\dot{x}_3^2 + \frac{m}{2}\sum_{i=1}^2\left(\dot{x}_3^2 + 2\dot{x}_3l\dot{\phi}_i\cos\phi_i + l^2\dot{\phi}_i^2\right) + mgl\sum_{i=1}^2(1 - \cos\phi_i) + \frac{k}{2}x_3^2 \geq 0. \quad (2.3)$$

The time derivative of V along the trajectories of the uncontrolled system, with undamped pendula (2.2) is equal to:

$$\dot{V} = -d_3\dot{x}_3^2 \leq 0. \quad (2.4)$$

By using LaSalle's invariance principle [35], it follows that all trajectories of system (2.2) tend to the set where

$$\phi_1 = -\phi_2, \quad \dot{\phi}_1 = -\dot{\phi}_2, \quad x_3 = \dot{x}_3 = 0. \quad (2.5)$$

Moreover, it should be noticed that if the pendula are released from identical initial conditions, i.e. $\phi_1(0) = \phi_2(0)$ and $\dot{\phi}_1(0) = \dot{\phi}_2(0) = 0$, the oscillations will decay completely independent of the values of $x_3(0)$ and $\dot{x}_3(0)$.

Although the freely oscillating pendula also show a kind of ‘‘sympathy’’ observed by Huygens, the limit amplitude of the oscillations will depend on the initial conditions. The damper supporting the bar dissipates a part of the initial energy. The closer to in-phase the pendula are released, the more energy is lost during the process to reach the anti-phase motion.

Note that the idealized case discussed here (no control of the system, no damping in pendula) can be related to Huygens' pendulum clocks experiment in the sense that, after transients, the energy loss due to damping is compensated by the escapement mechanism.

In the original Huygens experiment, the clocks were driven by a verge-and-crown-wheel escapement. In this analysis, however, the following energy-based escapement is considered [66]

$$\tau_i = -\gamma \dot{\phi}_i (H_i - H^*), \quad \text{for } i = 1, 2, \quad (2.6)$$

where $\gamma \in \mathbb{R}^+$ in [s], $H^* = mgl(1 - \cos \phi_{ref})$ is a reference energy level, $\phi_{ref} \in (0, \frac{\pi}{2})$ is the reference amplitude and H_i is the Hamiltonian for the uncoupled and unforced pendulum i , which is defined as:

$$H_i = \frac{1}{2}ml^2\dot{\phi}_i^2 + mgl(1 - \cos \phi_i), \quad \text{for } i = 1, 2. \quad (2.7)$$

2.3.1 Adjustment of the experimental setup to mimic Huygens' system

The experimental setup of Figure 2.3 can be adjusted to mimic Huygens' system of Figure 2.1(b) by using state feedback. This requires design of suitable controllers U_i , $i = 1, 2, 3$, in (2.1), which are required to satisfy two objectives. Namely, cancellation of the original dynamics of equation (2.1) and enforcing the dynamics of equation (2.2) corresponding to Huygens' clocks system. The cancellation part is achieved by using feed forward compensation as already discussed in Section 2.2.

The adjustment is as follows.

First, the coordinate system of the experimental setup is transformed to a new set of coordinates, in which translational displacements can be related to rotation angles. From Figure 2.1(b) it is clear that the horizontal projection of the rotation angle of pendulum i is given by

$$x_i = x_3 + l \sin \phi_i, \quad i = 1, 2, \quad (2.8)$$

with corresponding velocities

$$\dot{x}_i = \dot{x}_3 + l_i \dot{\phi}_i \cos \phi_i, \quad i = 1, 2. \quad (2.9)$$

Inversely, the translational coordinates x_i , $i = 1, 2$, corresponding to the experimental setup can be mapped to rotational coordinates ϕ_i , $i = 1, 2$, of the pendula according to

$$\phi_i = \arcsin \frac{\Delta x_i}{l} \quad \forall |\Delta x_i| \leq l, \quad i = 1, 2, \quad (2.10)$$

with corresponding angular velocities

$$\dot{\phi}_i = \frac{1}{\sqrt{1 - \left(\frac{\Delta x_i}{l}\right)^2}} \frac{\Delta \dot{x}_i}{l} \quad \forall |\Delta x_i| < l, \quad i = 1, 2, \quad (2.11)$$

where $\Delta x_i = x_i - x_3$, $i = 1, 2$. Consequently, the “translational” version of the Huygens system of Figure 2.1(b) is given by

$$\ddot{x}_i = (1 - \cos^2 \phi_i) \ddot{x}_3 - \frac{d}{ml} \dot{\phi}_i \cos \phi_i - g \cos \phi_i \sin \phi_i + \frac{\tau_i}{ml} \cos \phi_i - l \sin \phi_i \dot{\phi}_i^2, \quad (2.12)$$

$$\ddot{x}_3 = \frac{\sum_{i=1}^2 \left(\left(\frac{d}{l} \dot{\phi}_i + gm \sin \phi_i - \frac{\tau_i}{l} \right) \cos \phi_i + ml \sin \phi_i \dot{\phi}_i^2 \right) - d_3 \dot{x}_3 - k_3 x_3}{(m_3 + 2m - m \cos^2 \phi_1 - m \cos^2 \phi_2)}. \quad (2.13)$$

Secondly, the actuations in (2.1) are defined as:

$$U_i = \omega_{is}^2 (x_i - x_3) + 2\zeta_{is}\omega_i (\dot{x}_i - \dot{x}_3) + (1 - \cos^2 \phi_i) \ddot{x}_3 - \frac{d}{ml} \dot{\phi}_i \cos \phi_i - g \cos \phi_i \sin \phi_i + \frac{\tau_i}{ml} \cos \phi_i - l \sin \phi_i \dot{\phi}_i^2, \quad i = 1, 2, \quad (2.14)$$

$$U_3 = \sum_{i=1}^2 \mu_i \ddot{x}_i + \omega_{3s}^2 x_3 + 2\zeta_{3s}\omega_{3s} \dot{x}_3 + \ddot{x}_3, \quad (2.15)$$

where $\phi_i, \dot{\phi}_i$, $i = 1, 2$, are given in (2.10) and (2.11) respectively, \ddot{x}_i , $i = 1, 2$, as given in (2.12), \ddot{x}_3 as given in (2.13), and τ_i , $i = 1, 2$, as given in (2.6). In closed loop, the dynamics of equation (2.1) with controllers (2.14)-(2.15) coincide with the dynamics of system (2.12)-(2.13). Note that the first two terms on the right-hand side of (2.14) and the first three terms on the right-hand side of (2.15) cancel the original dynamics in equations (2.1). Clearly, the experimental setup has been “converted” into the classical Huygens model.

Note that in the ideal case, a perfect cancellation of the original dynamics (2.1) is achieved. However, in practice, the dynamics to be cancelled are not perfectly known and therefore a perfect cancellation cannot be achieved. From a control point of view this is not an issue because normally a controller should be robust enough such that the unavoidable mismatches between models and plants can be handled by the controller. In this case, an estimator of disturbances [71], i.e. the filter depicted in Figure 2.5, has been used.

2.3.2 Experimental results

The experimental setup is adjusted in order to mimic the controlled system (2.2) and (2.6). Here, only essential details are provided. For additional details regarding this experiment the reader is referred to [59]. The following parameter values are used: $m = 1$ [kg], $m_3 = 50$ [kg], $d_1 = d_2 = 0.01$ [Nms/rad], $d_3 = 20$ [Ns/m], $k_3 = 1$ [N/m], $g = 9.81$ [m/s²], and $l = 0.2184$ [m]. The reference energy level $H^* = mgl(1 - \cos \phi_{ref})$ of controllers (2.6) corresponds to the reference amplitude

$\phi_{ref} = 0.35$ [rad] and $\gamma = 5.3$ [s]. The pendula are released from the initial conditions $\phi_1(0) = -0.32$ [rad], $\phi_2 = -0.02$ [rad], and $\dot{\phi}_1(0) = \dot{\phi}_2(0) = x(0) = \dot{x}(0) = 0$. These initial conditions for model (2.2) are related to the initial conditions in the setup by means of (2.8)-(2.9).

Figure 2.6 shows the obtained results. Although the pendula are released from initial conditions close to in-phase, as depicted in Figure 2.6(a), after a time interval with transient behaviour, the pendula *practically* synchronize in anti-phase as shown in Figure 2.6(b) and 2.6(d). As a consequence, the oscillations in the coupling bar decay as illustrated in Figure 2.6(c).

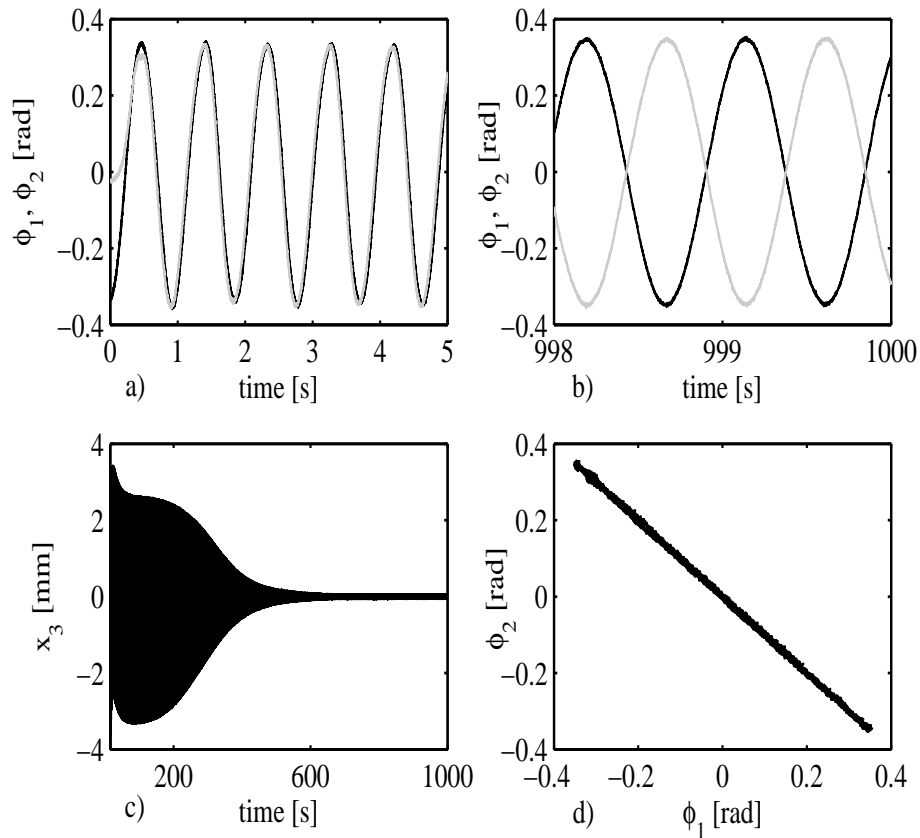


Figure 2.6 In this experiment, anti-phase synchronization is observed. In figures a) and b) black line: x_1 , grey line: x_2 .

2.4 Discussion

In conclusion, this chapter has introduced an adjustable experimental setup, which can be used in order to analyze robustness of synchronous behaviour in a real environment for a wide variety of dynamical oscillators. The research reported in the remaining chapters is largely supported by experimental results obtained with this experimental platform.

Chapter 3

Synchronization of nonlinear oscillators with limitations

The painter who draws merely by practice and by eye, without any reason, is like a mirror which copies everything placed in front of it without being conscious of their existence.

Leonardo da Vinci (1452–1519)

Abstract In this chapter, the occurrence of synchronization in pairs of (limited) nonlinear, self-sustained oscillators that interact via Huygens' coupling, i.e. a suspended rigid bar, is treated. Sufficient conditions for the existence and stability of synchronous solutions are derived using the Poincaré method. The obtained results are supported by experimental results. Ultimately, it is demonstrated that the mass of the coupling bar determines the limit synchronous behaviour in the oscillators.

3.1 Introduction

As mentioned in the introductory chapter, oscillations are common almost everywhere, be it in biology, in engineering, in economics, in physics or in other fields. These oscillations can occur naturally, as for example in the beats of the heart and lungs, in the rhythm of the waves approaching and receding the shore, in metronomes, in electrical circuits [84], and so on, or due to an external forcing, like for instance in the case of oscillations in structures and machines or in the case of chemical oscillations, like the ones produced by the Belousov-Zhabotinsky reaction [88].

Systems producing natural oscillations are called self-sustained oscillators. Essentially, one can distinguish four main properties in a self sustained oscillator namely:

- the system is nonlinear,
- there is an internal source of energy (in general this source is described by a nonlinear function),
- the oscillations are robust against small disturbances, and
- the form of the oscillations is determined by the parameters of the system and not by the initial conditions of the system.

Like other oscillatory systems, a pair or group of self-sustained oscillators may find their rhythms adjusted, i.e. they may synchronize. But, under what conditions? The famous example by Christiaan Huygens of two pendulum clocks exhibiting anti-phase or in-phase synchronized motion as brought forward in his notebook features exactly the crucial point: despite the lack of good modeling tools, Huygens did realize that there is a “medium” responsible for the synchronized motion, namely the bar to which both pendula are attached. This medium is referred to as *Huygens’ coupling*.

In this chapter, the onset of synchronization in pairs of constrained nonlinear self-sustained oscillators that interact via Huygens’ coupling is investigated. It is assumed that the nonlinear self-sustained oscillators are subject to the following *limitations*:

- small damping,
- weak nonlinearities and weak excitation forces, and
- small coupling strength.

Here, small has to be understood in the sense that the associated quantity is weighted by a (dimensionless) parameter which value is much less than unity. The term weak indicates that the influence of the nonlinear terms is almost negligible when compared to the influence that the linear terms have in the limit response of the system. In consequence, the dynamic behaviour of each nonlinear oscillator is close to a harmonic oscillator.

The original Huygens system is slightly modified in the sense that each pendulum clock is replaced by a constrained nonlinear oscillator. The coupling bar, i.e. the

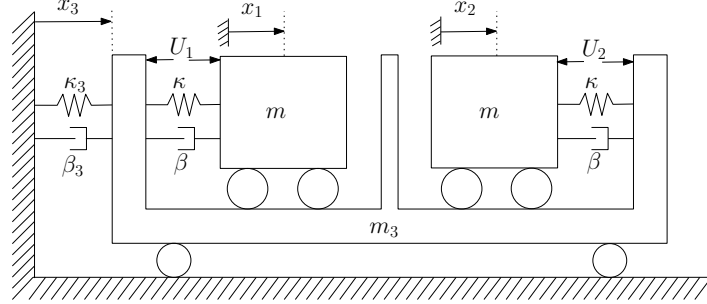


Figure 3.1 Schematic diagram of the generalized Huygens system.

Huygens coupling, is modeled as a one dof suspended rigid bar and it will be considered as the key element in the occurrence of synchronization.

Consequently, the generalized Huygens system introduced in Chapter 2 and depicted in Figure 3.1 is considered. It is assumed that the oscillators are identical and that the dynamic behaviour of the coupled system is, in general, described by a set of equations of the form

$$\ddot{x}_i = -\omega^2(x_i - x_3) + \mu F(x_i, \dot{x}_i, x_3, \dot{x}_3), \quad i = 1, 2, \quad (3.1)$$

$$\ddot{x}_3 = -\mu \sum_{i=1}^2 \ddot{x}_i - \omega_3^2 x_3 - 2\zeta_3 \omega_3 \dot{x}_3, \quad (3.2)$$

where $x_i \in \mathbb{R}$, $i = 1, 2$, denotes the displacement of oscillator i and $x_3 \in \mathbb{R}$ denotes the displacement of the coupling bar, $\omega = \sqrt{\frac{\kappa}{m}}$, $\kappa \in \mathbb{R}^+$, $m \in \mathbb{R}^+$ are the angular eigenfrequency, the stiffness, and the mass of each oscillator, respectively. The angular eigenfrequency of the coupling bar is denoted by $\omega_3 = \sqrt{\frac{\kappa_3}{m_3}}$ and $\kappa_3 \in \mathbb{R}^+$, $m_3 \in \mathbb{R}^+$, $\zeta_3 = \frac{\beta_3}{2\omega_3 m_3}$, $\beta_3 \in \mathbb{R}^+$ are the stiffness, the mass, the dimensionless damping coefficient, and the damping constant of the coupling bar, respectively. The dimensionless small parameter $0 < \mu = \frac{m}{m_3} \ll 1$ denotes the *coupling strength*. The function $F(x_i, \dot{x}_i, x_3, \dot{x}_3)$ describes the damping characteristic and the internal source of energy in each oscillator and is given by

$$F(x_i, \dot{x}_i, x_3, \dot{x}_3) = f(x_i, \dot{x}_i) - 2\zeta\omega(\dot{x}_i - \dot{x}_3), \quad i = 1, 2, \quad (3.3)$$

where $\zeta = \frac{\beta}{2\omega m}$, $\beta \in \mathbb{R}^+$ are the dimensionless damping coefficient and the damping constant of each oscillator, respectively. The nonlinear term $f(x_i(t), \dot{x}_i(t))$ (represented by U_i , $i = 1, 2$, in Figure 3.1) represents an internal energy source and compensates the energy loss in system (3.1)-(3.2). The need of having $f(x_i(t), \dot{x}_i(t))$ in (3.3) can be linked to Huygens' pendulum clocks where the energy loss due to damping and friction is compensated by an escapement mechanism.

The energy loss in the oscillators is assumed to be compensated by the *Hamiltonian escapement*

$$U_i = f(x_i, \dot{x}_i) = -\lambda(H_i - H^*)\dot{x}_i, \quad i = 1, 2, \quad (3.4)$$

as used earlier in Section 2.3 and by the *van der Pol escapement*

$$U_i = f(x_i, \dot{x}_i) = -\nu(ax_i^2 - 1)\dot{x}_i, \quad i = 1, 2. \quad (3.5)$$

It should be noted that these functions satisfy assumption [A-1] given in Section 1.4.

For the coupled system (3.1-3.3) together with either (3.4) or (3.5), it is possible to analyze, to a large extent, the occurrence of in-phase and anti-phase synchronization analytically. In fact, the natural existence of the small parameter μ (the ratio between the mass of the oscillator and the mass of the coupling bar) in the system and the aforementioned limitations on the oscillators, allow to describe the synchronization problem in a suitable form to be analyzed analytically by means of approximate methods of the theory of oscillations [4, 7, 41, 48].

Consequently, the Poincaré method described in Chapter 1 can be used in order to derive conditions, under which synchronous solutions in the pair of nonlinear oscillators with Huygens' coupling (3.1-3.2) exist and are stable. In particular, it will be shown that the mass of the coupling bar, which is directly associated with the coupling strength, determines the limit synchronized behaviour in the oscillators, namely in-phase or anti-phase synchronization. Section 3.2 presents this analysis for the case of constrained nonlinear oscillators driven by the Hamiltonian escapement (3.4), whereas in Section 3.3, a similar analysis is performed for the case of constrained nonlinear oscillators driven by the van der Pol escapement (3.5).

Finally, in Section 3.4, it is experimentally demonstrated for both types of escapements (3.4) and (3.5) that two constrained nonlinear oscillators may synchronize in-phase or in anti-phase without the influence of an explicit control action, i.e. in a natural way, provided that the oscillators are coupled through Huygens' coupling. All experiments are conducted by using the electro-mechanical device described in Chapter 2.

The chapter is concluded by a discussion of the obtained results.

3.2 Synchronization of oscillators driven by a Hamiltonian escapement

Consider the schematic model depicted in Figure 3.1 where it has been assumed that the oscillators are identical. Moreover, assume that the resupply of energy into the oscillators is provided by the Hamiltonian escapement (3.4), i.e. $U_i = f(x_i, \dot{x}_i) = -\lambda(H_i - H^*)\dot{x}_i$. Under these assumptions, the dynamic behaviour of the generalized Huygens system depicted in Figure 3.1 is described by the set of equations

$$\ddot{x}_i = -\omega^2(x_i - x_3) - 2\zeta\omega(\dot{x}_i - \dot{x}_3) - \lambda(H_i - H^*)\dot{x}_i, \quad i = 1, 2, \quad (3.6)$$

$$\ddot{x}_3 = -\mu \sum_{i=1}^2 \ddot{x}_i - \omega_3^2 x_3 - 2\zeta_3 \omega_3 \dot{x}_3, \quad (3.7)$$

where $\omega = \sqrt{\frac{\kappa}{m}}$ [rad/s], $\omega_3 = \sqrt{\frac{\kappa_3}{m_3}}$ [rad/s], $\zeta = \frac{\beta}{2\omega m}$ [-], and $\zeta_3 = \frac{\beta_3}{2\omega_3 m_3}$ [-] are positive parameters, which have been defined in the previous section, $\mu = \frac{m}{m_3}$ [-] is the coupling strength, λ [s/kgm²] is a positive parameter, $H^* = \frac{1}{2}\kappa x_{ref}^2$ [Nm] is a reference energy level with x_{ref} [m] being a reference amplitude, the displacements corresponding to the oscillators are denoted by x_i , $i = 1, 2$, and x_3 describes the displacement of the coupling bar. The Hamiltonian H_i for the uncoupled and unforced oscillator i is defined by

$$H_i = \frac{1}{2}m\dot{x}_i^2 + \frac{1}{2}\kappa x_i^2, \quad i = 1, 2. \quad (3.8)$$

Rescaling the time by $\tau = \omega t$ yields the system in the form

$$x_i'' = -(x_i - x_3) - p(x_i' - x_3') - \bar{\lambda}(ax_i'^2 + \kappa x_i^2 - \gamma)x_i', \quad i = 1, 2, \quad (3.9)$$

$$x_3'' = -\mu \sum_{i=1}^2 x_i'' - qx_3 - sx_3', \quad (3.10)$$

where the primes denote differentiation with respect to the dimensionless time τ , $p = 2\zeta$ [-], $\bar{\lambda} = \frac{\lambda}{2\omega}$ [s²/(kgm²rad)], $a = m\omega^2$ [kgrad²/s²], $\gamma = 2H^*$ [Nm], $q = \frac{\omega_3^2}{\omega^2}$ [-], and $s = \frac{2\zeta_3\omega_3}{\omega}$ [-].

In order to bring this system into the form (3.1)-(3.2), it will be assumed that the damping in the oscillators is small, i.e. $p = \mu d$ and that the nonlinearity is small, i.e. $\bar{\lambda} = \mu\alpha$.

The above assumptions yield the system

$$x_i'' = -(x_i - x_3) - \mu d(x_i' - x_3') - \mu\alpha \left(ax_i'^2 + \kappa x_i^2 - \gamma \right) x_i', \quad (3.11)$$

$$x_3'' = -\mu \sum_{i=1}^2 x_i'' - qx_3 - sx_3', \quad i = 1, 2. \quad (3.12)$$

In order to determine (the existence of) a periodic, synchronous solution in this system and its local stability, Theorem 1.1, which is based on the Poincaré method, is used. The analysis is as follows.

After neglecting quadratic terms in μ , (3.11-3.12) can be written in the form

$$x' = Ax + \mu\Phi(x) \quad (3.13)$$

with

$$A = \begin{bmatrix} 0 & 1 & 0 & 0 & 0 & 0 \\ -1 & 0 & 0 & 0 & 1 & 0 \\ 0 & 0 & 0 & 1 & 0 & 0 \\ 0 & 0 & -1 & 0 & 1 & 0 \\ 0 & 0 & 0 & 0 & 0 & 1 \\ 0 & 0 & 0 & 0 & -q & -s \end{bmatrix}, \quad \Phi(x) = \begin{bmatrix} 0 \\ -\alpha \left(ax_1'^2 + \kappa x_1^2 - \gamma \right) x_1' - d(x_1' - x_3') \\ 0 \\ -\alpha \left(ax_2'^2 + \kappa x_2^2 - \gamma \right) x_2' - d(x_2' - x_3') \\ 0 \\ x_1 + x_2 - 2x_3 \end{bmatrix}, \quad (3.14)$$

$$\text{and } x = [x_1 \quad x_1' \quad x_2 \quad x_2' \quad x_3 \quad x_3']^T.$$

The next step is to determine the transformation that leads to the canonical form (1.10). Since for $\mu = 0$ system (3.13) becomes linear, then such transformation can be easily obtained by diagonalizing A in the form $A = VDV^{-1}$, where D is a diagonal matrix containing the eigenvalues of A and V the matrix of corresponding eigenvectors, which are stored columnwise. For A as defined in (3.14), the diagonal matrix D verifies

$$D = \begin{bmatrix} i & 0 & 0 & 0 & 0 & 0 \\ 0 & -i & 0 & 0 & 0 & 0 \\ 0 & 0 & i & 0 & 0 & 0 \\ 0 & 0 & 0 & -i & 0 & 0 \\ 0 & 0 & 0 & 0 & \sigma_1 & 0 \\ 0 & 0 & 0 & 0 & 0 & \sigma_2 \end{bmatrix} \quad (3.15)$$

where $\sigma_1 = \frac{1}{2} \left(-s + \sqrt{s^2 - 4q} \right)$ and $\sigma_2 = \frac{1}{2} \left(-s - \sqrt{s^2 - 4q} \right)$. Note that since $s > 0$ and $q > 0$, $\text{Re}(\sigma_1) < 0$ and $\text{Re}(\sigma_2) < 0$. Note further that $k = 4$ and $l = 6$ in (1.13).

By defining $x = Vy$, system (3.13) takes the canonical form, see (1.10)¹

¹Note that this transformation is valid since the matrix of eigenvectors associated to (3.15)

$$y' = Dy + \mu V^{-1} \Phi(Vy). \quad (3.16)$$

According to (1.14), the generating system (1.11) associated to (3.16) has solutions of the form

$$y_1 = \alpha_1 e^{i\tau}, \quad y_2 = \alpha_2 e^{-i\tau}, \quad y_3 = \alpha_3 e^{i\tau}, \quad y_4 = \alpha_4 e^{-i\tau}, \quad y_5 = y_6 = 0. \quad (3.17)$$

The amplitudes of these solutions are assumed to be complex, i.e. $\alpha_i = r_i e^{i\phi_i}$, $i = 1, 2, 3, 4$, where $\alpha_i \in \mathbb{C}$, $r_i \in \mathbb{R}^+$, and $\phi_i \in \mathcal{S}^1$. In this way, it is easy to analyze phase synchronization by looking at the phase differences. At this point it is also worth to note that four eigenvalues of A appear in complex conjugate pairs, see (3.15). In order to have real solutions, it is necessary and sufficient that $\alpha_2 = \bar{\alpha}_1$ and $\alpha_4 = \bar{\alpha}_3$, i.e. $\phi_2 = -\phi_1$ and $\phi_4 = -\phi_3$ and correspondingly $r_1 = r_2$ and $r_3 = r_4$. This yields

$$\alpha_1 = r_1 e^{i\phi_1}, \quad \alpha_2 = r_1 e^{-i\phi_1}, \quad \alpha_3 = r_3 e^{i\phi_3}, \quad \alpha_4 = r_3 e^{-i\phi_3}. \quad (3.18)$$

One can set $\phi_3 = 0$ without loss of generality since time can be shifted by a constant, then synchronization is characterized by a single phase $\phi = \phi_1$. Moreover, it will be assumed that the amplitudes are the same, i.e. $r = r_1 = r_3$. Consequently, the solutions (3.17) of the generating system become

$$y_1 = r e^{i(\tau+\phi)}, \quad y_2 = r e^{-i(\tau+\phi)}, \quad y_3 = r e^{i\tau}, \quad y_4 = r e^{-i\tau}, \quad y_5 = y_6 = 0. \quad (3.19)$$

Next, the values of r and ϕ are determined. This can be done by writing conditions (1.15) of Theorem 1.1 as a system of equations in terms of r and ϕ . This yields

$$e^{i\phi} [\alpha (\gamma - (3a + \kappa) r^2) - d] - \frac{s(1 + e^{i\phi})}{(-1 + q)^2 + s^2} = 0, \quad (3.20)$$

$$\alpha (\gamma - (3a + \kappa) r^2) - d - \frac{f(s, \phi, q, i)}{(q - 1)^2 + s^2} = 0, \quad (3.21)$$

$$\frac{i(1 - e^{-2i\phi})}{-1 + q - is} = 0, \quad (3.22)$$

where

$$\frac{f(s, \phi, q, i)}{(q - 1)^2 + s^2} = \left[\frac{s + \frac{s}{2} (e^{i\phi} + e^{-i\phi}) + \frac{1}{2} (-1 + q) (e^{i\phi} + e^{-i\phi}) i}{(-1 + q)^2 + s^2} \right]. \quad (3.23)$$

Equation (3.22) directly implies

$$\phi = 0 \quad \text{or} \quad \phi = \pi.^2 \quad (3.24)$$

has full rank. Eigenvalue i as well as eigenvalue $-i$ have geometric and algebraic multiplicity equal to 2.

²Actually, Equation (3.22) is satisfied for $\phi = \pm n\pi$ with $n = 0, 1, 2, \dots$

Substituting these values into (3.20) or (3.21) yields the corresponding expressions for the half-amplitudes r of the periodic solutions:

- $\phi = 0$ (in-phase synchronization)

$$r = \sqrt{\frac{\gamma - \left(\frac{\sigma+d}{\alpha}\right)}{(3a + \kappa)}}, \quad (3.25)$$

with $\sigma = \frac{2s}{(-1+q)^2+s^2}$. Note that (3.25) is defined if $\gamma > \frac{\sigma+d}{\alpha}$.

- $\phi = \pi$ (anti-phase synchronization)

$$r = \sqrt{\frac{\gamma - \left(\frac{d}{\alpha}\right)}{(3a + \kappa)}}. \quad (3.26)$$

In this case, (3.26) will be defined if $\gamma > \frac{d}{\alpha}$.

Next, the stability of these solutions is investigated by using (1.18) in Theorem 1.1. This requires the computation of a characteristic polynomial for both the in-phase solution and the anti-phase solution.

- $\phi = 0$ (in-phase synchronization)

After elaborated computations, one finds the following characteristic polynomial:

$$p_{in}(\chi) = [\chi + 2\pi(\alpha\gamma - d - \sigma)] [((1 - q)^2 + s^2)\chi^2 + 2\pi(\alpha\gamma - d - 2\sigma)\chi + c], \quad (3.27)$$

where

$$\sigma = \frac{2s}{(1 - q)^2 + s^2}, \quad c = 4\pi^2 (1 + s\sigma - s(\alpha\gamma - d)). \quad (3.28)$$

This polynomial will have roots with negative real part if and only if

$$C_1 = \gamma - \left(\frac{\sigma + d}{\alpha}\right) > 0, \quad C_2 = \gamma - \left(\frac{2\sigma + d}{\alpha}\right) > 0, \quad \text{and} \quad C_3 = -\gamma + \left(\frac{\sigma + d + \frac{1}{s}}{\alpha}\right) > 0. \quad (3.29)$$

Note that condition $C_1 > 0$ is the same condition for the existence of the in-phase synchronous solution, see (3.25). Moreover, since $\sigma > 0$, condition $C_1 > 0$ is weaker than condition $C_2 > 0$. In other words, for (3.27) having negative roots, it is necessary and sufficient that $C_2 > 0$ and $C_3 > 0$.

By substituting the original parameters of (3.6)-(3.7) in (3.29), it is possible to rewrite the conditions for C_2 and C_3 in terms of the original parameters including m_3 , i.e. the mass of the coupling bar. This yields

$$C_2 = 2H^* - \frac{16\zeta_3\omega_3 m\omega^4}{\lambda m_3 [\omega^4 - 2\omega_3^2\omega^2 + \omega_3^4 + 4\zeta_3^2\omega_3^2\omega^2]} - \frac{4\zeta\omega}{\lambda} > 0, \quad (3.30)$$

$$C_3 = -2H^* + \frac{8\zeta_3\omega_3 m\omega^4}{\lambda m_3 [\omega^4 - 2\omega_3^2\omega^2 + \omega_3^4 + 4\zeta_3^2\omega_3^2\omega^2]} + \frac{4\zeta\omega}{\lambda} + \frac{\omega^2 m}{\lambda\zeta_3\omega_3 m_3} > 0. \quad (3.31)$$

- $\phi = \pi$ (anti-phase synchronization)

Again, after elaborated computations, one finds the following characteristic polynomial:

$$p_{anti}(\chi) = [\chi + 2\pi(\alpha\gamma - d)] [z\chi^2 + (2\pi z(\alpha\gamma - d)\chi + 4\pi^2(1 + s(\alpha\gamma - d)))] , \quad (3.32)$$

where $z = (1 - q)^2 + s^2$. In this case the roots of $p_{anti}(\chi)$ will have negative real parts if and only if

$$C_4 = \gamma - \left(\frac{d}{\alpha}\right) > 0, \quad C_5 = \gamma - \left(\frac{d - \frac{1}{s}}{\alpha}\right) > 0, \quad (3.33)$$

Since σ and s are positive, it follows that $p_{anti}(\chi)$ is Hurwitz iff $C_4 > 0$. Note that, again, stability condition $C_4 > 0$ coincides with the condition for the existence of the solution, see (3.26).

Again, C_4 can be rewritten in terms of the original parameters, i.e.

$$C_4 = 2H^* - \frac{4\zeta\omega}{\lambda}. \quad (3.34)$$

Clearly, the condition for the existence and stability of the anti-phase regime does not depend on m_3 , i.e. the mass of the coupling bar. Note that this coincides with the fact that the coupling bar comes to standstill when the oscillators synchronize in anti-phase, i.e. the coupling ‘disappears’ during the anti-phase motion. Furthermore, it should be noted that condition (3.33) is ‘softer’ than condition (3.29) for in-phase synchronization because if (3.29) is satisfied, then (3.33) will be satisfied too, whereas the opposite is not true.

Finally, the period of the synchronous solutions is computed. From Theorem 1.1 and (1.19) it follows that the in-phase synchronous solutions of system (3.13) which

is in terms of dimensionless time τ have period

$$T_{in} = T + \tau_c(\mu) = 2\pi \left[1 + \mu \frac{q-1}{q^2 - 2q + s^2 + 1} \right] + \mathcal{O}(\mu^2), \quad (3.35)$$

whereas the anti-phase synchronous solutions will have period

$$T_{anti} = T + \tau_c(\mu) = 2\pi + \mathcal{O}(\mu^2). \quad (3.36)$$

This result is very intuitive: when the oscillators synchronize in anti-phase, the coupling bar has no influence because it will be in rest and the oscillation frequency will closely approximate the eigenfrequency of the uncoupled, undamped, oscillators. On the other hand, when the oscillators synchronize in-phase, the coupling bar converges to an oscillatory motion, which will influence the oscillation frequency of the oscillators.

As mentioned before, the coupling strength in a pair of oscillators with Huygens' coupling is defined as the ratio of the mass of one oscillator over the mass of the coupling bar, i.e. $\mu = \frac{m}{m_3}$. For the application of the Poincaré method to be valid μ should be a small parameter, i.e. $\mu \ll 1$.

The above results are summarized in the following two theorems and corollary.

Theorem 3.1. *Consider system (3.11)-(3.12). Assume $\mu \ll 1$ and that the parameter values satisfy conditions (3.29). Then, in-phase synchronized solutions exist in system (3.11)-(3.12) and these solutions are (asymptotically) stable, i.e.*

$$\lim_{t \rightarrow \infty} e_{in}(t) := x_1(t) - x_2(t) = 0, \quad \lim_{t \rightarrow \infty} \dot{e}_{in}(t) := \dot{x}_1(t) - \dot{x}_2(t) = 0. \quad (3.37)$$

Moreover, the limit solutions corresponding to the oscillators have amplitude

$$A_{in-phase}(\mu) = 2r = 2\sqrt{\frac{\gamma - \left(\frac{\sigma+d}{\alpha}\right)}{(3a + \kappa)}} = 2\sqrt{\frac{2H^* - \mu h_1 - \frac{4\zeta\omega}{\lambda}}{3m\omega^2 + \kappa}} \quad (3.38)$$

with $h_1 = \frac{8\zeta_3\omega_3\omega^4}{\lambda[\omega^4 - 2\omega_3^2\omega^2 + \omega_3^4 + 4\zeta_3^2\omega_3^2\omega^2]}$ and period

$$T_{in-phase} = T + \tau_c(\mu) = 2\pi \left[1 + \mu \frac{q-1}{q^2 - 2q + s^2 + 1} \right] + \mathcal{O}(\mu^2). \quad (3.39)$$

Theorem 3.2. *Consider system (3.11)-(3.12). Assume that $\mu \ll 1$ and that the parameter values satisfy conditions (3.33). Then, anti-phase synchronized solutions exist and are (asymptotically) stable, i.e.*

$$\lim_{t \rightarrow \infty} e_{an}(t) := x_1(t) + x_2(t) = 0, \quad \lim_{t \rightarrow \infty} \dot{e}_{an}(t) = \dot{x}_1(t) + \dot{x}_2(t) = 0, \quad (3.40)$$

$$\text{and} \quad \lim_{t \rightarrow \infty} x_3(t) = \dot{x}_3(t) = 0. \quad (3.41)$$

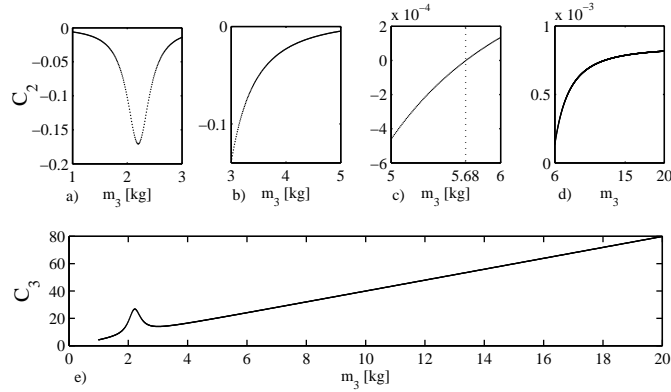


Figure 3.2 Conditions (3.29) for in-phase synchronization plotted as a function of the mass of the coupling bar, i.e. m_3 . Figures a) to d): C_2 . Figure e): C_3 .

Moreover, the limit solutions corresponding to the oscillators have amplitude

$$A_{anti-phase} = 2r = 2\sqrt{\frac{\gamma - \frac{d}{\alpha}}{(3a + \kappa)}} = 2\sqrt{\frac{2H^* - \frac{4\zeta\omega}{\lambda}}{3m\omega^2 + \kappa}} \quad (3.42)$$

and period

$$T_{anti-phase} = T + \tau_c(\mu) = 2\pi + \mathcal{O}(\mu^2). \quad (3.43)$$

Corollary 3.1. *If $\mu \ll 1$ and condition (3.29) is satisfied then system (3.11)-(3.12) admits both in-phase and anti-phase synchronized solutions and both solutions are locally asymptotically stable.*

Finally, the above analytical results are illustrated and supported by means of numerical simulations.

Consider system (3.11)-(3.12) with the following parameter values: $a = 37.1080$ [-], $\gamma = 1.6 \times 10^{-3}$ [-], $\kappa = 37.1080$ [-], $d = \frac{1.43 \times 10^{-2}}{\mu}$ [-], $\alpha = \frac{1.99 \times 10^1}{\mu}$ [s²/(kgm²rad)], $q = 1.309 \times 10^{-1}$ [-], $s = 1.46 \times 10^{-2}$ [-] and $\mu = \frac{2.1 \times 10^{-1}}{m_3}$ [-]. It follows that for these parameter values conditions (3.29) are satisfied if $m_3 > 5.68$ [kg], see Figure 3.2. Here, a value of $m_3 = 16.8$ [kg] is considered. Consequently $\mu = 0.0125$ [-].

Figure 3.3 shows the obtained simulation results. The nonzero initial conditions are $x_1(0) = 3 \times 10^{-3}$ [m], $x_2(0) = 2 \times 10^{-3}$ [m]. After initial transient behaviour, the oscillators synchronize in-phase, as depicted in Figure 3.3. By using (3.38) the limit amplitude of the synchronized solution is computed. It follows that for the given

parameters $A_{in-phase} = 4.713 \times 10^{-3}$ [m]. This value and its negative counterpart are denoted by the horizontal dotted lines in Figure 3.3b). The agreement between the analytical and the numerical results is evident. In fact, the difference between the actual amplitude and predicted amplitude is 2.256%. Additionally, the period of the synchronous solution is computed by using (3.39). This yields $T_{in-phase} = 6.1928$ [-]. Again, this result is very close (with an error of 0.033%) to the obtained result by numerical integration of (3.11)-(3.12) as depicted in Figure 3.3b) (vertical dotted lines). Moreover, since for the given parameter values also condition (3.33), see Theorem 3.2, holds with $C_4 = 8.487 \times 10^{-4}$, it follows that also anti-phase synchronization exists. This case is presented in Figure 3.3c) and Figure 3.3d). These results have been obtained by using the same parameter values as used above except for the initial condition of oscillator 2, which now is $x_2(0) = -5 \times 10^{-4}$ [m]. Clearly, the oscillators are synchronized in anti-phase. The amplitude of the anti-phase solution, computed by using (3.42) in Theorem 3.2, is $A_{anti-phase} = 4.782 \times 10^{-3}$ [m]. Again, this value and its negative counterpart are indicated by two horizontal lines in Figure 3.3d). The error in the predicted amplitude and the actual amplitude of the solution is 0.083%. The period of the solution, indicated by two vertical lines in Figure 3.3d), is $T_{anti-phase} = 6.2827$ [-], whereas the expected value from (3.43) in Theorem 3.2 is $T = 2\pi$, i.e. there is a difference of 0.0063%.

In order to illustrate the influence of the coupling strength $\mu = \frac{m}{m_3}$ in the limit synchronizing behaviour of the oscillators, system (3.11)-(3.12) is again numerically integrated by using the same parameter values and initial conditions as used in the first simulation presented above, except for the coupling strength, which is increased by decreasing m_3 to $m_3 = 4.1$ [kg]. This yields $\mu = 0.0512$ [-]. Consequently, condition (3.29), see Theorem 3.1, is not fulfilled. However, condition (3.33), see Theorem 3.2, is satisfied and consequently the only stable synchronous solution is anti-phase synchronization, as depicted in Figure 3.4. It can be seen that although the initial conditions of the system are very close to in-phase, after initial transient behaviour, the system synchronizes in anti-phase. Next, the limit amplitude of the synchronous solutions can be computed by using (3.42) and it follows that $A_{anti-phase} = 4.782 \times 10^{-3}$ [m]. Again, this value and its negative counterpart are shown by two horizontal lines in Figure 3.4b). The error between the predicted amplitude and the real amplitude is 0.020%. The corresponding period, according to (3.43) is $T_{anti-phase} = 2\pi = 6.2832$ [-] and this result again is very approximated to the computer simulation result, see the vertical lines in Figure 3.4b), which is 6.2824 [-], i.e. an error of 0.01%.

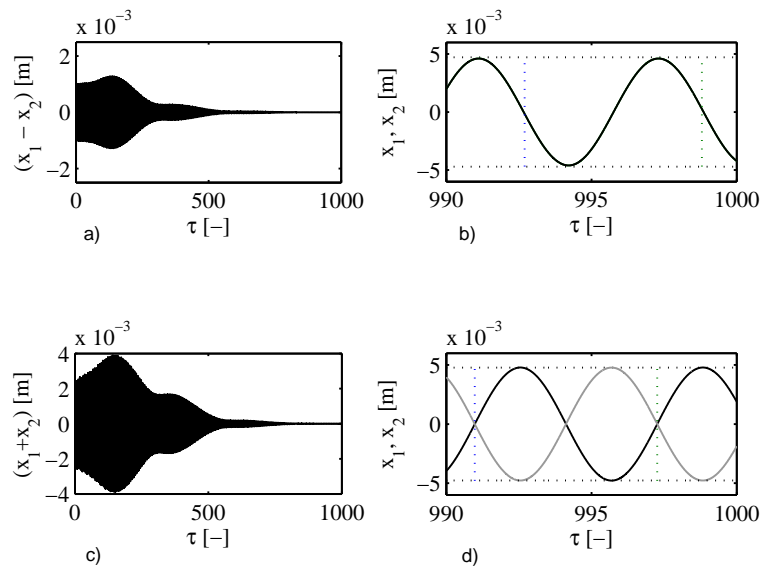


Figure 3.3 For a small coupling strength (m_3 large) and initial conditions close to in-phase, system (3.II-3.12) synchronizes in-phase as depicted in figures a) and b). For the same coupling strength and initial conditions far from in-phase, the oscillators synchronize in anti-phase, as shown in figures c) and d), where black line: x_1 , grey line: x_2 .

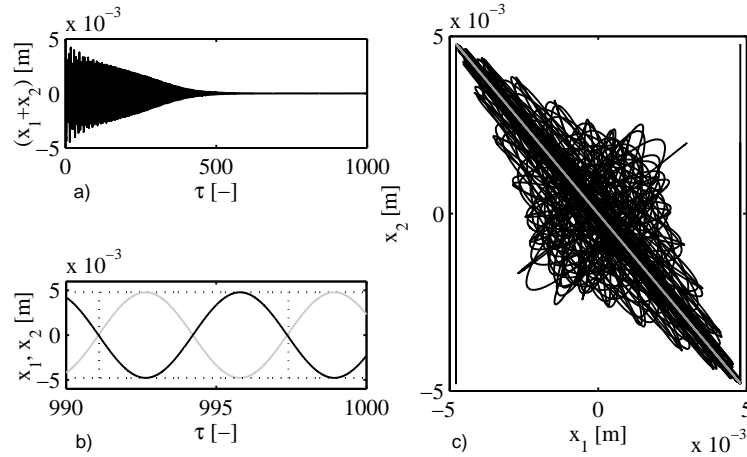


Figure 3.4 When the coupling strength is increased (by decreasing m_3) the only synchronous solution in system (3.11-3.12) is anti-phase synchronization. In b), black line: x_1 , grey line: x_2 . In c), black line: transient behaviour, grey: long term behaviour.

3.3 Synchronization of oscillators driven by a van der Pol term

A classical model of a nonlinear oscillator showing self-sustained oscillations is due to van der Pol [85]. The key feature in the model is the presence of a nonlinear damping term, which dissipates energy for large amplitudes - acting like ordinary positive damping - and generates energy at low amplitudes - acting like negative damping. It should be noticed that this term has more or less the same effect as an escapement mechanism in a pendulum clock: energy is delivered to the system such that the oscillations do not damp out. Consequently, it is not surprising that there exist several works related to the classical Huygens system where the escapement mechanism has been modelled by using the nonlinear damping term of the van der Pol equation, see e.g. [8, 55, 82]. This facilitates the modelling of the real escapement mechanism and allows to perform a fairly complete analytic analysis of the in-phase and anti-phase synchronized motion, which becomes tremendously involved if the escapement is modelled for instance by an impulsive function [43, 72].

This section investigates the occurrence of synchronization in the system of coupled oscillators depicted in Figure 3.1 for the case where the resupply of energy into

the oscillators is provided by the nonlinear term (3.5).

By again assuming identical oscillators, it can be shown that the dynamic behaviour of the coupled system is described by

$$\ddot{x}_i = -\omega^2(x_i - x_3) - 2\zeta\omega(\dot{x}_i - \dot{x}_3) - \nu(ax_i^2 - 1)\dot{x}_i \quad i = 1, 2, \quad (3.44)$$

$$\ddot{x}_3 = -\mu \sum_{i=1}^2 \ddot{x}_i - \omega_3^2 x_3 - 2\zeta_3 \omega_3 \dot{x}_3, \quad (3.45)$$

where again as defined in Section 3.1, $\omega, \omega_3, \zeta, \zeta_3$ are positive parameters and μ is the coupling strength. Parameter $\nu \in \mathbb{R}^+$ in [1/s] determines the amount of nonlinearity and the strength of the damping and $a \in \mathbb{R}^+$ in [1/m²] is a parameter, which defines the switching between positive and negative damping. For $x_i < \frac{1}{\sqrt{a}}$, the velocity in oscillator i is increased and for $x_i > \frac{1}{\sqrt{a}}$, it is decreased.

It is clear that the system under consideration resembles a pair of van der Pol oscillators with Huygens' coupling. In order to derive conditions for the onset of in-phase and anti-phase synchronized motion in the coupled system (3.44)-(3.45), the Poincaré method presented in Chapter 1 is used again. This requires to transform the system into the form (1.10). By setting $\tau = \omega t$ [-], $p = 2\zeta$ [-], $q = \frac{\omega_3^2}{\omega^2}$ [-], $s = \frac{2\zeta_3\omega_3}{\omega}$ [-], and $\bar{\lambda} = \frac{\nu}{\omega}$ [-], and assuming that the damping in the oscillators and the amplitude of the nonlinear van der Pol term are small, i.e. $p = \mu d$ [-] and $\bar{\lambda} = \mu\alpha$, it is possible to rewrite (3.44)-(3.45) in the form

$$x' = Ax + \mu\Phi_1(x) + \mu^2\Phi_2(x) \quad (3.46)$$

where the prime denotes differentiation with respect to the dimensionless time τ , $x = [x_1 \ x_1' \ x_2 \ x_2' \ x_3 \ x_3']^T$ is the state vector, A is as given in (3.14), and

$$\Phi_1 = \begin{bmatrix} 0 \\ -d(x_1' - x_3') - \alpha(ax_1^2 - 1)x_1' \\ 0 \\ -d(x_2' - x_3') - \alpha(ax_2^2 - 1)x_2' \\ 0 \\ x_1 + x_2 - 2x_3 \end{bmatrix}, \quad \Phi_2 = \begin{bmatrix} 0 \\ 0 \\ 0 \\ 0 \\ 0 \\ \sum_{i=1}^2 (dx_i' + \alpha(ax_i^2 - 1)x_i') - 2dx_3' \end{bmatrix}. \quad (3.47)$$

The following two theorems are derived for system (3.46). For simplicity, their proof is omitted but it can be derived by following the procedure presented in Section 3.2.

Theorem 3.3. *Consider system (3.46). Assume $\mu \ll 1$ and that the parameter values satisfy the following conditions:*

$$C_1 = 1 - \left(\frac{2\sigma + d}{\alpha}\right) > 0, \quad \text{and} \quad C_2 = -1 + \left(\frac{\sigma + d + \frac{1}{s}}{\alpha}\right) > 0. \quad (3.48)$$

Then, in-phase synchronized solutions exist in system (3.46) and these solutions are (asymptotically) stable, i.e.

$$\lim_{t \rightarrow \infty} e_{in}(t) := x_1(t) - x_2(t) = 0, \quad \lim_{t \rightarrow \infty} \dot{e}_{in}(t) := \dot{x}_1(t) - \dot{x}_2(t) = 0. \quad (3.49)$$

Moreover, the limit solutions corresponding to the oscillators have amplitude

$$A_{in-phase}(\mu) = 2r = 2\sqrt{\frac{\alpha - (\sigma + d)}{a\alpha}} = 2\sqrt{\frac{1 - \mu h_1 - \frac{2\zeta\omega}{\nu}}{a}} \quad (3.50)$$

with $h_1 = \frac{4\zeta_3\omega_3\omega^4}{\lambda[\omega^4 - 2\omega_3^2\omega^2 + \omega_3^4 + 4\zeta_3^2\omega_3^2\omega^2]}$ and period

$$T_{in-phase} = T + \tau_c(\mu) = 2\pi \left[1 + \mu \frac{q-1}{q^2 - 2q + s^2 + 1} \right] + \mathcal{O}(\mu^2). \quad (3.51)$$

Theorem 3.4. Consider system (3.46). Assume $\mu \ll 1$ and that the following condition holds

$$\alpha - d > 0. \quad (3.52)$$

Then, anti-phase synchronized solutions exist and are (asymptotically) stable, i.e.

$$\lim_{t \rightarrow \infty} e_{an}(t) := x_1(t) + x_2(t) = 0, \quad \lim_{t \rightarrow \infty} \dot{e}_{an}(t) = \dot{x}_1(t) + \dot{x}_2(t) = 0, \quad (3.53)$$

$$\text{and} \quad \lim_{t \rightarrow \infty} x_3(t) = \dot{x}_3(t) = 0. \quad (3.54)$$

Moreover, the limit solutions corresponding to the oscillators have amplitude

$$A_{anti-phase} = 2r = 2\sqrt{\frac{1 - \frac{d}{\alpha}}{a}} = 2\sqrt{\frac{1 - \frac{2\zeta\omega}{\nu}}{a}} \quad (3.55)$$

and period

$$T_{anti-phase} = T + \tau_c(\mu) = 2\pi + \mathcal{O}(\mu^2). \quad (3.56)$$

These results again show that the coupling strength influences the limit synchronizing behaviour as stated in the previous section.

Note that condition (3.52) is weaker than condition (3.48). Hence, when (3.48) is satisfied, in-phase and anti-phase synchronous solutions exist and are locally asymptotically stable. On the other hand, when (3.52) is satisfied and condition (3.48) is not satisfied, then the only stable synchronous solution is anti-phase synchronization. By means of numerical integration it is possible to show countless examples. However, all of them will have the same essence as those depicted in Figures 3.3 and 3.4, namely the occurrence of in-phase and anti-phase synchronization being influenced by the mass of the coupling bar, i.e. by m_3 .

3.4 Experimental results

The obtained results in the previous sections have been derived under the assumption that the oscillators are *identical*. Obviously, in a real physical system, it is impossible to have two identical oscillators. A mathematical treatment, in which external perturbations (like noise) and unmodelled dynamics are taken into account, turns out to be complicated and the available mathematical tools are limited. Therefore, in this section, an experimental analysis is performed in order to get insight into the existence of synchronization in a real system where there are unavoidable small mismatches/disturbances in the oscillators. The analysis is conducted by using the experimental setup depicted in Figure 2.3. All parameter values and initial conditions are fixed and the only parameter that is modified from experiment to experiment is m_3 , the mass of the coupling bar, which influences the coupling strength $\mu = \frac{m}{m_3}$.

3.4.1 Hamiltonian escapement

In a first set of experiments, the inherent mechanical properties of the experimental setup of Figure 2.3 are adjusted such that its dynamic behaviour is described by the set of equations (3.11)-(3.12). This is achieved by defining the actuations U_i in (2.1) as follows

$$U_i = \omega_{is}^2(x_i - x_3) + 2\zeta_{is}\omega_{is}(\dot{x}_i - \dot{x}_3) - \omega^2(x_i - x_3) - \mu d\omega(\dot{x}_i - \dot{x}_3) - \mu\alpha\omega\left(\frac{a}{\omega^2}\dot{x}_i^2 + \kappa x_i^2 - \gamma\right)\dot{x}_i, \quad i = 1, 2, \quad (3.57)$$

$$U_3 = 0. \quad (3.58)$$

Clearly, the closed loop (2.1)-(3.57-3.58) coincides with the dynamics (3.11)-(3.12) expressed in terms of the original time t . Consequently, the mass-spring-damper oscillators in the experimental platform of Figure 2.3 have been converted into a pair of constrained nonlinear self-sustained oscillators driven by a Hamiltonian escapement.

The parameter values for the experiments are given in Table 2.1 and Table 3.1. The nonzero initial conditions are $x_1(0) = 4$ [mm], $x_2(0) = 3.5$ [mm]. Note that in the experiment the intention still is to make the oscillators identical but it should be noted that it will be practically impossible to realize this.

In a first experiment, no extra mass is added to the coupling bar, hence $m_3 = 4.1$ [kg] and, consequently, $\mu = 0.0512$ [-]. For the given parameter values, condition

Table 3.1 Parameter values for the experiments.

Oscillator 1		Oscillator 2		Coupling bar	
$m = 2.10 \times 10^{-1}$	[kg]	$m = 2.10 \times 10^{-1}$	[kg]	$m_3 \in \{4.1, 15.95\}$	[kg]
$\kappa = 3.7108 \times 10^1$	$[\frac{N}{m}]$	$\kappa = 3.7108 \times 10^1$	$[\frac{N}{m}]$	$\kappa_3 = 3.8871 \times 10^2$	$[\frac{N}{m}]$
$\beta = 5 \times 10^{-2}$	$[\frac{Ns}{m}]$	$\beta = 5 \times 10^{-2}$	$[\frac{Ns}{m}]$	$\beta_3 = 3.2656$	$[\frac{Ns}{m}]$
$d = \frac{1.791 \times 10^{-2}}{\mu}$	[-]	$d = \frac{1.791 \times 10^{-2}}{\mu}$	[-]	—	—
$\alpha = \frac{2.241 \times 10^1}{\mu}$	[-]	$\alpha = \frac{2.241 \times 10^1}{\mu}$	[-]	—	—
$a = 3.7108 \times 10^1$	[-]	$a = 3.7108 \times 10^1$	[-]	—	—
$\gamma = 1.567 \times 10^{-3}$	[-]	$\gamma = 1.567 \times 10^{-3}$	[-]	—	—

(3.33), see Theorem 3.2, is satisfied, whereas condition (3.29), see Theorem 3.1, is not fulfilled³. Hence, anti-phase synchronization is expected to occur in this experiment.

Figure 3.5 summarizes the main results. Although the oscillators are released close to in-phase, as depicted in Figure 3.5, after initial transient behaviour, the oscillators *practically* synchronize in anti-phase, as shown in Figures 3.5b) and 3.5d). Although initially the oscillations in the coupling bar are large due to the nearly in-phase startup, in the limit, when the oscillators practically synchronize in anti-phase, the amplitude of these oscillations becomes relatively small as depicted in Figure 3.5c). Ideally, for identical oscillators, the oscillations in the coupling bar should decay. However, in the experiment, the oscillators are not identical as can be seen from Figures 3.5b),d). Roughly speaking, the “pushing force” of one oscillator exerted to the coupling bar is larger than the “pulling force” exerted by the other oscillator and, consequently, the coupling bar does not come to a complete standstill.

In a second experiment, the mass of the coupling bar is increased by adding five steel plates with a mass of approximately 2.370 [kg] each. This yields $m_3 \approx 15.95$ [kg], i.e. $\mu = 0.0131$ [-]. The remaining parameter values and initial conditions are the same as used in the previous experiment. Note that in this case, condition (3.29) in Theorem 3.1 is satisfied. As a consequence of adding mass to the coupling bar, the oscillators now *practically* synchronize in-phase as depicted in Figure 3.6. The coupling bar converges to an oscillatory motion with fixed amplitude and frequency, as shown in Figure 3.6c). Moreover, the frequency of the in-phase synchronous solution is approximately the same as the frequency of the coupling bar. The amplitude of the vibrations in the coupling bar is of the same order in Figures 3.5 and 3.6. Note, however, that the mass of the coupling bar is about four times higher in Figure 3.6.

³For the given parameters, condition (3.29) is satisfied if $m_3 > 6.1267$ [kg].

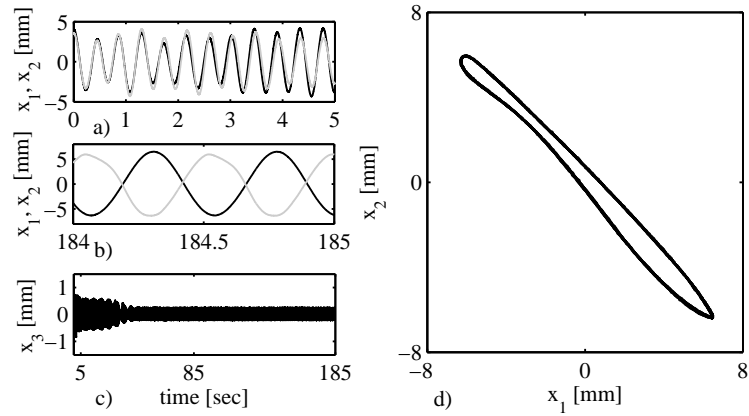


Figure 3.5 Experimental results. For relatively large coupling strength, the oscillators practically synchronize in anti-phase. In figures a) and b), black line: x_1 , grey line: x_2 . Figure d) does not contain transient behaviour.

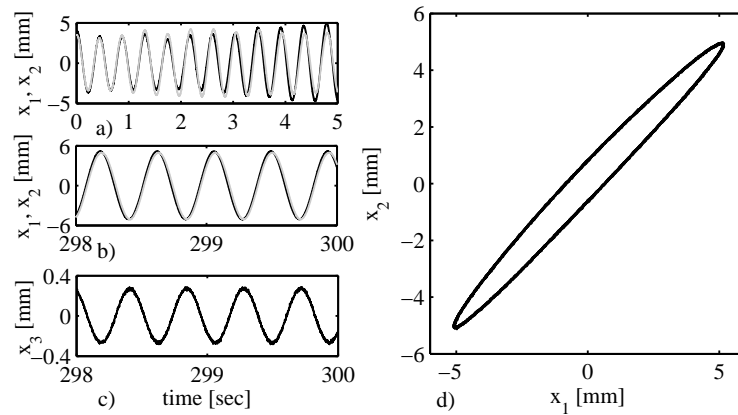


Figure 3.6 In this experiment, the mass of the coupling bar is increased to $m_3 = 15.95$ [kg] (coupling strength is decreased). As a consequence the oscillators practically synchronize in-phase. In figures a) and b), black line: x_1 , grey line: x_2 . Figure d) does not contain transient behaviour.

In both experiments, the amplitudes and frequencies of the synchronous solutions differ from the analytical values given by Theorems 3.1 and 3.2 respectively. For instance, in the case of the first experiment, the amplitude of the anti-phase synchronous solution is 6.47 [mm] for the first oscillator and 6.31 [mm] for the second one. If the parameter values used during the experiment are substituted in (3.42), then the expected amplitude is 4.551 [mm]. Regarding the frequency of the synchronous solution, the same experiment reveals that the oscillators synchronize in anti-phase with a frequency of 2.1155 Hz, i.e. $T = 0.4727$ [sec], whereas (3.43) in Theorem 3.2 yields $T = 0.4726$ [sec] (converting dimensionless time τ back to the real time t). For the second experiment, the amplitude of the oscillations in oscillator 1 is 5.166 [mm] and 4.939 [mm] for the second oscillator, whereas the predicted amplitude from Theorem 3.1 is 4.479 [mm]. The frequency of the in-phase synchronous solution in the experiment is $T = 0.4342$ [sec], whereas the predicted period from Theorem 3.1 is $T = 0.4654$ [sec]. These differences should not be surprising since, as has been mentioned before, the oscillators in the experimental setup are not identical and moreover the original dynamics are not cancelled perfectly.

Notwithstanding these quantitative rather than qualitative differences, the experiments confirm that the mass of the coupling bar, which determines the coupling strength μ , influences the type of limiting synchronous solutions in the system: increasing the mass of the coupling bar (decreasing the coupling strength) facilitates the onset of in-phase synchronization, whereas for a light coupling bar (increasing the coupling strength) anti-phase synchronization is the only expected stable synchronous mode.

3.4.2 van der Pol escapement

Similar experiments have been conducted for the case where the experimental setup is adjusted to mimic the dynamics (in terms of the time t) of the coupled system (3.46) analyzed in Section 3.3. In this case, the experimental setup is adjusted by defining the actuations U_i in (2.1) as follows

$$\begin{aligned} U_i &= \omega_{is}^2(x_i - x_3) + 2\zeta_{is}\omega_{is}(\dot{x}_i - \dot{x}_3) - \omega^2(x_i - x_3) - \mu d\omega(\dot{x}_i - \dot{x}_3) \\ &\quad - \mu\alpha\omega(ax_i^2 - 1)\dot{x}_i, \quad i = 1, 2. \end{aligned} \quad (3.59)$$

$$U_3 = 0. \quad (3.60)$$

The parameter values for ω_{is} and ζ_{is} are summarized in Table 2.1. Furthermore, $\omega = 13.29$ [rad/s], $\beta = 8 \times 10^{-3}$ [Ns/m], $d = \frac{2.865 \times 10^{-3}}{\mu}$ [-], $\alpha = \frac{7.522 \times 10^{-3}}{\mu}$ [-], and $a = 1 \times 10^5$ [1/m²]. The nonzero initial conditions are $x_1(0) = 3$ [mm] and $x_2(0) = 2.8$ [mm].

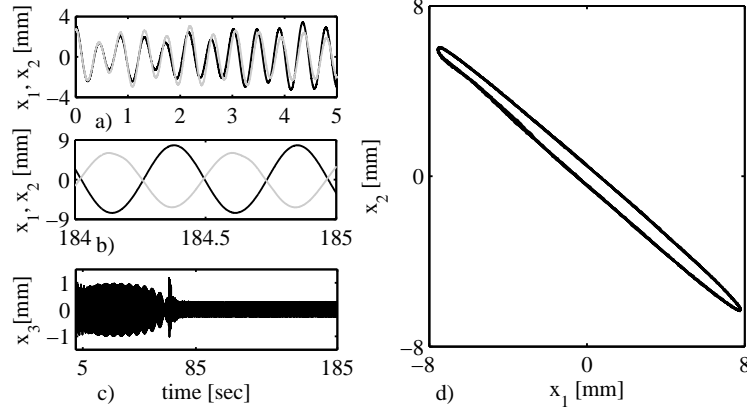


Figure 3.7 Experimental results. For a light coupling bar $m_3 = 4.1$ [kg] (relatively large coupling strength μ) practical anti-phase synchronization occurs. In figures a) and b), black line: x_1 , grey line: x_2 . In figure d), transient behaviour has been omitted.

Again, in the first experiment, a light coupling bar, i.e. $m_3 = 4.1$ [kg], i.e. $\mu = 0.0512$ [-], is used. For the given parameter values, condition (3.52) in Theorem 3.4 is satisfied, whereas condition (3.48) in Theorem 3.3 is not fulfilled⁴. Hence, for this experiment anti-phase synchronization is expected to occur.

As becomes clear from Figures 3.7b) and 3.7d), the oscillators practically synchronize in anti-phase, although they were released close to in-phase synchronization as depicted in Figure 3.7a). The behaviour of the coupling bar is depicted in Figure 3.7c). Initially, the transient part of the displacement of the bar is relatively large due to the nearly in-phase startup of the oscillators. Later, when the phase difference between the oscillators tends to π [rad], the amplitude of the oscillations in the bar reduces to a small value. In the experiment, the amplitude of the oscillations is 7.776 [mm] for the first oscillator and 6.09 [mm] for the second oscillator. Furthermore, the period of the synchronous solution is $T = 0.4729$ [sec]. The amplitude and period of the synchronous solution when computed by using (3.55) and (3.56) is 4.976 [mm] and 0.4726 [sec], respectively.

In a second experiment, the mass of the coupling bar is increased by adding ten steel plates of approximately 2.370 [kg] each one. This yields $m_3 \approx 27.8$ [kg], i.e. $\mu = 0.0075$ [-]. The remaining parameters and initial conditions are the same as used in the previous experiment. Note that in this case, condition (3.48)

⁴For the given parameters, condition (3.48) in Theorem 3.3 is satisfied if $m_3 > 8.8519$ [kg].

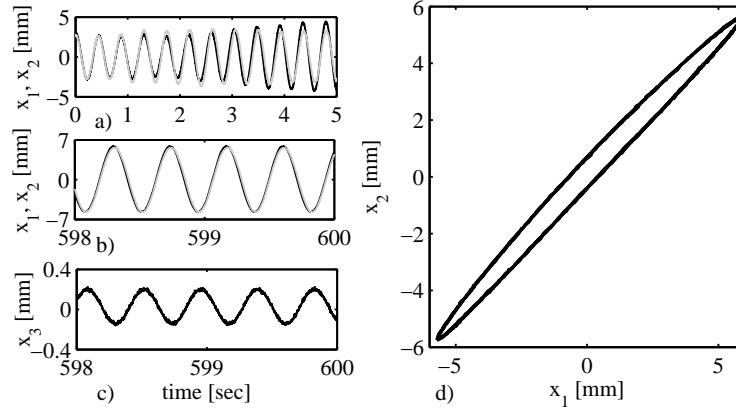


Figure 3.8 In this experiment, the oscillators practically synchronize in-phase. The oscillators have been released from initial conditions close to in-phase and the mass of the coupling bar has been increased to $m_3 = 27.8$ [kg]. In figures a) and b), black line: x_1 , grey line: x_2 . In figure d), transient behaviour has been omitted.

in Theorem 3.3 is satisfied. In fact, as a consequence of adding mass to the coupling bar, the oscillators practically synchronize in-phase as depicted in Figure 3.8. The coupling bar converges to an oscillatory motion with fixed amplitude and frequency, as shown in Figure 3.8c). Moreover, the frequency of the in-phase synchronous solution is approximately the same as the frequency of the coupling bar. The oscillations in the first oscillator have amplitude 5.871 [mm], whereas for the second oscillator the amplitude of the oscillations is 5.603 [mm]. The in-phase synchronous solution has period $T = 0.4340$ [sec]. For the given parameter values, Theorem 3.3 predicts a synchronous solution with amplitude equal to 4.891 [mm] and period $T = 0.4687$ [sec].

Finally, in order to illustrate the influence of the initial conditions in the limit synchronizing behaviour of the system, experiment 2 is repeated by only changing the initial condition of oscillator 2, which now is $x_2(0) = 0$ [rad]. As can be seen in Figure 3.9, the oscillators now synchronize in anti-phase.

Summarizing, the analytical results obtained in Section 3.2 and Section 3.3 are qualitatively in large agreement with the experimental analysis conducted in this section. Quantitative differences, as explained before, originate from the fact that in the real physical system the oscillators are not identical and original dynamics cannot be completely cancelled. However, analytical results and experimental

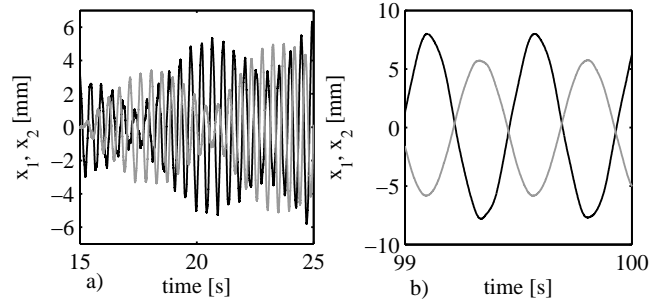


Figure 3.9 For initial conditions far from in-phase the oscillators synchronize in anti-phase.

results convey the same message: the mass of the coupling bar m_3 (or rather the coupling strength μ) influences the limit synchronizing behaviour in the oscillators.

3.5 Discussion

In this chapter, the occurrence of synchronized motion in pairs of constrained nonlinear oscillators interacting via Huygens' coupling has been investigated. Sufficient conditions for the existence and stability of synchronous solutions have been derived using the Poincaré method based on a small parameter. For the present case, this small parameter appears naturally in the system and corresponds to the coupling strength μ , i.e. the ratio between the oscillators' mass m and the mass of the coupling bar m_3 ⁵.

The analysis has revealed that the coupling strength influences the limit synchronized behaviour in the system, namely anti-phase or in-phase synchronization. Decreasing the coupling strength, i.e. increasing the mass of the coupling bar, facilitates the onset of in-phase synchronization. On the other hand, when the coupling strength is increased, i.e. by decreasing the mass of the coupling bar, anti-phase synchronization is the only expected stable synchronous mode.

Moreover, Corollary 3.1 establishes that by decreasing the coupling strength μ , it is possible to have two coexisting types of *stable* synchronous motion: in-phase and anti-phase. Consequently, the limit behaviour in this case is determined by

⁵Clearly, the coupling strength may be affected by modifying m and/or m_3 . However, modifying m requires to modify the dynamics of the uncoupled oscillators, which is not intended in the present study. Hence, in the analysis presented in this chapter, the coupling strength has been modified by means of the mass of the coupling bar m_3

the *initial conditions*. Computer simulations have revealed that when the oscillators are released *close* to in-phase then the limit behaviour of the system will be in-phase synchronization, whereas for the remaining initial conditions the limit behaviour is anti-phase synchronization, i.e. the region of attraction for anti-phase is larger than the attraction region for in-phase.

Additionally, the onset of synchronization in the coupled oscillators has been investigated in a real system, i.e. by means of experiments. These experiments are in large agreement with the theoretical investigations presented in Section 3.2 and Section 3.3. In fact, the experiments have confirmed that a light coupling bar yields to anti-phase synchronous motion in the oscillators, whereas with a heavier coupling bar in-phase synchronization can be observed.

Note that the results obtained here are largely in agreement with other (experimental) results available in the literature. Consider for example the system described in [54]. It consists of two metronomes attached to a bar that can move horizontally, see Figure 2.2(c). The authors observed that anti-phase synchronization was the ‘dominant’ synchronous solution. Moreover, the authors mention that in-phase synchronization was observed only when the mass of the bar was increased. Likewise, in [55], where the setup consists of a pair of metronomes placed on a freely moving rigid bar, which rests on top of two soda cans, see Figure 2.2(b), the author explains that anti-phase synchronization was observed only when the coupling strength was increased.

The results presented in this chapter suggest that the occurrence of synchronization is not influenced by the type of ‘escapement’ used to compensate the energy loss in the oscillators. The escapement mechanism only guarantees self-sustained oscillations but it does not determine how the oscillators synchronize. The mass of the coupling bar, to which the oscillators are attached, is one of the possible key parameters determining the limit behaviour.

Chapter 4

Synchronization of nonlinear oscillators

... great difficulties are felt at first and these cannot be overcome except by starting from experiments ... and then by conceiving certain hypotheses ... But even so, very much hard work remains to be done and one needs not only great perspicacity but often a degree of good fortune...

Christiaan Huygens (1629–1695)

Abstract This chapter focuses on getting insight into the synchronized motion of a pair of strongly nonlinear oscillators with Huygens' coupling, mainly by means of experiments. Some analytic conditions for the stability of the anti-phase synchronized motion are also derived under the assumption of small oscillations in the system. Additionally, a brief comparison between the obtained results and the results derived in the previous chapter, is presented. The results confirm that also in the strongly nonlinear case, the synchronization observed by Huygens in his clocks is still observed even if the clocks are replaced by different oscillators.

4.1 Introduction

In the previous chapter, it has been shown that a pair of limited nonlinear oscillators with Huygens' coupling may synchronize. Analytic conditions have been derived for the occurrence of in-phase and anti-phase synchronization and experimental analyses have been conducted. Moreover, it has been shown that the

analytic results are in good agreement with the experimental results. The analytic conditions have been derived by means of the Poincaré method. However, this analytic method, and in general any perturbation method, is only valid for the case that the nonlinearities in the system are “small” in some sense.

The problem addressed in this chapter is to determine, under which conditions a pair of arbitrarily chosen nonlinear oscillators with Huygens’ coupling shows synchronized behaviour. The limitations on the oscillators regarding small damping and weak nonlinearities/excitation forces, considered in previous chapter, are disregarded. In order to get a complete answer, one can distinguish two approaches. The first approach consists of determining the existence of synchronous solutions and their stability via a rigorous mathematical analysis, i.e. via a theoretical approach. In the second approach, more insight in the synchronous motion of the oscillators is obtained by means of experiments. This is in line with current works about the study of Huygens’ synchronization occurring in *metronomes*. For results regarding the theoretical approach, the reader may consider to study [16, 17, 29, 31, 33, 52, 66, 75]. With respect to the second approach, several experimental setups have been created by researchers in order to reproduce the observations made by Huygens and find mathematical arguments for the synchronized motion of the clocks. Some of these experimental setups are presented in [5, 54, 55] and depicted in Figure 2.2.

For the present case (high damping and strong nonlinearities), if one attempts to perform a theoretical analysis in order to derive conditions for the existence and stability of synchronous solutions in the coupled system, then a mathematical apparatus, or an ad hoc theoretical framework does not exist, as far as the author knows. A Lyapunov-based analysis is not useful in most of the cases because the system (in this case the synchronization error dynamics) cannot be written in a suitable form. Then, in order to obtain analytic results, it is unavoidable to make some simplifications and assumptions in the system under consideration. Obviously, the obtained results may be conservative or only valid under some idealized conditions.

This chapter focuses in getting insight into the synchronized motion of oscillators, mainly by means of experiments. However, some analytic results (by using linearization) are also given and it is shown that the obtained analytic results are in agreement, to a large extent, with the experimental results. In fact, it is the belief of the author that the experimental analysis presented here, provides important and illuminating insight in the old and intriguing synchronization problem considered by Huygens. Moreover, these results may motivate the future derivation of a suitable mathematical machinery in order to obtain a rigorous stability analysis of the synchronous motion occurring in the oscillators.

In the analysis, the generalized Huygens system depicted in Figure 2.4 is considered and by means of three particular examples, it is demonstrated that two self-driven oscillators with Huygens' coupling may exhibit in-phase and anti-phase synchronization. The first two examples are presented in Sections 4.2 and 4.3. These examples correspond to the cases where the energy loss in the oscillators is compensated by respectively the *Hamiltonian escapement* (3.4) and by the *van der Pol escapement* (3.5). Then, in Section 4.4, a pair of nonlinear oscillators self-driven by a *discontinuous escapement* is considered. It is shown that the synchronized motion in the oscillators seems to be independent of the kind of escapement used to maintain the oscillations. The mass of the coupling bar, however, appears to be an important parameter, which determines the eventual synchronized behaviour in the oscillators, namely in-phase or antiphase synchronization.

The chapter is concluded by a discussion about the influence of the coupling strength in the onset of synchronization. In particular, the results obtained for nonlinear oscillators with limitations, see Chapter 3, are compared against the results for the case of nonlinear oscillators presented in this chapter.

4.2 Oscillators self-driven by a Hamiltonian escapement: revisited

Consider the system depicted in Figure 2.4 consisting of two mass-spring-damper oscillators linked via a one dof suspended rigid bar. As discussed in Chapter 2, the equations of motion of the (idealized) system are given by

$$\begin{aligned}\ddot{x}_1 &= -\omega^2(x_1 - x_3) - 2\zeta\omega(\dot{x}_1 - \dot{x}_3) + U_1 \\ \ddot{x}_2 &= -\omega^2(x_2 - x_3) - 2\zeta\omega(\dot{x}_2 - \dot{x}_3) + U_2 \\ \ddot{x}_3 &= \mu \sum_{i=1}^2 [\omega^2(x_i - x_3) + 2\zeta\omega(\dot{x}_i - \dot{x}_3) - U_i] \\ &\quad - \omega_3^2 x_3 - 2\zeta_3 \omega_3 \dot{x}_3 + U_3.\end{aligned}\tag{4.1}$$

Due to the damping present in the system, a control signal should be designed such that the oscillations do not damp out. This requirement of having a control input to sustain the oscillations can be linked either to Huygens' pendulum clocks, where each pendulum is equipped with an escapement mechanism, which provides an impulsive force to the pendulum in order to keep the clocks running, or to the case of a metronome, where the energy loss due to friction is compensated by an escapement consisting of a spring, which loads a toothed wheel.

In this section, the control input U_i , $i = 1, 2$, to the oscillators is assumed to be

given by the Hamiltonian escapement (3.4) and $U_3 = 0$. Consequently, the system under consideration is given by

$$\ddot{x}_i = -\omega^2(x_i - x_3) - 2\zeta\omega(\dot{x}_i - \dot{x}_3) - \lambda(H_i - H^*)\dot{x}_i, \quad i = 1, 2, \quad (4.2)$$

$$\ddot{x}_3 = -\mu \sum_{i=1}^2 \ddot{x}_i - \omega_3^2 x_3 - 2\zeta_3 \omega_3 \dot{x}_3. \quad (4.3)$$

Note that this system coincides with (3.6)-(3.7). However, the limitations on the oscillators regarding small damping and weak nonlinearities/excitation forces, mentioned in the introduction of Chapter 3, are discarded.

4.2.1 Analysis of the anti-phase synchronization

The analysis is conducted under the assumption of small oscillations, i.e. by linearizing system (4.2)-(4.3). This yields

$$\begin{aligned} \ddot{x}_1 &= -\omega^2(x_1 - x_3) - 2\zeta\omega(\dot{x}_1 - \dot{x}_3) + \lambda H^* \dot{x}_1 \\ \ddot{x}_2 &= -\omega^2(x_2 - x_3) - 2\zeta\omega(\dot{x}_2 - \dot{x}_3) + \lambda H^* \dot{x}_2 \\ \ddot{x}_3 &= \mu \sum_{i=1}^2 [\omega^2(x_i - x_3) + 2\zeta\omega(\dot{x}_i - \dot{x}_3) - \lambda H^* \dot{x}_i] - \omega_3^2 x_3 - 2\zeta_3 \omega_3 \dot{x}_3. \end{aligned} \quad (4.4)$$

Furthermore, it will be assumed that $\lambda H^* > 2\zeta\omega$. If system (4.2)-(4.3) synchronizes in anti-phase, then all trajectories converge to the anti-phase manifold $M_{anti} := \{(x_1, \dot{x}_1) = (-x_2, -\dot{x}_2), x_3 = \dot{x}_3 = 0\}$. Therefore, it is quite natural to define anti-phase synchronization errors and their time derivatives as

$$\begin{aligned} e_1 &= x_1 + x_2, & \dot{e}_1 &= \dot{x}_1 + \dot{x}_2, \\ e_2 &= x_3, & \dot{e}_2 &= \dot{x}_3. \end{aligned} \quad (4.5)$$

Writing the error dynamics as a set of first order differential equations yields

$$\frac{d}{dt} \begin{bmatrix} e_1 \\ \dot{e}_1 \\ e_2 \\ \dot{e}_2 \end{bmatrix} = \underbrace{\begin{bmatrix} 0 & 1 & 0 & 0 \\ -\omega^2 & -(2\zeta\omega - \lambda H^*) & 2\omega^2 & 4\zeta\omega \\ 0 & 0 & 0 & 1 \\ \frac{m\omega^2}{m_3} & \left(\frac{2\zeta\omega m}{m_3} - \frac{\lambda H^* m}{m_3} \right) & a & b \end{bmatrix}}_A \begin{bmatrix} e_1 \\ \dot{e}_1 \\ e_2 \\ \dot{e}_2 \end{bmatrix}. \quad (4.6)$$

where $a = -\left(\frac{2\omega^2 m}{m_3} + \omega_3^2\right)$ and $b = -\left(\frac{4\zeta\omega m}{m_3} + 2\zeta_3 \omega_3\right)$. It is well-known from stability theory for linear systems that (4.6) is asymptotically stable, if and only if the real parts of the eigenvalues of matrix A are negative. Then, the following proposition holds.

Proposition 4.1. *System (4.4) will converge to the set where $x_1(t) = -x_2(t)$, $\dot{x}_1(t) = -\dot{x}_2(t)$, $x_3(t) = 0$, $\dot{x}_3(t) = 0$ provided that the roots of the characteristic polynomial:*

$$\begin{aligned} p(\chi) = & \chi^4 + (2\zeta\omega - \lambda H^* + 2\zeta_3\omega_3 + 4\zeta\omega \frac{m}{m_3})\chi^3 \\ & + (4\zeta\omega\zeta_3\omega_3 - 2\lambda H^*\zeta_3\omega_3 + \omega_3^2 + \omega^2 + 2\frac{m}{m_3}\omega^2)\chi^2 \\ & + (2\zeta\omega\omega_3^2 - \lambda H^*\omega_3^2 + 2\omega^2\zeta_3\omega_3)\chi + \omega^2\omega_3^2 \end{aligned} \quad (4.7)$$

all have negative real parts.

For a given set of fixed parameters $m, \omega, \omega_3, \lambda, H^*, \zeta$, and ζ_3 , the only way to modify the roots of the characteristic polynomial (4.7) is by varying m_3 . Actually, this is the situation in the experimental setup of Figure 2.4, where the masses of the oscillators, denoted by m , are fixed but the mass of the supporting bar, denoted by m_3 may be varied by a factor 10, see Chapter 2.

Using computer simulations, Figure 4.1 is made in order to illustrate Proposition 4.1 using m_3 as a design parameter. Consider the characteristic polynomial (4.7) with parameter values given in Table 4.1. Furthermore, assume $\lambda = 13.0268 \times 10^3$ [s/kgm²] and $H^* = 7.8390 \times 10^{-4}$ [Nm]. Note that for the given values, it holds that $\lambda H^* > 2\zeta\omega$.

Table 4.1 Parameter values for system (4.1).

Oscillators	Coupling bar
$\omega = 13.2930$ [rad/s]	$\omega_3 = \sqrt{\frac{388.71}{m_3}}$ [rad/s]
$\zeta = 0.3829$ [-]	$\zeta_3 = \frac{0.0828}{\sqrt{m_3}}$ [-]
$m = 0.210$ [kg]	$m_3 \in [0.1, 230]$ [kg]

Next, define the parameter $\rho := \max \{\text{Re} \{\chi_1\}, \text{Re} \{\chi_2\}, \text{Re} \{\chi_3\}, \text{Re} \{\chi_4\}\}$, which corresponds to the largest real part of the roots of (4.7). From Figure 4.1, it is clear that ρ is negative for $4.36 \leq m_3 \leq 216.29$ [kg]. Therefore, in this interval for m_3 , Proposition 4.1 is applicable and the oscillators are expected to synchronize in anti-phase. For small values of m_3 , i.e. $0 < m_3 < 4.36$ [kg], the polynomial (4.7) has at least one root with positive real part, as can be seen again in Figure 4.1. In this interval, computer simulations have revealed that the oscillators may synchronize in-phase. Also, for $m_3 > 216.29$ [kg], it holds that $\rho > 0$ as can be seen in Figure 4.1. It has been found, again by computer simulations, that in this case the oscillators can show uncoupled behaviour, which is expected, since for such large values of m_3 it is as if the bar is fixed and the oscillators run uncoupled.

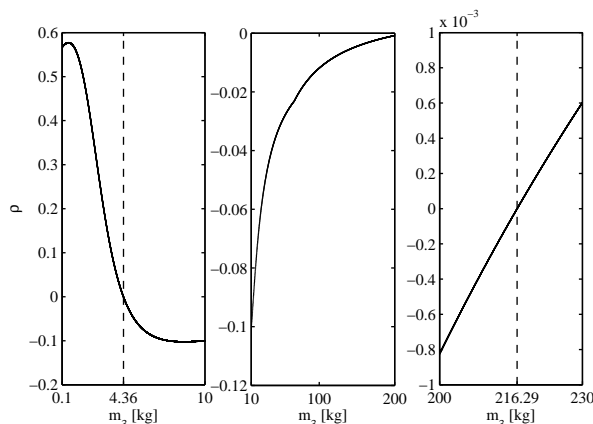


Figure 4.1 Influence of m_3 on the roots of (4.7).

Remark 4.1. When the oscillators reach anti-phase synchronization - i.e. $x_1 = -x_2$, and $\dot{x}_1 = -\dot{x}_2$ - the displacement of the bar converges to zero, while for the in-phase motion, where $x_1 = x_2$, and $\dot{x}_1 = \dot{x}_2$, the displacement of the bar converges to a small periodic motion. Therefore, it is quite plausible that a relatively light bar will facilitate the in-phase synchronization and for a relatively heavy bar the anti-phase synchronization seems more feasible. Consequently, for relatively small values of the mass m_3 , in comparison with the mass of the oscillators, (large μ) in-phase synchronization is expected. For larger values of the mass m_3 , in comparison with the masses of the oscillators, (small μ) anti-phase synchronization is expected, and for a really heavy bar ($\mu \rightarrow 0$) no coupling behaviour is expected. This reasoning can be linked to the Huygens situation, where the coupling strength μ (the ratio of the mass of the two clocks to the wooden bar mass) was small due to the fact that Huygens had placed some extra mass (around 45 kg) in the cases of the clocks (so this mass adds to the coupling bar mass and not to the pendula mass) in order to keep them upright in stormy seas. In such situations (small μ), Huygens always observed anti-phase synchronization [5]). Furthermore, the case of a (very) heavy bar ($\mu \rightarrow 0$) can also be linked to the Huygens experiment. Based on his observations of two pendulum clocks, Huygens drew the conclusion that the reason behind the sympathy of the pendulum clocks was the imperceptible movements of the wooden beam, to which the pendula were connected. These imperceptible movements are rather negligible if the mass of the coupling bar is much larger than the mass of the oscillators, i.e. $\mu \rightarrow 0$, and as a consequence the pendula cannot “communicate” with each other and synchronization is not possible. This is also clear from (4.3), because if $\mu \rightarrow 0$, then the oscillators, described by (4.2) run uncoupled.

Finally, it should be noticed that the approach used for analyzing the anti-phase motion does not lead to insight in the stability of the in-phase synchronized behaviour because the corresponding (linearized) error system is independent of m_3 .

4.2.2 Experimental analysis

In this Subsection, experimental results are presented in order to show different synchronizing limit behaviours in the system described by equations (4.2-4.3). For the experiments, the experimental setup of Figure 2.3 is used and its dynamic behaviour is modified such that in closed-loop the setup mimics the dynamics of system (4.2)-(4.3). The parameter values are assumed to be as given in Table 4.1 and the inputs of the setup, see (2.1), are defined as follows

$$U_i = -\lambda(H_i - H^*)\dot{x}_i = -\lambda\left(\frac{1}{2}m\dot{x}_i^2 + \frac{1}{2}\kappa x_i^2 - \frac{1}{2}\kappa x_{ref}^2\right), \quad i = 1, 2, \quad (4.8)$$

with $\lambda = 13.244 \cdot 10^3$ [s/kgm²], $m = 0.210$ [kg], $\kappa = 37.108$ [N/m], and $x_{ref} = 6.5$ [mm].

In the experiments, only m_3 , the mass of the coupling bar, is varied. Two experiments are presented: one corresponding to a *light* coupling bar, where in-phase sync is observed, and a second experiment corresponding to a *heavier* bar, where anti-phase synchronization occurs.

In the first experiment, no extra mass is added to the coupling bar, hence $m_3 = 4.1$ [kg]. The oscillators are released from the initial conditions $x_1(0) = 2.7$ [mm], $x_2(0) = -2.9$ [mm], $\dot{x}_1(0) = \dot{x}_2(0) = x_3(0) = \dot{x}_3(0) = 0$. Although the oscillators are released close to anti-phase synchronization, as shown in Figure 4.2a) after a transient behaviour the system practically synchronizes in-phase, as depicted in Figures 4.2b) and 4.2d).

Initially, the displacement of the bar, i.e. x_3 , is very small due to the anti-phase start-up. However, when the oscillators tends to the in-phase synchronized motion, the oscillations in the coupling bar increase and once the oscillators are synchronized in-phase, the bar keeps oscillating with a fixed frequency as depicted in Figure 4.2c).

In a second experiment, the mass of the coupling bar is increased by adding two steel plates of 2.359 [kg] each. This yields $m_3 = 8.818$ [kg]. The oscillators are released from initial conditions close to in-phase, $x_1(0) = 2.7$ [mm], $\dot{x}_1(0) = 0$, $x_2(0) = 2.9$ [mm], $\dot{x}_2(0) = 0$, and $x_3(0) = \dot{x}_3(0) = 0$. In this case, the system practically synchronizes in anti-phase as can be seen in Figures 4.3b) and

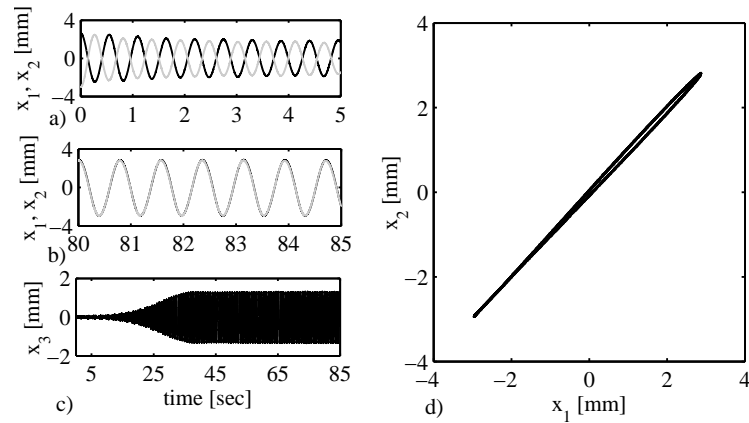


Figure 4.2 Experimental results. Practical in-phase synchronization occurs for a light coupling bar ($m_3 = 4.1$ [kg]), i.e. for a relatively large coupling strength μ . In figures a) and b) black line: x_1 , grey line: x_2 . Figure d) does not contain transient behaviour.

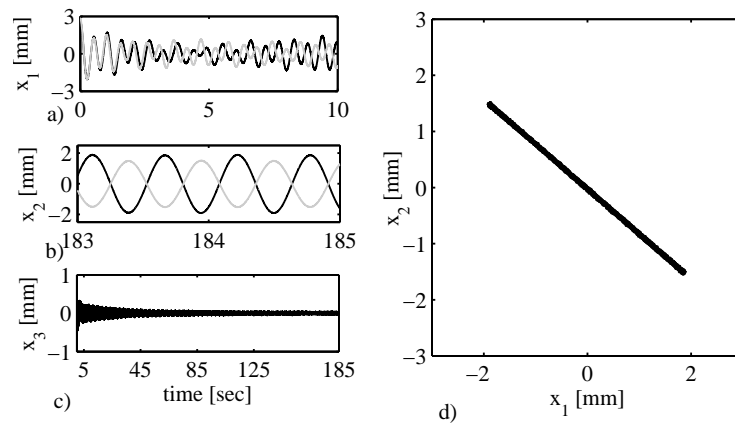


Figure 4.3 The mass of the coupling bar is increased ($m_3 = 8.818$ [kg]). As a consequence, the oscillators practically synchronize in anti-phase (in figures a) and b) black line: x_1 , grey line: x_2). Figure d) does not contain transient behaviour.

4.3d). Ideally, the displacement of the coupling bar denoted as x_3 should go to zero. However, due to the fact that the amplitudes of the oscillators differ by a factor approximately equal to 1.2, the coupling bar does not come to a complete standstill as depicted in Figure 4.3c). Nevertheless, the phase difference between the oscillators is approximately π [rad].

Note that for the parameter values considered in experiment one, the eigenvalues of matrix A in (4.6) have positive real parts, whereas for the parameter values used in experiment two, all eigenvalues of A have negative real parts, i.e. the anti-phase error system (4.6) is asymptotically stable.

4.3 Oscillators self-driven by a van der Pol term: revisited

Consider again the coupled system (3.44)-(3.45) given in Section 3.2

$$\ddot{x}_i = -\omega^2(x_i - x_3) - 2\zeta\omega(\dot{x}_i - \dot{x}_3) - \nu(ax_i^2 - 1)\dot{x}_i \quad i = 1, 2, \quad (4.9)$$

$$\ddot{x}_3 = -\mu \sum_{i=1}^2 \ddot{x}_i - \omega_3^2 x_3 - 2\zeta_3 \omega_3 \dot{x}_3. \quad (4.10)$$

The small parameter limitations regarding damping and nonlinearities, considered in Chapter 3, are again discarded.

By again assuming small oscillations, it is possible to analytically analyze the (local) stability of the anti-phase synchronized motion by writing the anti-phase error dynamics similar to (4.6) where λH^* should be replaced by ν . Consequently, Proposition 4.1 applies to the linearized system associated to (4.9)-(4.10) with (4.7) replaced by

$$\begin{aligned} p(\chi) = & \chi^4 + (2\zeta\omega - \nu + 2\zeta_3\omega_3 + 4\zeta\omega\frac{m}{m_3})\chi^3 \\ & + (4\zeta\omega\zeta_3\omega_3 - 2\nu\zeta_3\omega_3 + \omega_3^2 + \omega^2 + 2\frac{m}{m_3}\omega^2)\chi^2 \\ & + (2\zeta\omega\omega_3^2 - \nu\omega_3^2 + 2\omega^2\zeta_3\omega_3)\chi + \omega^2\omega_3^2. \end{aligned} \quad (4.11)$$

At this point, it is also worth mentioning that for certain set of parameters and moderate coupling strength, the limit synchronizing behaviour is also influenced by the initial conditions as depicted in Figure 4.4, which has been obtained by numerical integration of (4.9)-(4.10) with parameter values: $\omega = 11.1217$ [rad/s], $\omega_3 = 9.7369$ [rad/s], $\zeta = 0.3203$ [-], $\zeta_3 = 0.0409$ [-], $\nu = 20$ [1/s], $a = 1 \times 10^5$ [1/m²],

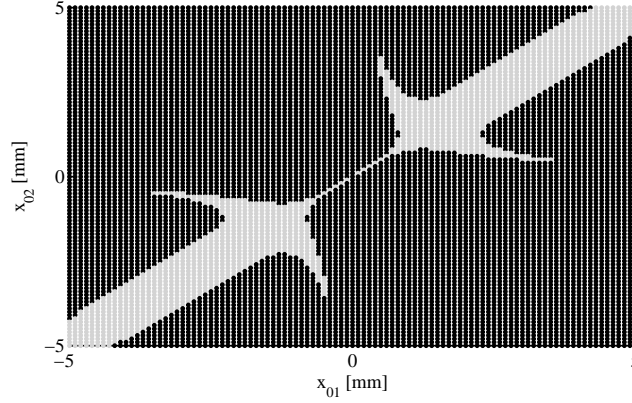


Figure 4.4 Projection of the limit behaviour onto the plane with initial conditions (x_{01}, x_{02}) for a set of fixed parameters. Black points represent initial conditions converging to anti-phase motion, while grey points represent initial conditions converging to in-phase motion.

and $\mu = 0.0731$ [-]. Only a subset of the possible initial conditions has been varied, namely the ones corresponding to the initial positions of the oscillators. All other initial conditions are zero. In Figure 4.4, black points represent initial conditions that converge to anti-phase motion, i.e. $e = x_1 + x_2 \rightarrow 0$, whereas grey points represent initial conditions that converge to in-phase motion, i.e. $e = x_1 - x_2 \rightarrow 0$. In other words, there exist values of the coupling strength, for which both in-phase and anti-phase synchronization exist (see Corollary 3.1). In [26], a similar ‘arrow’ pattern as shown in Figure 4.4 has been observed for a system consisting of two pendula.

4.3.1 Experimental results

The experimental setup depicted in Figure 2.3 is adjusted to mimic system (4.9)-(4.10) by defining the actuator forces of system (2.1) as follows

$$U_i = -\nu(ax_i^2 - 1)\dot{x}_i \quad i = 1, 2. \quad U_3 = 0. \quad (4.12)$$

The parameter values for the oscillators (4.9) are $\omega = 16.57$ [rad/s] and $\zeta = 0.4775$ [-], and the parameter values for the coupling bar (4.10) are given in Table 1 for $m_3 = 4.1$ [kg]. The parameter values of the input (4.12) are $\nu = 25$ [1/s], $a = 1 \times 10^5$ [1/m²].

In a first experiment, the oscillators are released from the initial conditions $x_1(0) =$

3 [mm], $x_2(0) = 1$ [mm]. The remaining initial conditions are zero. The coupling strength is $\mu=0.0329$. After initial transient behaviour the system converges

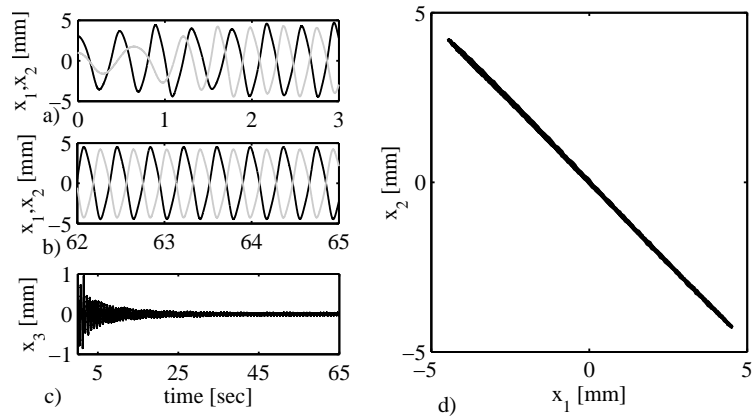


Figure 4.5 Experimental results: For a small coupling strength ($\mu = 0.0329$), the van der Pol oscillators practically synchronize in anti-phase. In figures a) and b), black line: x_1 , grey line: x_2 . In Figure d) the transient behaviour has been omitted.

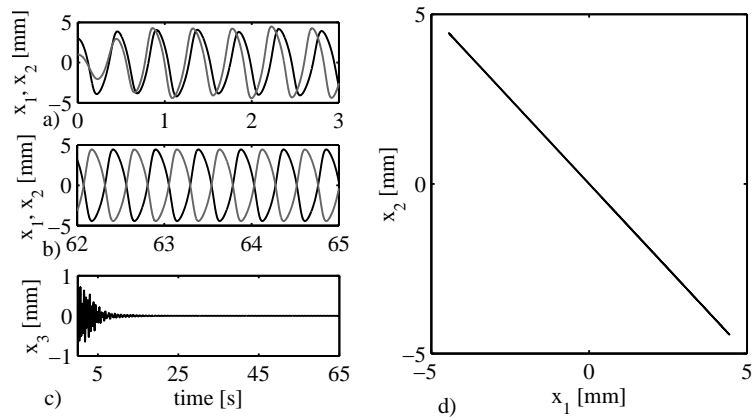


Figure 4.6 Numerical results for system (4.9)-(4.10) with parameter values as used in experiment one. Compare this figure with Figure 4.5.

to anti-phase motion as becomes clear from Figure 4.5b) and as a consequence

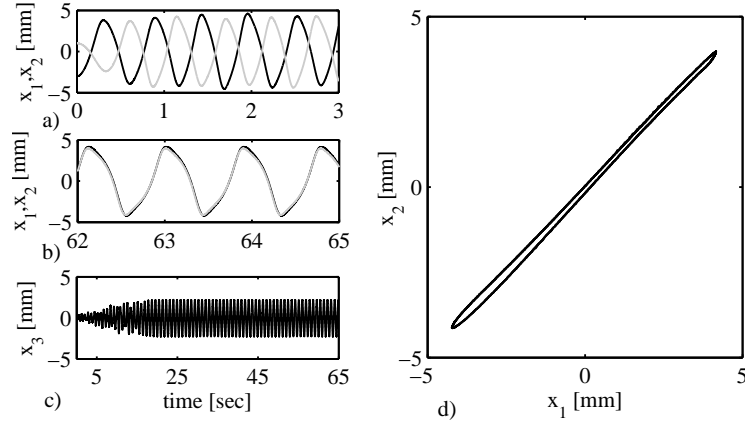


Figure 4.7 When the coupling strength is increased, the van der Pol oscillators practically synchronize in-phase. In figures a) and b), black line: x_1 , grey line: x_2 . Figure d) does not contain transient behaviour.

the oscillations in the coupling bar decay as shown in Figure 4.5c). The anti-phase synchronization of the coupled van der Pol oscillators is illustrated further by projecting the synchronized displacements corresponding to the oscillators in the plane (x_1, x_2) as depicted in Figure 4.5d). Furthermore, these results are in good agreement with the numerical results depicted in Figure 4.6, which has been obtained by numerical integration of (4.9)-(4.10) with parameter values as used in the experiment above discussed. In the experiment the oscillators are practically synchronized in anti-phase with oscillation frequency $f = 2.6226$ [Hz], whereas the result obtained by computer simulations is $f = 2.5986$ [Hz]. Obviously, there are (unavoidable) quantitative differences between the experimental results and the numerical results. However, qualitatively, both results are comparable.

In a second experiment, the oscillators are released from initial conditions close to anti-phase motion, i.e. $x_1(0) = -3$ [mm] and $x_2(0) = 1$ [mm], as depicted in Figure 4.7a). The remaining initial conditions are again zero. The coupling strength is increased to $\mu = 0.1176$ by increasing m to 0.4821 [kg]¹, and $\nu = 20$ [1/s]. As a result, the van der Pol oscillators converge to in-phase motion, as depicted in Figures 4.7b) and 4.7d). The coupling bar, which is initially at rest, starts moving until it reaches an oscillation with constant amplitude and frequency as depicted in Figure 4.7c). Again, these experimental results are in good agreement with numerical results, which are depicted in Figure 4.8. In the experiments, the

¹Note that for the given value of m the eigenfrequency in the oscillators becomes $\omega = 8.77$ [rad/s] and the dimensionless damping coefficient is $\zeta = 0.2527$ [-].

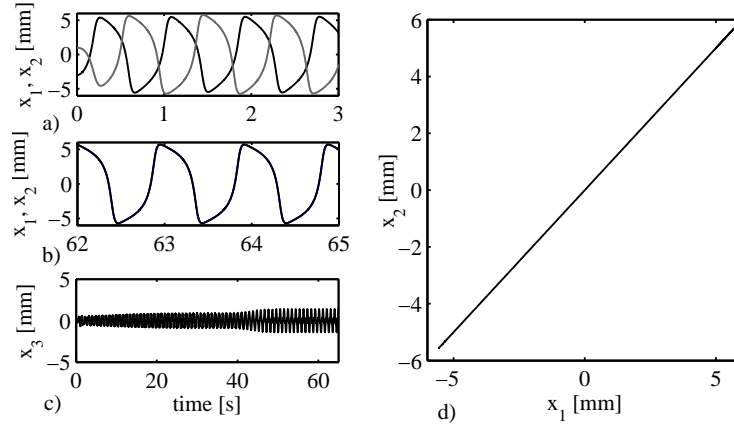


Figure 4.8 Numerical results for system (4.9)-(4.10) with parameter values as used in experiment two. Compare this figure with Figure 4.7.

oscillators synchronize in-phase with frequency $f = 1.12$ [Hz] which is very close to the frequency observed in the numerical analysis, which is $f = 1.037$ [Hz].

4.4 Oscillators self-driven by a discontinuous force

In this section, the following state dependent discontinuous control inputs for the coupled oscillators (4.1) are considered

$$U_i = -\alpha \dot{x}_i \text{sign}(|x_i| - x_{ref}), \quad i = 1, 2, \quad (4.13)$$

$$U_3 = 0, \quad (4.14)$$

where $\alpha \in \mathbb{R}^+$ influences the amplitude of the force U_i , $i = 1, 2$, the constant $x_{ref} \in \mathbb{R}^+$ represents a threshold displacement value, and

$$\text{sign}(x) = \begin{cases} 1 & x > 0, \\ 0 & x = 0, \\ -1 & x < 0. \end{cases} \quad (4.15)$$

The input U_3 is taken to be zero because it is desired that the bar oscillates freely. The controllers (4.13)-(4.14) convert system (4.1) into a self-driven discontinuous piecewise-linear system.

Obviously, in this case a linearization approach cannot be used due to the discontinuous function (4.13). In order to derive an analytic result, a hybrid approach seems in order. For the present case, only experimental results are provided.

4.4.1 Experimental results

In this subsection, experimental results are presented in order to show different synchronizing limit behaviours in the system described by equations (4.1),(4.13),(4.14). This requires to adjust the dynamics (2.1) of the experimental setup in order to mimic the dynamics (4.1),(4.13),(4.14). All experiments are performed by using the parameter values given in Table 4.1 and $\alpha = 10.187$ [1/s]. Only m_3 , the mass of the coupling bar, is varied. Three experiments are presented: one corresponding to a light coupling bar ($m_3 = 4.1$ [kg]), where in-phase synchronization is observed, a second one corresponding to a heavier bar ($m_3 = 8.8$ [kg]) where anti-phase synchronization does occur, and a third experiment where a transition from in-phase to anti-phase (due to a sudden change in the mass of the coupling bar from 4.1 [kg] to 8.8 [kg]) is observed.

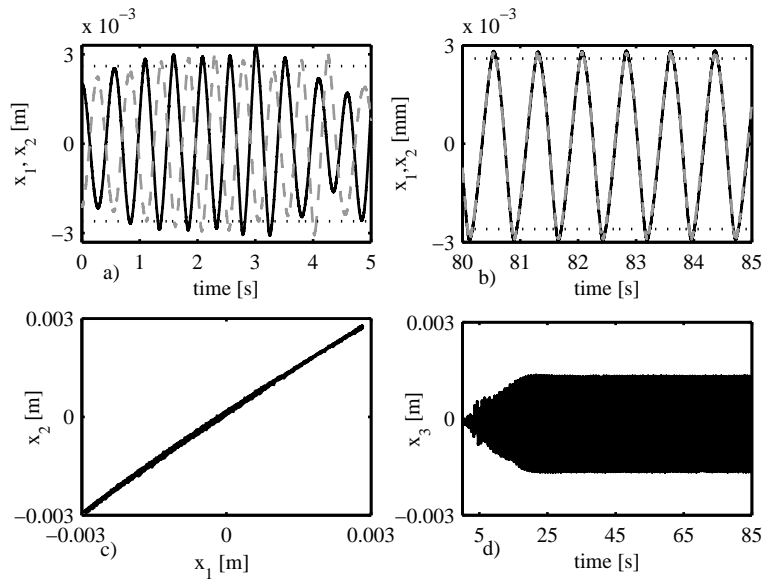


Figure 4.9 Experimental results: the oscillators synchronize in-phase. Solid line: x_1 , dashed line: x_2 .

In the first experiment, no extra mass is added to the coupling bar, hence $m_3 = 4.1$

[kg]. The oscillators are released from the initial conditions $x_1(0) = 1.97$ [mm], $\dot{x}_1(0) = 0$, $x_2(0) = -2.13$ [mm], $\dot{x}_2(0) = 0$, and $x_3(0) = \dot{x}_3(0) = 0$, and the threshold displacement value of the control input (4.13) is taken to be $x_{ref} = 2.65$ [mm]. In Figures 4.9a) and 4.9b), this value and its negative counterpart are indicated by two horizontal black dotted lines.

Although the oscillators are released close to anti-phase synchronization, see Figure 4.9a), in steady-state the oscillators synchronize in-phase as depicted in Figure 4.9b) with frequency $f = 1.3007$ [Hz]. Additionally, Figure 4.9c) shows the projection of the displacements corresponding to the oscillators onto the plane (x_1, x_2) . The transient behaviour has been omitted.

The behaviour of the coupling bar is depicted in Figure 4.9d). Initially, the displacement of the bar is very small due to the anti-phase start-up. As long as the phase difference between the oscillators tends to zero, the oscillation corresponding to the displacement of the bar increases until the oscillators synchronize in-phase. Then, the bar keeps oscillating with fixed frequency ($f = 1.3007$ [Hz]) and amplitude.

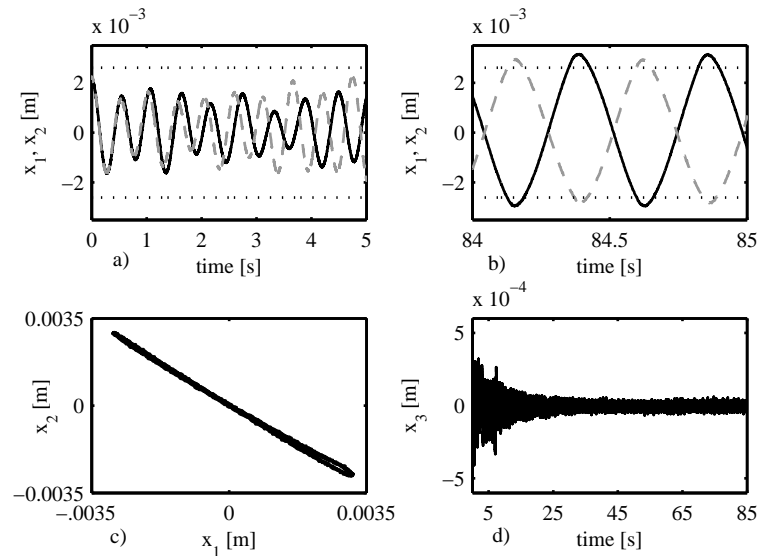


Figure 4.10 In this experiment, the oscillators synchronize in anti-phase. Solid line: x_1 , dash-dot line: x_2 .

In a second experiment, the mass of the coupling bar is increased by adding two steel plates of 2.359 [kg] each. This yields $m_3 = 8.818$ [kg]. As depicted in Figure

4.10a), the oscillators are released from initial conditions close to in-phase, $x_1(0) = 1.97$ [mm], $\dot{x}_1(0) = 0$, $x_2(0) = 2.13$ [mm], $\dot{x}_2(0) = 0$, and $x_3(0) = \dot{x}_3(0) = 0$. After the transient behaviour, the oscillators synchronize in anti-phase as can be seen in Figure 4.10b) with frequency $f = 2.1208$ [Hz]. Figure 4.10c) shows the projection of the limit displacements corresponding to the oscillators onto the plane (x_1, x_2) . Ideally, the displacement of the coupling bar should go to zero. However, due to the fact that the amplitudes of the oscillators differ slightly, because in the experimental setup the oscillators are not completely identical, the coupling bar does not come to a complete standstill as can be seen in Figure 4.10d). As a matter of fact, the anti-phase synchronized motion observed in this experiment can also be seen if the oscillators are released from the same initial conditions as used in experiment one.

Finally, an experiment, in which there is a transition from in-phase to anti-phase synchronization, due to a sudden change in the mass of the coupling bar, is presented. Actually, this experiment is a combination of experiment one with experiment two. Initially, experiment one is repeated, i.e. the oscillators are released from the initial conditions $x_1(0) = 1.97$ [mm], $\dot{x}_1(0) = 0$, $x_2(0) = -2.13$ [mm], $\dot{x}_2(0) = 0$, and $x_3(0) = \dot{x}_3(0) = 0$, the threshold displacement value of the control input (4.13) is again taken to be $x_{ref} = 2.65$ [mm], and the mass of the coupling bar is $m_3 = 4.1$ [kg]. The result is in-phase synchronization as depicted in Figure 4.11a). Then, at $t \approx 91$ [s], two additional steel plates (the same ones as used in experiment two) are suddenly added to the coupling bar in order to increase its mass from 4.1 [kg] to 8.818 [kg]. As a result, the in-phase synchrony is lost as depicted in Figure 4.11b). After a short transient, anti-phase synchronization is observed as shown in Figure 4.11c). The transition from in-phase to anti-phase motion is evident.

In addition, Figure 4.12 shows the time series corresponding to the displacement of the coupling bar. When the motion of the oscillators is in-phase, the bar oscillates with fixed amplitude and frequency. After adding the extra mass, the oscillations in the bar (almost) damp out.

This section is concluded with a short discussion. The experimental results show that when the system synchronizes in anti-phase, the oscillation frequency is approximately the same as the natural frequency $\frac{\omega}{2\pi} = 2.1156$ [Hz] of the (undamped/undriven) oscillators, whereas for the in-phase synchronization case, the oscillation frequency is approximately $\frac{\omega_3}{2\pi} = 1.5467$ [Hz], i.e. the natural frequency of the coupling bar.

As stated above, and as shown in Figure 4.10b), when the oscillators synchronize in anti-phase, their amplitudes are (slightly) different. The most probable cause of this is again the fact that in the experiment the oscillators and their actuators are

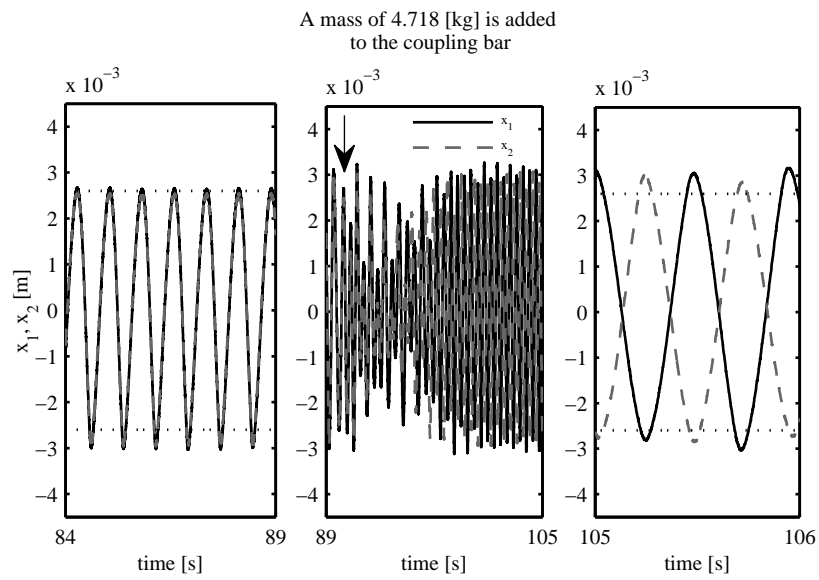


Figure 4.11 Transition from in-phase to anti-phase synchronization.

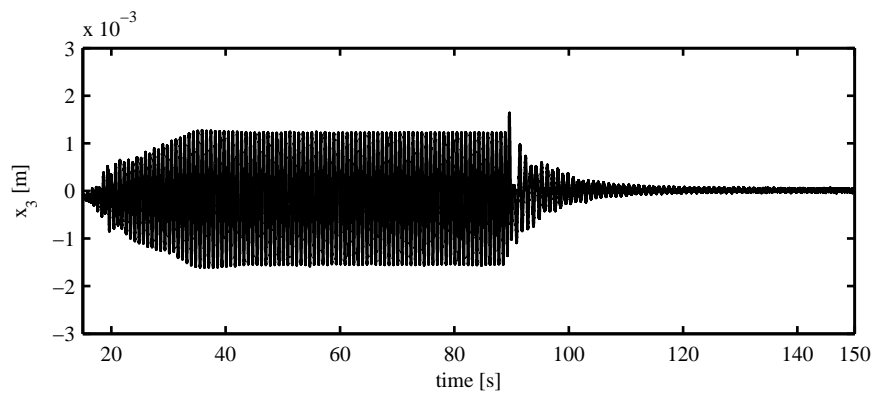


Figure 4.12 Displacement of the coupling bar.

not completely identical. This means that for the same input force their amplitude responses are expected to be (slightly) different. However, in the case where the oscillators synchronize in-phase, their amplitudes are almost equal (see Figure 4.9). The cause seems to be the “additional” harmonic excitation provided by x_3 .

4.5 Discussion

This chapter has illustrated, mainly by means of experiments, that a pair of nonlinear oscillators that interact via Huygens’ coupling may show in-phase and anti-phase synchronized behaviour. The experimental analyses have revealed that when the coupling strength is large (small mass of the coupling bar) the oscillators synchronize in-phase. On the other hand, when the coupling strength is small (relatively large mass of the coupling bar) the oscillators show anti-phase motion. For this, an intuitive and quite physical interpretation can be given, as presented in Remark 4.1. Some analytic conditions related to the stability of the anti-phase synchronous motion have been derived by assuming small amplitudes in the displacements of the oscillators. Notwithstanding these assumptions, the obtained analytic conditions are in good agreement with computer simulations and with the experiments.

Regarding the stability of the in-phase synchronous motion the following should be noted. The natural choice is to define the in-phase synchronization error $e = x_1 - x_2$, obtain the error dynamics and analyze its stability. However, this will not lead to any insight into the stability of the in-phase synchronized motion in terms of the coupling strength μ . The reason is because both oscillators receive the same “input” (the influence of the bar on them is the same) and, therefore, the obtained error dynamics $\ddot{e} = (\ddot{x}_1 - \ddot{x}_2)$ is independent of m_3 . Therefore, only focusing in the stability of \ddot{e} and ignoring the dynamics of the dynamic coupling is a conceptual flaw. Further research is needed in order to derive a global stability analysis of the in-phase and anti-phase synchronized motion of the oscillators (without the assumption of small amplitude in the oscillations) and some recommendations on this issue are provided in Chapter 8.

The results presented in this chapter are largely in agreement with Huygens observations. In Huygens’ original experiment, the coupling strength μ (the ratio between the clocks’ masses and the mass of the wooden bar) was small due to the fact that Huygens had placed some extra mass in the cases of the clocks in order to keep them upright in stormy seas. In such situations (of small μ), Huygens *only* observed anti-phase synchronization [30]. The experiments presented here reveal the same: when the mass of the coupling bar is increased, the oscillators

synchronize in anti-phase. The obtained results regarding in-phase synchronization suggest that if Huygens' would have removed the extra load at the bottom² then he would also had reported the existence of the in-phase synchronous motion.

In conclusion, this chapter has exploited and extended the serendipitous observations made by Huygens, who correctly explained that the sympathy of his clocks was due to the small vibrations of the wooden bar. In fact, it has been shown that Huygens' coupling can be used to synchronize several dynamical oscillators and likewise it has been demonstrated (via experiments) that the properties of this coupling determine the limit synchronizing behaviour in the oscillators, namely in-phase or anti-phase synchronization.

4.6 The influence of the coupling strength

In this final section, a brief discussion related to the influence of the coupling strength on the onset of synchronization in second order, self-sustained, nonlinear oscillators is presented.

On the one hand, the results presented in Chapter 3 have shown that in order to observe in-phase synchronization, the coupling strength should be *decreased* (by increasing the mass of the coupling bar), and anti-phase synchronization occurs for the cases where the coupling strength is *increased* (by reducing the mass of the coupling bar). On the other hand, the results presented in this chapter, reveal the contrary: in-phase synchronization is only observed when the coupling strength is *increased* and correspondingly, anti-phase synchronization has been observed when the coupling strength is *decreased*. Hence, a natural question is what is the reason behind this seemingly "opposite" effect of the coupling strength?

Note that there is a subtle but key difference between the systems analyzed in Chapter 3 and the ones analyzed here: the amount of damping and energy resupplied to the oscillators. In Chapter 3, the damping in the oscillators is assumed to be small (of the order μ) and consequently, the system only requires a small amount of energy to compensate the effect of damping. On the other hand, the results presented in this chapter correspond to systems where the damping in the oscillators is larger (at least one order greater than μ) and obviously, in this case the amount of energy that needs to be resupplied to the system is larger.

²In order to determine the origin of the 'sympathy' in his clocks, Huygens' did try several things like placing them far away from each other, placing them transversally to each other, etc [63]. However, as far as the author knows, experiments where the extra masses in the clocks are removed are not reported.

Moreover, from the experimental results (presented in Chapter 3 and here) it can be concluded that the energy required to achieve in-phase synchronization is larger than the energy required for anti-phase synchronization. This follows from the fact that during an in-phase motion of the oscillators, the coupling bar converges to a small oscillatory movement, whereas in anti-phase motion the vibrations in the coupling bar are rather negligible. In consequence, for the case discussed in Chapter 3 (small resupply of energy), by increasing the mass of the coupling bar, it is possible to keep more energy in the system (since the effective damping in the suspended bar is decreased) and in consequence the in-phase motion is likely to occur.

In conclusion, the limit synchronizing behaviour of the coupled oscillators not only depends on the magnitude of the coupling strength but also the amount of damping in the system has an important influence on the type of synchronized behaviour.

If the reader reflects on the broad picture resulting from Chapter 3 and this chapter, then the following must be clear: given a pair of arbitrary self-driven oscillators (with large or small damping/nonlinearities) it is possible to observe in-phase and anti-phase synchronization when they interact via Huygens' coupling. In other words, the synchronization phenomenon observed by Huygens more than 300 years ago in a pair of pendulum clocks can also be observed if the pendulums are replaced by other *second order, self-driven, nonlinear* oscillators.

Chapter 5

Controlled synchronization of chaotic oscillators with Huygens' coupling

Does the flap of a butterfly's wings in Brazil set off a tornado in Texas?

Edward Lorenz (1917–2008)

Abstract In this chapter, synchronization of chaotic oscillators interacting via Huygens' coupling is studied from a control point of view. The synchronization phenomenon does not occur naturally but it is induced by means of a suitable controller. Two well-known nonlinear oscillators are used in the analysis, namely Duffing and van der Pol oscillators. The controlled synchronized motion of the oscillators is validated by means of experiments.

5.1 Introduction

There are oscillating systems where synchronization occurs naturally, like for example biological systems, where it has been found that two or more cells, independently of their nature, or functioning, can show sympathetic behaviour, i.e. they synchronize by using signaling messengers (as for example light) as the coupling signal [36]. This is also the case of nonlinear self-driven oscillators interacting via Huygens' coupling, as already discussed in Chapters 3 and 4.

In other cases, the synchronization phenomenon is artificially induced by for instance a control law. This kind of synchronization is called, for obvious reasons,

controlled synchronization [49, 51]. As an example, the reader may consider the synchronization of wireless network terminals, which are of vital importance in communication systems [87].

Synchronized behavior can also be observed in chaotic systems. Due to their sensitivity to initial conditions, these systems are not expected to synchronize in a natural way. However, it is possible to find suitable couplings/controllers such that two (or more) chaotic systems may synchronize, see e.g. [2, 27, 56], and more recently [10].

In this chapter, a pair of identical chaotic oscillators linked via Huygens' coupling is considered. Since self-synchronization does not occur, a suitable controller is designed in order to induce *controlled* synchronized motion in the chaotic oscillators. Two well-known oscillators are used in the analysis, namely the (forced) Duffing and van der Pol oscillators.

The outline of this chapter is as follows. In Section 5.2, the synchronization of two Duffing oscillators with Huygens' coupling is analyzed. It is shown that by driving the coupling bar with a periodic signal, it is possible to induce chaotic behaviour in the oscillators. Then, a nonlinear controller is designed such that (in-phase and anti-phase) synchronization is achieved in the oscillators when they behave in a chaotic fashion. This is experimentally validated. Next, in Section 5.3, a similar analysis is conducted for a pair of van der Pol oscillators. Finally, a discussion of the obtained results is presented in Section 5.4.

5.2 Synchronization of two chaotic Duffing oscillators

The first objective of this section is to show that, by *driving* the coupling bar with an external periodic excitation it is possible to trigger the onset of chaos in two second order nonlinear oscillators coupled through a suspended rigid bar (i.e. with Huygens' coupling). When the oscillators are behaving chaotically, the phase synchronization phenomenon will not occur naturally. Consequently, the second objective is to show that by using the well known master/slave configuration, cf. [46], it is possible to achieve (controlled) synchronization, i.e. the slave system will be forced to follow the chaotic dynamics of the master oscillator. Figure 5.1 visualizes this. Notice that, a mutual synchronization scheme can be considered as an alternative [65], but this is not worked out here.

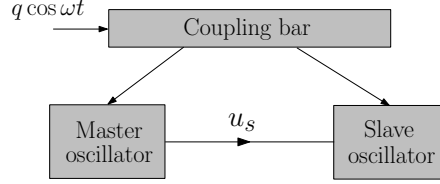


Figure 5.1 Two oscillators with Huygens' coupling and master/slave configuration. The slave control input is indicated by u_s .

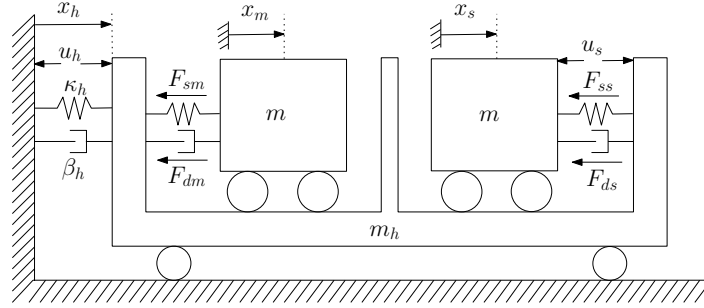


Figure 5.2 Schematic representation of two oscillators with Huygens' coupling.

Consider the system depicted in Figure 5.2 and assume that the nonlinear spring force is given by:

$$F_{si} = k(x_i - x_h) + k_3(x_i - x_h)^3, \quad i = m, s, \quad (5.1)$$

where $k_3 \in \mathbb{R}^+$ and $k \in \mathbb{R}^-$ (negative linear stiffness). Subscripts $i = m, s$ refer to the master and slave oscillator, respectively. Furthermore, assume linear damping force

$$F_{di} = \beta(\dot{x}_i - \dot{x}_h), \quad i = m, s, \quad (5.2)$$

where $\beta \in \mathbb{R}^+$. Then, the equations of motion of the system become

$$\begin{aligned} \ddot{x}_m &= -\frac{\beta}{m}(\dot{x}_m - \dot{x}_h) - \frac{k}{m}(x_m - x_h) - \frac{k_3}{m}(x_m - x_h)^3 \\ \ddot{x}_s &= -\frac{\beta}{m}(\dot{x}_s - \dot{x}_h) - \frac{k}{m}(x_s - x_h) - \frac{k_3}{m}(x_s - x_h)^3 + \frac{1}{m}u_s \\ \ddot{x}_h &= -\frac{m}{m_h}(\ddot{x}_m + \ddot{x}_s) - \frac{k_h}{m_h}x_h - \frac{\beta_h}{m_h}\dot{x}_h + \frac{u_h}{m_h}, \end{aligned} \quad (5.3)$$

where u_s is the slave control input to be designed. Note that this set of equations describes a pair of identical Duffing oscillators, with a double potential well, linked via Huygens' coupling.

The rigid coupling bar is externally excited with the periodic force

$$u_h = q \cos \omega t, \quad (5.4)$$

where q is the amplitude of the force and $\omega = 2\pi f$ is the angular frequency of the external excitation.

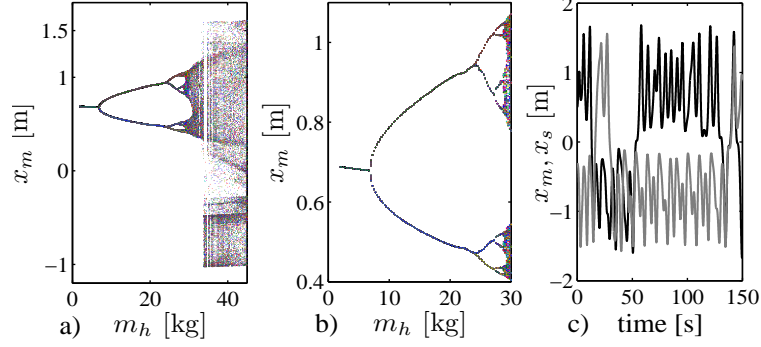


Figure 5.3 Left: bifurcation diagram for x_m as a function of m_h . Center: enlargement of plot a) in the interval $m_h \in [4.1, 30]$ [kg]. Right: chaotic time histories of the oscillators.

The following parameter values are considered (compare with [11]): $\beta = 0.0840$ [Ns/m], $k = -0.2310$ [N/m], $k_3 = 0.210$ [N/m³], $\omega = 1.2$ [rad/s], $q = 89$ [N], $k_h = 388.71$ [N/m], $\beta_h = 3.2656$ [Ns/m], and $m = 0.210$ [kg]. The slave control input is not active yet, i.e. $u_s = 0$ [N].

Different to other works, where chaotic behaviour of the Duffing equation is observed by varying the amplitude or frequency of the external periodic excitation, see e.g. [11, 28, 38], here, the mass of the coupling bar m_h is considered as a bifurcation parameter taking values in the range $m_h \in [4.1, 45]$ [kg]. The coupling strength $\mu = \frac{m}{m_h}$ is therefore considered in the range $\mu \in [4.667 \times 10^{-3}, 5.12 \times 10^{-2}]$ [-]. The bifurcation diagram is depicted in Figures 5.3a) and 5.3b). A cascade of period-doubling bifurcations ultimately resulting in a chaotic response can be observed. Starting from $x_m(0) = 0.5$, $x_s(0) = -0.3$, and other initial conditions equal zero, Figure 5.3c) shows the chaotic time histories of both oscillators for $m_h = 42$ [kg].

5.2.1 Case A: in-phase synchronization

When the synchronized motion of the oscillators is in-phase, the following equations should be satisfied:

$$e = x_s - x_m = 0, \quad \dot{e} = \dot{x}_s - \dot{x}_m = 0. \quad (5.5)$$

Writing down the error dynamics for system (5.3) yields:

$$\ddot{e} = \frac{1}{m} [-\beta\dot{e} - ke - k_3e^3 - f(e + x_m, x_m, x_h)e + u_s]. \quad (5.6)$$

where $f(e + x_m, x_m, x_h) = 3k_3(x_m - x_h)(e + x_m - x_h)$. Similar to [50], the control input u_s is defined:

$$u_s = -k_p e - k_v \dot{e} + \eta, \quad (5.7)$$

where k_p, k_v are the controller gains, and η is a compensation term to be designed. Substitution of this control in (5.6) yields the following closed-loop error dynamics

$$\ddot{e} = \frac{1}{m} [-(\beta + k_v)\dot{e} - (k + k_p)e - k_3e^3 - f(e + x_m, x_m, x_h)e + \eta]. \quad (5.8)$$

Proposition 5.1. *If the gains k_p, k_v satisfy*

$$k_p > -k, \quad k_v > -\beta, \quad (5.9)$$

and the compensation term η is designed such that

$$\eta = 3k_3e(x_m - x_h)(e + x_m - x_h), \quad (5.10)$$

then, system (5.8) is asymptotically stable, i.e.

$$\lim_{t \rightarrow \infty} e = 0, \quad \lim_{t \rightarrow \infty} \dot{e} = 0. \quad (5.11)$$

Proof. The closed-loop (5.6)-(5.7), with η as given in (5.10) is described by

$$\ddot{e} = \frac{1}{m} [-(\beta + k_v)\dot{e} - (k + k_p)e - k_3e^3]. \quad (5.12)$$

Now, consider the candidate Lyapunov function

$$V = \frac{1}{2}(\dot{e} + \alpha e)^2 + \frac{1}{2} \left[\left(\frac{k + k_p}{m} \right) + \alpha \left(\frac{\beta + k_v}{m} \right) - \alpha^2 \right] e^2 + \frac{k_3}{4m} e^4, \quad (5.13)$$

where $\alpha \in \mathbb{R}^+$ is a constant. Function (5.13) is positive definite if α satisfies

$$\alpha < \frac{(\beta + k_v)}{m}. \quad (5.14)$$

The time derivative of (5.13) along the solutions of system (5.12) is given by

$$\dot{V} = - \left(\frac{\beta + k_v}{m} - \alpha \right) \dot{e}^2 - \frac{\alpha(k + k_p)}{m} e^2 - \frac{\alpha k_3}{m} e^4. \quad (5.15)$$

Next, assume that α satisfies (5.14). If the gains of the controller (5.7) are chosen according to (5.9) then the closed-loop system (5.12) is asymptotically stable and therefore

$$\lim_{t \rightarrow \infty} (x_s - x_m) = 0, \quad \lim_{t \rightarrow \infty} (\dot{x}_s - \dot{x}_m) = 0. \quad (5.16)$$

□

5.2.2 Case B: anti-phase synchronization

Now, a control input is designed (in analogy with the in-phase synchronization case) to realize anti-phase synchronization of the slave oscillator with respect to the chaotic motion of the master oscillator.

The anti-phase synchronization errors are defined by

$$e_1 = x_s + x_m = 0, \quad e_2 = \dot{e}_1 = \dot{x}_s + \dot{x}_m = 0. \quad (5.17)$$

Then, the error dynamics of the coupled Duffing oscillators (5.3) are

$$\begin{aligned} \dot{e}_1 &= e_2 \\ \dot{e}_2 &= \frac{1}{m} [-\beta e_2 - k e_1 - k_3 e_1^3 + \gamma(e_1 - x_m, x_m, x_h) + u_s], \end{aligned} \quad (5.18)$$

where

$$\gamma(\cdot) = -k_3 [3e_1 ((x_m - x_h)e_1 + (x_m + x_h)^2 - 2x_m^2) - 6x_h x_m^2 - 2x_h^3] + 2k x_h + 2\beta \dot{x}_h. \quad (5.19)$$

As before, the control input u_s is defined as:

$$u_s = -\gamma(x_m, x_s, e_1) - k_p e_1 - k_v e_2. \quad (5.20)$$

Note that the closed-loop dynamics (5.18)-(5.20) coincides with the closed-loop dynamics (5.12) with $e = e_1 = (x_s + x_m)$ and $\dot{e} = e_2 = (\dot{x}_s + \dot{x}_m)$. Now, by following the same reasoning as used in Proposition 5.1, it is possible to show that system (5.18)-(5.20) with k_p and k_v satisfying (5.9) is asymptotically stable, i.e. the oscillators will asymptotically synchronize in anti-phase.

5.2.3 Experimental validation

The synchronized motion of the chaotic Duffing oscillators with Huygens' coupling is experimentally verified in this section. As a testbed, the electro-mechanical setup schematically depicted in Figure 2.3 is used. By means of feedback control (see Section 2.2), the inherent mechanical properties are adjusted such that the dynamical behaviour of the setup is described by the set of equations¹ (5.3). In all experiments, the following parameter values are considered: $\beta = 0.0840$ [Ns/m], $k = -0.2310$ [N/m], $k_3 = 0.210$ [N/m³], $\omega = 1.2$ [rad/s], $q = 89$ [N], $k_h = 388.71$ [N/m], $\beta_h = 3.2656$ [Ns/m], $m = 0.210$ [kg], and $m_h = 42$ [kg].

¹For the experiments, equations (5.3) have been escaled. The reason is due to the fact that, in the experimental setup, the maximum displacement of each oscillator is approximately 5 [mm].

In the first experiment, the in-phase synchronized motion of oscillators (5.3) is investigated. The nonlinear feedback controller (5.7) is implemented for the slave oscillator. For this experiment, the oscillators are released from the initial conditions $x_m(0) = 5$ [mm], $x_s(0) = -3$ [mm], and $x_h(0) = \dot{x}_h(0) = \dot{x}_m(0) = \dot{x}_s(0) = 0$. The values of the gains in the controller are $k_p = 1.3$ [N/m] and $k_v = 0.5$ [Ns/m]. With this choice, (5.9) is satisfied.

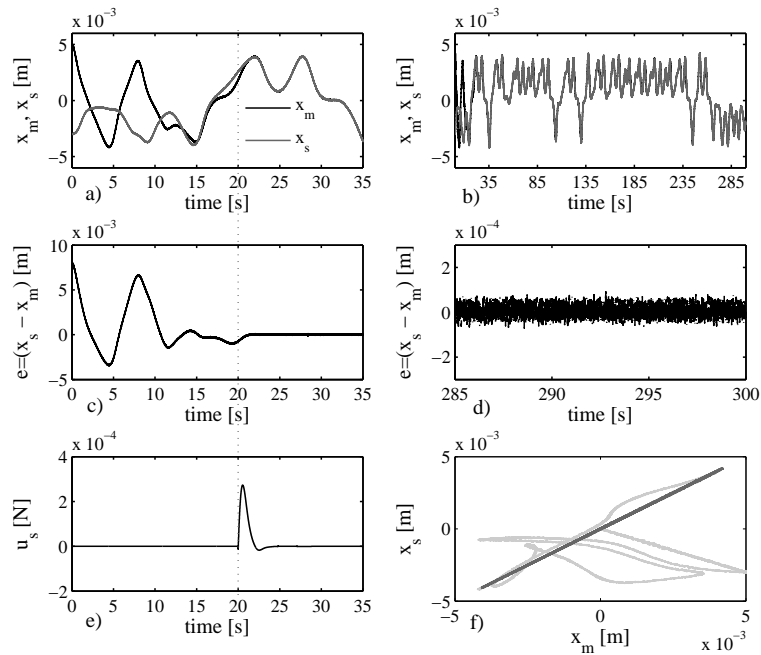


Figure 5.4 Experimental result: oscillators synchronize in-phase.

The corresponding experimental results are depicted in Figure 5.4. The transient responses for the displacements, the synchronization error, and the control input are shown in Figures 5.4a), 5.4c), and 5.4e), respectively.

For $t \in [0, 20)$, the controller is not activated and the behaviour in the oscillators is uncorrelated as depicted in Figure 5.4a). At $t = 20$ [s], the controller is activated and as a consequence, the slave oscillator synchronizes in-phase with the chaotic trajectory of the master. This can be seen in Figure 5.4b), where the complete time series corresponding to the displacements of the oscillators and synchronized chaotic behaviour is achieved. The synchronization error $e = x_s - x_m$ obviously is large when the control action is not applied yet, but once the

controller is activated, this error becomes practically zero as illustrated in Figure 5.4c) and Figure 5.4d), respectively. In theory, this error should become exactly zero. However, in practice the oscillators are not exactly equal and consequently in the experimental result there is a small error. Figure 5.4e) shows that the control effort stays very small once in-phase synchronization is realized. Figure 5.4f) presents a projection of the displacements corresponding to the oscillators onto the (x_m, x_s) plane. The light grey part of the curve corresponds to the transient behaviour, whereas the dark grey part of the curve indicates the synchronized limit behaviour.

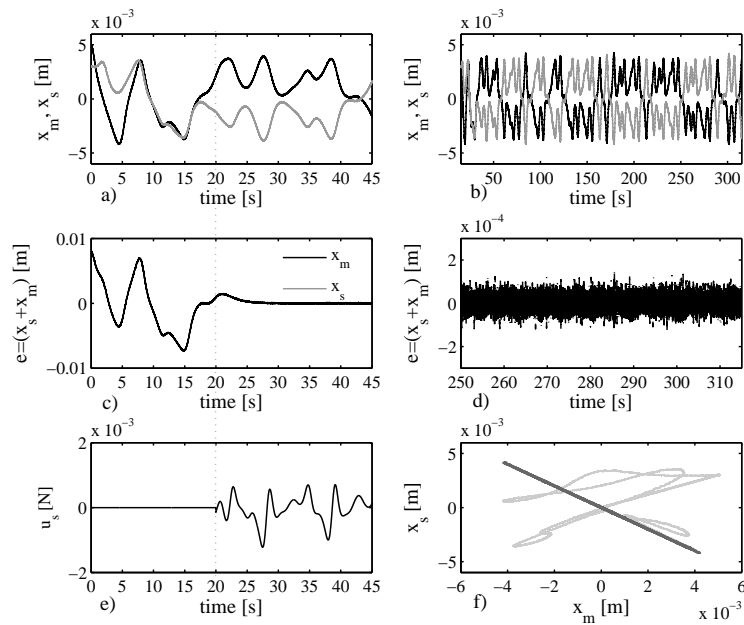


Figure 5.5 Anti-phase synchronization is achieved in two chaotic Duffing oscillators with Huygens' coupling.

In a second experiment, anti-phase synchronization is investigated. In this case, the control input (5.20) is used with $k_p = 1.1$ [N/m] and $k_v = 0.5$ [Ns/m]. In order to better illustrate the effect of the control action, the controller is again activated at $t = 20$ [s]. After this time, the displacement and velocity of the slave oscillator synchronize in anti-phase with the trajectories of the master, so the control objective is achieved. Figure 5.5 summarizes the main results of this experiment. Figures 5.5a) and 5.5c) correspond to the initial transient responses, whereas plots 5.5b), 5.5d), and 5.5e) show the limit behaviour for the displacements x_m and x_s

of the oscillators, the synchronization error $e = x_m + x_s$, and the control input u_s , respectively. The anti-phase synchronization of the coupled Duffing oscillators becomes immediately clear by drawing the projection of the displacements corresponding to the oscillators onto the (x_m, x_s) plane as depicted in Figure 5.5f). As before, the light grey part of the curve corresponds to the transient behaviour, whereas the dark grey part of the curve indicates the synchronized limit behaviour.

Note that in contrast to Figure 5.4e), the control force in Figure 5.5e) does not converge to zero.

5.3 Synchronization of two chaotic van der Pol oscillators

Consider again the system depicted in Figure 5.2 and assume that the nonlinear damping force corresponding to both oscillators is given by

$$F_{di} = -b(1 - ax_i^2)(\dot{x}_i - \dot{x}_h), \quad i = m, s, \quad (5.21)$$

where $a, b \in \mathbb{R}^+$. Furthermore, assume that the linear spring force is given by:

$$F_{si} = k(x_i - x_h), \quad i = m, s, \quad (5.22)$$

where $k \in \mathbb{R}^+$. Then, the equations of motion of the system become

$$\begin{aligned} \ddot{x}_m &= \frac{b}{m}(1 - ax_m^2)(\dot{x}_m - \dot{x}_h) - \frac{k}{m}(x_m - x_h) \\ \ddot{x}_s &= \frac{b}{m}(1 - ax_s^2)(\dot{x}_s - \dot{x}_h) - \frac{k}{m}(x_s - x_h) + \frac{1}{m}u_s \\ \ddot{x}_h &= -\frac{m}{m_h}(\ddot{x}_m + \ddot{x}_s) - \frac{k_h}{m_h}x_h - \frac{b_h}{m_h}\dot{x}_h + \frac{1}{m_h}u_h. \end{aligned} \quad (5.23)$$

This set of equations describes a pair of van der Pol oscillators with Huygens' coupling. The case $u_h = 0$ is considered.

It has been found that (5.23) shows chaotic behaviour for $b = 18.3135$ [Ns/m], $b_h = 3.2656$ [Ns/m], $k = 6.315$ [N/m], $k_h = 388.71$ [N/m], $a = 55 \cdot 10^5$ [1/m²], $m = 4.210$ [kg], and $m_h = 5$ [kg]. Similar to the case of Duffing oscillators discussed before, the ratio $\mu = \frac{m}{m_h}$ is an important parameter in the onset of chaotic behaviour. Note, however, that now the coupling bar is not driven.

Also here, in the chaotic regime, the coupled van der Pol oscillators may show synchronized behaviour provided that a control action is applied to one of them.

5.3.1 In-phase synchronization

By defining in-phase synchronization errors (5.5), the corresponding error dynamics for system (5.23) can be written as

$$\ddot{e} = \frac{1}{m} [b\dot{e} - ba(x_m^2\dot{e} + (2x_m + e)(\dot{x}_m + \dot{e} - \dot{x}_h)e) - ke + u_s]. \quad (5.24)$$

In order to achieve in-phase synchronized motion in the chaotic oscillators, the following controller may be considered

$$u_s = -k_p e - k_v \dot{e} + \eta, \quad (5.25)$$

where k_p, k_v are the controller gains and η can be chosen as

$$\eta = ba(x_m^2\dot{e} + (2x_m + e)(\dot{x}_m + \dot{e} - \dot{x}_h)e). \quad (5.26)$$

Following the approach used in Proposition 5.1, it can be proven that the controller (5.25)-(5.26) yields global asymptotic stability for system (5.24), i.e. the coupled oscillators asymptotically synchronize in-phase, provided that $k_v > b$ and $k_p > -k$.

5.3.2 Anti-phase synchronization

If the two van der Pol oscillators with Huygens' coupling show in-phase synchronized chaotic behaviour, the coupling bar will vibrate. However, when anti-phase synchronization is induced in the oscillators, the oscillations in the coupling bar will die out, i.e. $x_h \rightarrow 0$ and the coupling bar converges to a standstill as in the original Huygens system, see also the third equation in (5.23). Therefore, if anti-phase synchronization is achieved, the originally chaotic motion will change to periodic motion in both (now uncoupled) van der Pol oscillators. An uncoupled, unforced van der Pol oscillator can not show chaotic behaviour according to the Poincaré-Bendixon theorem [28]. To avoid this scenario and maintain chaotic motion for anti-phase synchronization, the external periodic excitation (5.4) is applied to the coupling bar.

The anti-phase synchronized motion in the chaotic oscillators is achieved by considering controller (5.25) with $e = (x_m + x_s)$, $\dot{e} = (\dot{x}_m + \dot{x}_s)$, and $\eta(\cdot)$ chosen as

$$\eta(\cdot) = ba(x_m^2\dot{e} + (e - 2x_m)(\dot{e} - \dot{x}_m - \dot{x}_h)e - 2x_m^2\dot{x}_h) - 2kx_h + 2b\dot{x}_h. \quad (5.27)$$

As before, the control gains are chosen according to $k_v > b$ and $k_p > -k$.

5.3.3 Experimental results

The synchronized chaotic motion of two van der Pol oscillators is validated by means of experiments. System (5.23) is implemented in the experimental setup with the following parameter values: $b = 18.3135$ [Ns/m], $b_h = 3.2656$ [Ns/m], $k = 6.315$ [N/m], $k_h = 388.71$ [N/m], $a = 55 \cdot 10^5$ [1/m²], $m = 4.210$ [kg], and $m_h = 5$ [kg].

In a first experiment, the oscillators are synchronized in-phase by applying to one of them the control input (5.25)-(5.26) with $k_p = 25$ [N/m] and $k_v = b + 10$ [Ns/m]. The controller is activated at $t = 20$ [s]. The oscillators are released from the initial conditions $x_m(0) = 1$ [mm] and $x_s(0) = -1.5$ [mm]. The remaining initial conditions are set to zero. The obtained experimental results are presented in Figure 5.6. When the controller is off, the chaotic trajectories of the oscillators are not synchronized and consequently the error $e = (x_s - x_m)$ is large, but once the controller is activated, this error becomes practically zero as depicted in Figures 5.6a) and 5.6c). Although theoretically this error should asymptotically converge to zero, in practice the error signal keeps showing small vibrations caused by measurement noise and (slight) differences in the oscillators. The control effort is depicted in Figure 5.6d) and becomes practically zero once the in-phase synchronization is achieved.

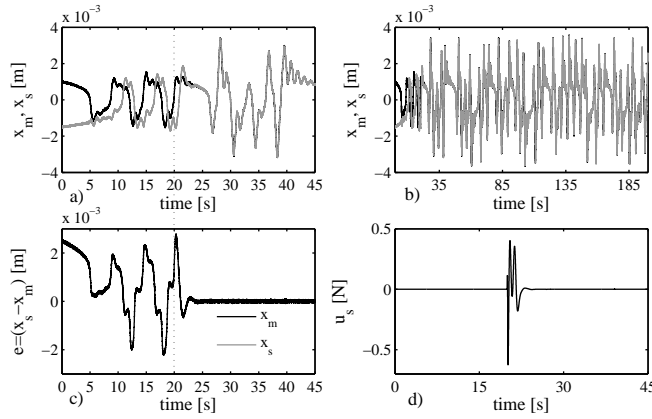


Figure 5.6 In-phase synchronization of two chaotic van der Pol oscillators with Huygens' coupling.

Next, it is desired to experimentally synchronize the coupled oscillators (5.23) in anti-phase. Therefore, control law (5.25),(5.27) with $e = (x_m + x_s)$, $\dot{e} = (\dot{x}_m + \dot{x}_s)$ is applied. Moreover, in this experiment, the coupling bar is not externally driven, i.e. $u_h = 0$.

To better illustrate the influence of the control law, the controller is now switched on at $t = 115$ [s]. As can be seen from Figure 5.7, when the control action is not active, the system behaves chaotically and unsynchronized. When the controller is activated, the oscillators asymptotically synchronize in anti-phase but in a periodic regime. As discussed above, the chaotic behaviour disappears because the coupling bar comes to a standstill and as a consequence the *unforced* oscillators run uncoupled. And it is well-known that an unforced van der Pol oscillator can not show chaotic motion.

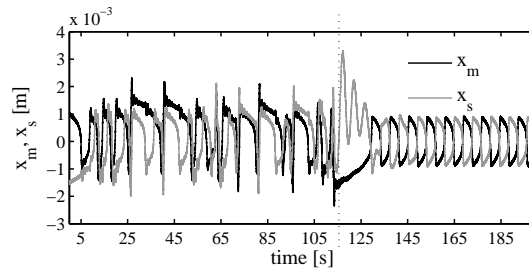


Figure 5.7 Although in this experiment the oscillators synchronize in anti-phase, the chaotic behaviour disappears.

To avoid the disappearance of the chaotic behaviour, the external periodic force (5.4) is applied to the coupling bar, i.e. $u_h = q \cos \omega t$ with $q = 0.5$ [N] and $\omega = 3.5$ [rad/s]. The remaining structural and control parameter values are identical to the first and second experiment. The non-zero initial conditions are $x_m(0) = 2.5$ [mm] and $x_s(0) = 2$ [mm]. The control action (5.25), (5.27) with $e = (x_m + x_s)$, $\dot{e} = (\dot{x}_m + \dot{x}_s)$ is applied from $t = 10$ [s]. As observed in Figure 5.8, the chaotic trajectories of the oscillators asymptotically synchronize in anti-phase. The control input (not shown here) does not converge to zero.

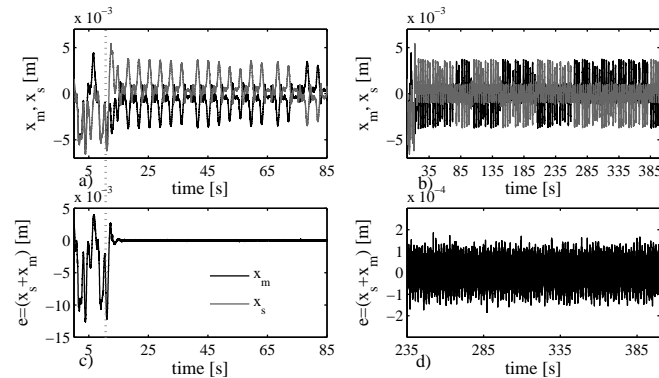


Figure 5.8 Chaotic anti-phase synchronization is experimentally achieved.

5.4 Discussion

The contributions of this chapter can be summarized as follows:

- It has been shown that the onset of chaotic behaviour in a pair of nonlinear oscillators coupled through a suspended rigid bar (i.e. with Huygens' coupling) can be triggered by driving the coupling bar with a periodic excitation. The mass of the coupling bar, which determines the coupling strength, has been considered as the bifurcation parameter leading to chaos.
- Huygens' coupling can be used to synchronize not only pendulum clocks as in the original experiment of Huygens, but also to synchronize other type of oscillators like van der Pol and piecewise linear oscillators as shown in Chapters 3 and 4. However, it is important to emphasize that if the oscillators behave chaotically, then Huygens' coupling will not lead to self-synchronization.
- The experimental results presented here validate that it is possible by adding a control input to induce synchronized behaviour in a pair of chaotic oscillators with Huygens' coupling.

It should be noted that the nonlinear controllers used to synchronize the oscillators, see e.g. (5.7), require inclusion of a compensation term η in order to deal with the nonlinearities and/or to cancel the influence of the coupling bar, see e.g. (5.10). Sometimes, however, it is desired to have a controller that on the one hand is as simple as possible, but on the other hand should be robust enough to guarantee that the stability is not compromised [6, 50]. In other words, it should be assured that the error dynamics at least remains ultimately uniformly bounded. For these reasons, the following simple feedback controller may be used

$$u_s = -k_p e - k_v \dot{e}. \quad (5.28)$$

This control law has the advantage that it does not require knowledge of the parameters of the oscillator to be controlled. Computer simulations and experimental results have revealed that in some cases, by using (5.28), the oscillators numerically (asymptotically) synchronize, whereas experimentally the so-called practical synchronization will appear. The stability proof of this turns out to be involved but it will be worthwhile to address this problem in the future also because experimental results and computers simulations have revealed that the control effort needed is small. This has several (beneficial) implications. First, the probability to have saturation effects in the actuators is considerably reduced. Secondly, small

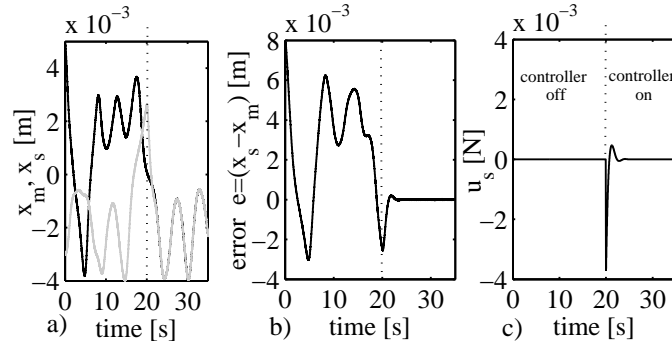


Figure 5.9 Experimental in-phase synchronization induced in system (5.3) by using controller (5.28).

control signals result in low energy consumption. For the sake of illustration, an experimental result corresponding to system (5.3) with parameter values as given in Subsection 5.2.3 and with controller (5.28), with $k_p = 1.2$ and $k_k = 0.5$ is presented in Figure 5.9.

Chapter 6

Synchronization of oscillators with time-delayed Huygens' coupling

Time flees away without delay

Abstract In this chapter, the influence of time delay on the onset of synchronization in pairs of nonlinear oscillators interacting via Huygens' coupling is examined, numerically and experimentally, from a control point of view. Namely, a suitable control input is applied to a pair of self-driven oscillators such that the closed-loop system resembles a pair of oscillators with Huygens' coupling, where the interaction between the oscillators and the control input is subject to a time delay. In particular, the occurrence of in-phase and anti-phase synchronization in the coupled/controlled oscillators is studied as a function of the coupling strength and the time delay. An eigenvalue-based numerical test is used as a first step to investigate the stability of the anti-phase synchronized motion and experimental validation is provided.

6.1 Introduction

As already mentioned in the introductory chapter, synchronization is a phenomenon that can be observed in a wide class of (oscillating) systems. An interesting situation occurs when the interaction between the systems is not instantaneous but occurs after some (small) time delay. This is the case in for example biological oscillators [36], neurosystems [73], and remote synchronization of mechanical systems [3, 22].

Several studies have analyzed the influence of time delay in the synchronization of coupled systems, see e.g. [11], [53], and [77]. In particular, in [67, 68], it has been found that the synchronized motion of two oscillators with coupling with time delay may experience a *phase-flip* bifurcation, i.e. an abrupt change from in-phase to anti-phase synchronization due to a variation in the time delay. This phase-flip may find application in for instance coupled laser systems where transition from in-phase to anti-phase synchronization may lead to a high degree of constant output [68].

In this study, the Huygens' experiment on synchronization is examined from a control point of view. The pendulum clocks (see Figure 2.1(a)) are replaced by two self-driven oscillators and the coupling structure, i.e. the wooden bar on two chairs, is replaced by a representative dynamical system. This dynamical system generates a suitable control input for the oscillators such that in closed loop the system resembles a pair of oscillators with Huygens' coupling. Note that in this case, the oscillators do not need to be at the same location in contrast to previous chapters and moreover, the dynamical system generating the control input should be implemented separately, using for instance a computer. Consequently, the possibility of having communication time-delays (either in the oscillators or in the applied control input) comes into play.

Hence, this chapter will focus in determining the influence of time delay in the limit behaviour of the (controlled) oscillators. The study is conducted for three different pairs of self-driven oscillators: oscillators self-driven by a Hamiltonian escapement (Section 6.3), van der Pol oscillators (Section 6.4), and oscillators self-driven by a discontinuous force (Section 6.5). For each of these pairs, two cases are considered: delayed unidirectional coupling, where only the input to the oscillators is time-delayed and delayed bidirectional coupling where both the input and output of the oscillators are time-delayed.

6.2 Preliminaries

Consider a pair of identical oscillatory systems of the form:

$$\ddot{x}_i(t) = F(x_i(t), \dot{x}_i(t)) + u(t), \quad i = 1, 2, \quad (6.1)$$

$$y_i(t) = h(x_i(t), \dot{x}_i(t)) \quad i = 1, 2, \quad (6.2)$$

with $x_i(t), \dot{x}_i(t) \in \mathbb{R}$, input $u(t) \in \mathcal{L}_\infty(\mathbb{R}, \mathbb{R})$ ¹, and output $y_i(t) \in \mathbb{R}$. The function $F : \mathbb{R}^2 \rightarrow \mathbb{R}$ is locally Lipschitz in $(x_i(t), \dot{x}_i(t))$ and is assumed to be given by

$$F(x_i(t), \dot{x}_i(t)) = f(x_i(t), \dot{x}_i(t)) - \omega^2 x_i(t) - 2\zeta\omega\dot{x}_i(t), \quad i = 1, 2, \quad (6.3)$$

¹ $\mathcal{L}_\infty(X, Y)$ is the space of bounded functions that map elements of X into elements of Y .

where $\omega \in \mathbb{R}^+$ is the angular eigenfrequency of the unforced oscillators and $\zeta \in \mathbb{R}^+$ is the dimensionless damping coefficient. The nonlinear term $f(x_i(t), \dot{x}_i(t))$ represents an internal energy source and compensates the energy loss in oscillator i . Furthermore, the output of each oscillator is assumed to be given by

$$y_i(t) = 2\zeta\omega\dot{x}_i(t) + \omega^2x_i(t) - f(x_i(t), \dot{x}_i(t)), \quad i = 1, 2. \quad (6.4)$$

Let the systems (6.1) interact via the dynamic system

$$\ddot{\eta}(t) = \frac{1}{\gamma} \sum_{i=1}^2 y_i(t) + g(\eta(t), \dot{\eta}(t)), \quad (6.5)$$

where $\eta(t), \dot{\eta}(t) \in \mathbb{R}$, $1/\gamma \in \mathbb{R}^+$ is the coupling strength (here, $\frac{1}{\gamma}$ plays the same role as μ in (2.1)) and the function $g : \mathbb{R}^2 \rightarrow \mathbb{R}$ is given by

$$g(\eta(t), \dot{\eta}(t)) = -\alpha_1\eta(t) - \alpha_2\dot{\eta}(t), \quad (6.6)$$

where $\alpha_1, \alpha_2 \in \mathbb{R}^+$.

The control input $u(t)$, which is *the same* for each oscillator, is constructed as follows

$$u(t) = \omega^2\eta(t) + 2\zeta\omega\dot{\eta}(t). \quad (6.7)$$

Hence, the closed-loop system (6.1),(6.3),(6.5)-(6.7) is given by

$$\ddot{x}_i(t) = -\omega^2(x_i(t) - \eta(t)) - 2\zeta\omega(\dot{x}_i(t) - \dot{\eta}(t)) + f(x_i(t), \dot{x}_i(t)), \quad i = 1, 2, \quad (6.8)$$

$$\ddot{\eta}(t) = \frac{1}{\gamma} \sum_{i=1}^2 y_i(t) - \alpha_1\eta(t) - \alpha_2\dot{\eta}(t). \quad (6.9)$$

with $y_i(t)$ as given in (6.4).

Note that system (6.8)-(6.9) resembles a pair of identical oscillators with Huygens' coupling (compare (6.8)-(6.9) with (2.1)). This terminology is explained as follows. In the generalized Huygens system depicted in Figure 2.4 the oscillators are *physically* coupled via the suspended rigid bar. In the analysis presented in this chapter, the coupling bar has been removed and the possibly remote oscillators interact via the dynamics (6.9) with coupling strength $1/\gamma$. The influence of the coupling bar in the oscillators is represented by the control input (6.7). However, the behaviour of the closed-loop system (6.8)-(6.9) coincides with the behaviour of the physically coupled system of Figure 2.4.

In the following, the influence of time delay in the limit behaviour of the (controlled) coupled system (6.8)-(6.9) is studied. Two cases are considered: *delayed*

unidirectional coupling, where only the control input (6.7) to the oscillators is delayed, and *delayed bidirectional coupling* where both the control input (6.7) and the output (6.4) of each oscillator are delayed, as schematically depicted in Figures 6.1(a) and 6.1(b) respectively.

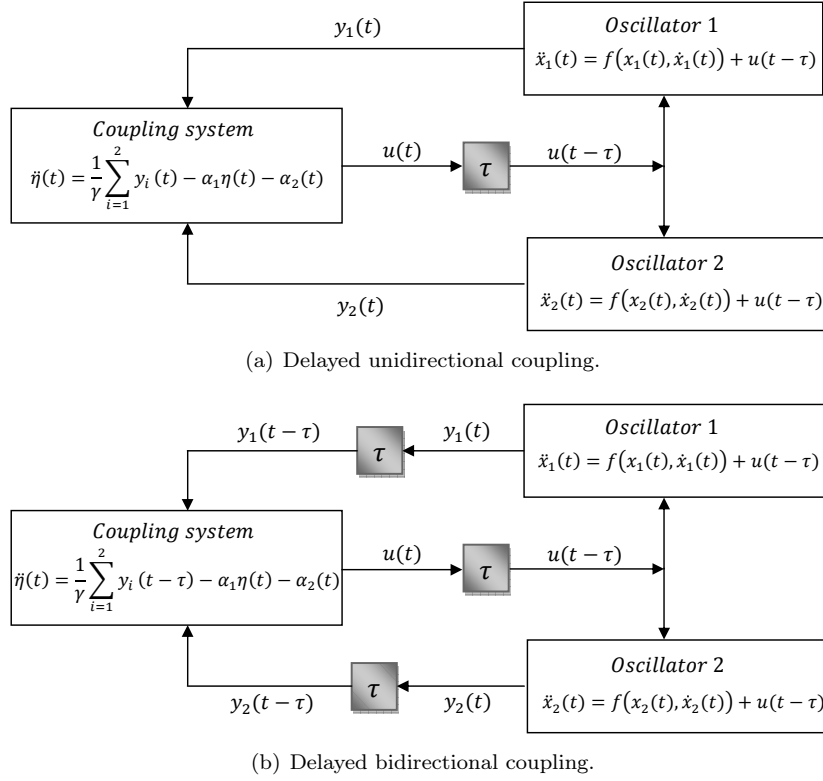


Figure 6.1 Two time-delayed coupling schemes. Time delay is indicated by τ .

6.3 Oscillators self-driven by a Hamiltonian escapement

Consider system (6.1) and assume that the nonlinear function in the oscillators is given by (3.4), i.e.

$$f(x_i(t), \dot{x}_i(t)) = -\lambda(H_i - H^*) \dot{x}_i(t), \quad i = 1, 2, \quad (6.10)$$

where $\lambda \in \mathbb{R}^+$, $H^* = \frac{1}{2} \kappa x_{ref}^2 \in \mathbb{R}^+$ is a reference energy level with x_{ref} being a reference amplitude, and $\kappa \in \mathbb{R}^+$. H_i is the Hamiltonian for the uncoupled and unforced oscillator i and is defined by $H_i = \frac{1}{2} m \dot{x}_i^2 + \frac{1}{2} \kappa x_i^2$, $i = 1, 2$.

6.3.1 Delayed unidirectional coupling

In the case of delayed unidirectional coupling, only the input to the oscillators is delayed, hence

$$u(t) = \omega^2 \eta(t - \tau) + 2\zeta \omega \dot{\eta}(t - \tau). \quad (6.11)$$

The resulting closed-loop system (6.1),(6.3)-(6.6),(6.10),(6.11) is given by:

$$\begin{aligned} \ddot{x}_i(t) &= -\omega^2(x_i(t) - \eta(t - \tau)) - 2\zeta\omega(\dot{x}_i(t) - \dot{\eta}(t - \tau)) \\ &\quad -\lambda(H_i - H^*)\dot{x}_i(t), \quad i = 1, 2, \end{aligned} \quad (6.12)$$

$$\ddot{\eta}(t) = \frac{1}{\gamma} \sum_{i=1}^2 y_i(t) - \alpha_1 \eta(t) - \alpha_2 \dot{\eta}(t). \quad (6.13)$$

Limit behaviour for varying γ and τ .

Next, the dynamic behaviour of the coupled system (6.12)-(6.13) is studied as a function of the coupling strength $1/\gamma$ and the time delay τ . The system's response is simulated for $\tau \in [0, 2.5]$ [s] (in steps of $\Delta_\tau = 0.01$), $\gamma \in [0.04, 100]$ [-] (in steps of $\Delta_\gamma = 1$), and parameter values: $\omega = 13.29$ [rad/s], $\zeta = 0.3829$ [-], $\lambda = 13.244 \times 10^3$ [s/kg·m²], $m = 0.210$ [kg], $\kappa = 37.108$ [N/m], $H^* = 7.83 \times 10^{-4}$ [Nm], $\alpha_1 = 2204.4095\gamma^{-1}$ [1/s²], $\alpha_2 = 35.9104\gamma^{-1}$ [1/s], and initial conditions $x_1(0) = 0.0027$ [m] and $x_2(0) = -0.0023$ [m]. The remaining initial conditions are set to zero².

The simulation results are illustrated in Figure 6.2(a), where different colors have been used to indicate when the system reaches anti-phase synchronization (cyan), in-phase synchronization (orange), or unstable behaviour (brown). Clearly, the time delay is a parameter that influences the limit behaviour of the coupled oscillators.

For very small values of τ ($\tau < 10$ [ms]), see Figure 6.2(c), the qualitative behaviour of the coupled oscillators is unaffected, i.e. the behaviour is as described in [60] and in Section 4.2: increasing γ (decreasing μ) results in a transition from in-phase synchronization to anti-phase synchronization. However, when τ increases, the synchronized behaviour of the system switches from in-phase to anti-phase and vice versa, i.e. the coupled system (6.12)-(6.13) experiences a phase-flip bifurcation. It should also be noticed that there are intermediate values of τ , for which the coupled

²In the particular case considered here, parameters α_1 and α_2 are depending on γ because it is desired to mimic Huygens' system, see (2.1), in which the angular eigenfrequency ω_3 and the dimensionless damping coefficient ζ_3 of the coupling bar are dependent on m_3 .

system will exhibit unstable oscillations, i.e. each oscillator becomes unstable. As depicted in Figure 6.2(a), for small values of γ ($\gamma < 15.51$ [-]), unstable behaviour does not seem to occur.

Analysis of the anti-phase motion

An initial step in the stability analysis of the anti-phase synchronized motion in the coupled self-driven oscillators (6.12)-(6.13) is conducted under the assumption of small oscillations. Then, the closed-loop system (6.12)-(6.13) becomes

$$\begin{aligned} \ddot{x}_i(t) &= -\omega^2(x_i(t) - \eta(t - \tau)) - 2\zeta\omega(\dot{x}_i(t) - \dot{\eta}(t - \tau)) \\ &+ \lambda H^* \dot{x}_i(t), \quad i = 1, 2, \end{aligned} \quad (6.14)$$

$$\ddot{\eta}(t) = \frac{1}{\gamma} \sum_{i=1}^2 y_i(t) - \alpha_1 \eta(t) - \alpha_2 \dot{\eta}(t), \quad (6.15)$$

with $y_i(t) = (2\zeta\omega - \lambda H^*)\dot{x}_i(t) + \omega^2 x_i(t)$, $i = 1, 2$.

Note that if the oscillators synchronize in anti-phase, then the coupling vanishes, i.e. $x_1(t) = -x_2(t)$ implies that $y_1(t) = -y_2(t)$ and consequently $\eta(t)$ and $\dot{\eta}(t)$ in (6.15) tend to zero.

The anti-phase synchronization errors are defined as follows

$$e_1(t) = x_1(t) + x_2(t), \quad \dot{e}_1(t) = \dot{x}_1(t) + \dot{x}_2(t), \quad (6.16)$$

$$e_2(t) = \eta(t), \quad \dot{e}_2(t) = \dot{\eta}(t). \quad (6.17)$$

The error dynamics can be written in the form

$$\dot{e}(t) = A_0 e(t) + A_1 e(t - \tau), \quad (6.18)$$

where the error state is given by $e = [e_1 \ e_2 \ \dot{e}_1 \ \dot{e}_2]^T$ and

$$A_0 = \begin{bmatrix} 0 & 0 & 1 & 0 \\ 0 & 0 & 0 & 1 \\ -\omega^2 & 0 & a & 0 \\ \frac{1}{\gamma}\omega^2 & -\alpha_1 & b & -\alpha_2 \end{bmatrix}, \quad A_1 = \begin{bmatrix} 0 & 0 & 0 & 0 \\ 0 & 0 & 0 & 0 \\ 0 & 2\omega^2 & 0 & 4\zeta\omega \\ 0 & 0 & 0 & 0 \end{bmatrix}, \quad (6.19)$$

with $a = -(2\zeta\omega - \lambda H^*)$ and $b = \frac{1}{\gamma}(2\zeta\omega - \lambda H^*)$. It is well-known that the stability of a system like (6.18) is determined by the *rightmost* roots of the *characteristic equation* [42]

$$p(\chi) = \det(\chi I - A_0 - A_1 e^{-\chi\tau}) = 0. \quad (6.20)$$

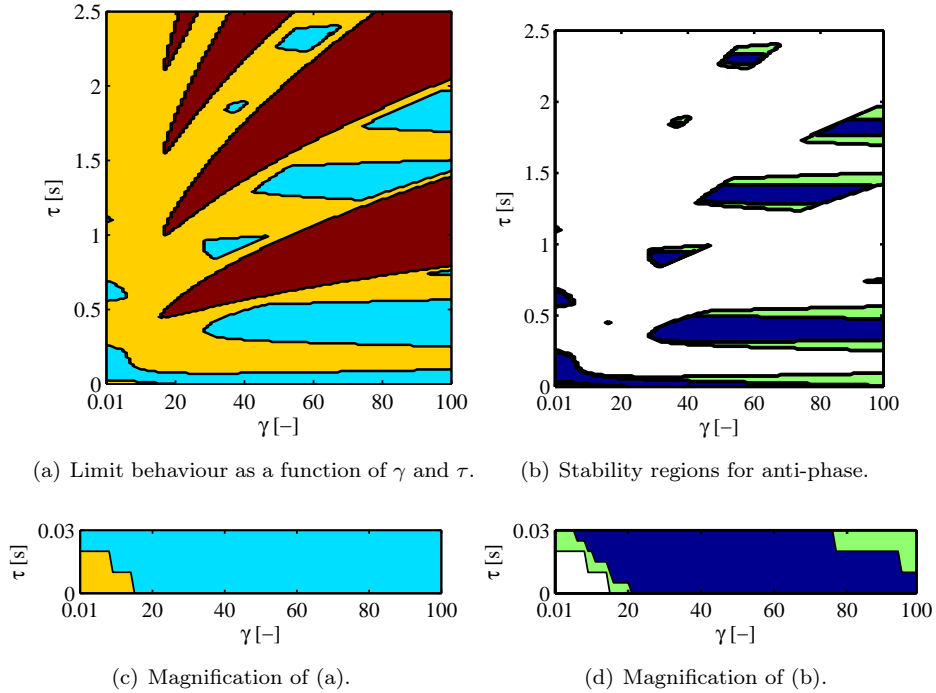


Figure 6.2 Hamiltonian escapement and delayed unidirectional coupling: numerical results. In figures (a),(c) cyan: anti-phase synchronization, orange: in-phase synchronization, and brown: unstable behaviour. In figures (b),(d) dark blue: stable anti-phase synchronization calculated by DDE-BIFTOOL, green: stable anti-phase synchronization according to the simulations presented in figure (a).

Here, the rightmost roots of (6.20) are computed (for a certain combination of parameter values) using DDE-BIFTOOL, a Matlab package for numerical bifurcation and stability analysis of delayed differential equations [21].

In the analysis, matrices A_0 and A_1 with the same parameter values as used earlier in this subsection are considered. The obtained results are shown in Figure 6.2(b). The plot shows the different regions where stable anti-phase synchronization occurs according to the linearized stability analysis based on (6.20) (dark blue areas) and compares these regions with the green areas, which were obtained in the numerical simulations based on (6.12)-(6.13). These green areas were presented by the cyan areas in Figure 6.2(a). As can be seen, the region where anti-phase motion is stable, according with the numerical stability test, forms a subset of the anti-phase region obtained by numerical integration of (6.12)-(6.13).

6.3.2 Delayed bidirectional coupling

Consider again the closed-loop system (6.1), (6.3), (6.5)-(6.6), (6.10), (6.11), i.e.

$$\begin{aligned} \ddot{x}_i(t) &= -\omega^2(x_i(t) - \eta(t - \tau)) - 2\zeta\omega(\dot{x}_i(t) - \dot{\eta}(t - \tau)) \\ &\quad - \lambda(H_i - H^*)\dot{x}_i(t), \quad i = 1, 2, \end{aligned} \quad (6.21)$$

$$\ddot{\eta}(t) = \frac{1}{\gamma} \sum_{i=1}^2 y_i(t) - \alpha_1\eta(t) - \alpha_2\dot{\eta}(t). \quad (6.22)$$

but now with $y_i(t)$, $i = 1, 2$, defined by

$$y_i(t) = 2\zeta\omega\dot{x}_i(t - \tau) + \omega^2x_i(t - \tau) - f(x_i(t - \tau), \dot{x}_i(t - \tau)). \quad (6.23)$$

Limit behaviour for varying γ and τ .

The response of system (6.21)-(6.22) is numerically investigated as a function of γ and the time delay τ . The same parameter values are used as in the unidirectional case discussed in Subsection 6.3.1. The simulation results are depicted in Figure 6.3(a). Among others, transitions from in-phase to anti-phase synchronization and vice versa, i.e. a phase-flip bifurcation, again can be clearly seen. An important difference between the results obtained for the unidirectional delayed coupling and for the present coupling is that the regions where the in-phase or anti-phase synchronized motion of the oscillators are stable, are smaller and therefore, the instability region is larger.

Analysis of the anti-phase motion

An initial step in the stability analysis of the anti-phase synchronized motion is again carried out under the assumption of small oscillations.

The anti-phase error dynamics are the same as defined in (6.18) but now with

$$A_0 = \begin{bmatrix} 0 & 0 & 1 & 0 \\ 0 & 0 & 0 & 1 \\ -\omega^2 & 0 & a & 0 \\ 0 & -\alpha_1 & 0 & -\alpha_2 \end{bmatrix}, \quad A_1 = \begin{bmatrix} 0 & 0 & 0 & 0 \\ 0 & 0 & 0 & 0 \\ 0 & 2\omega^2 & 0 & 4\zeta\omega \\ \frac{1}{\gamma}\omega^2 & 0 & b & 0 \end{bmatrix}, \quad (6.24)$$

where $a = -(2\zeta\omega - \lambda H^*)$ and $b = \frac{1}{\gamma}(2\zeta\omega - \lambda H^*)$.

Next, the same eigenvalue-based stability test for the linearized system as already used for the delayed unidirectional coupling case is carried out. The results are

shown in Figure 6.3(b). Also for the delayed bidirectional coupling, the stability regions for anti-phase synchronization identified by DDE-BIFTOOL are subsets of the stability regions resulting from the simulations.

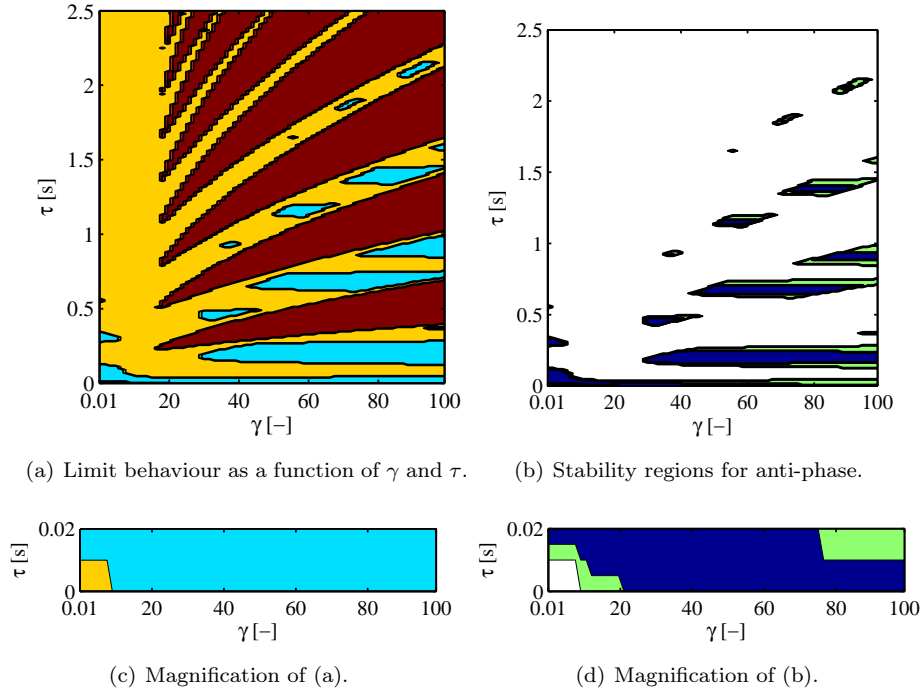


Figure 6.3 Hamiltonian escapement and delayed bidirectional coupling: numerical results. In figures (a),(c), cyan: anti-phase synchronization, orange: in-phase synchronization, and brown: unstable behaviour. In figure (b),(d), dark blue: stable anti-phase synchronization calculated by DDE-BIFTOOL, green: stable anti-phase synchronization according to the simulations presented in figure (a).

6.4 Oscillators self-driven by a van der Pol term

In this section, a similar analysis as presented in the previous section is conducted but now for the case where the loss of energy in the oscillators due to dissipation is compensated by the van der Pol term (3.5), i.e,

$$f(x_i(t), \dot{x}_i(t)) = -\nu(ax_i^2(t) - 1)\dot{x}_i(t), \quad i = 1, 2. \quad (6.25)$$

where $\nu \in \mathbb{R}^+$ determines the amount of nonlinearity and the strength of the damping and $a \in \mathbb{R}^+$ is a parameter, which defines the switching between positive and negative damping.

For the delayed unidirectional coupling, numerical integration of the coupled system (6.1), (6.3)-(6.6), (6.11), (6.25) is carried out with parameter values $\nu = 10.49$ [s^{-1}] and $a = 100000$ [m^{-2}]. Other parameter values and initial conditions are as discussed in Subsection 6.3.1. For the considered ranges of γ and τ , this yields the results depicted in Figure 6.4(a). The regions where the oscillators synchronize in anti-phase are denoted by the cyan color, the in-phase regions by the orange color, and the regions where the oscillators behave unstable are denoted by the brown color.

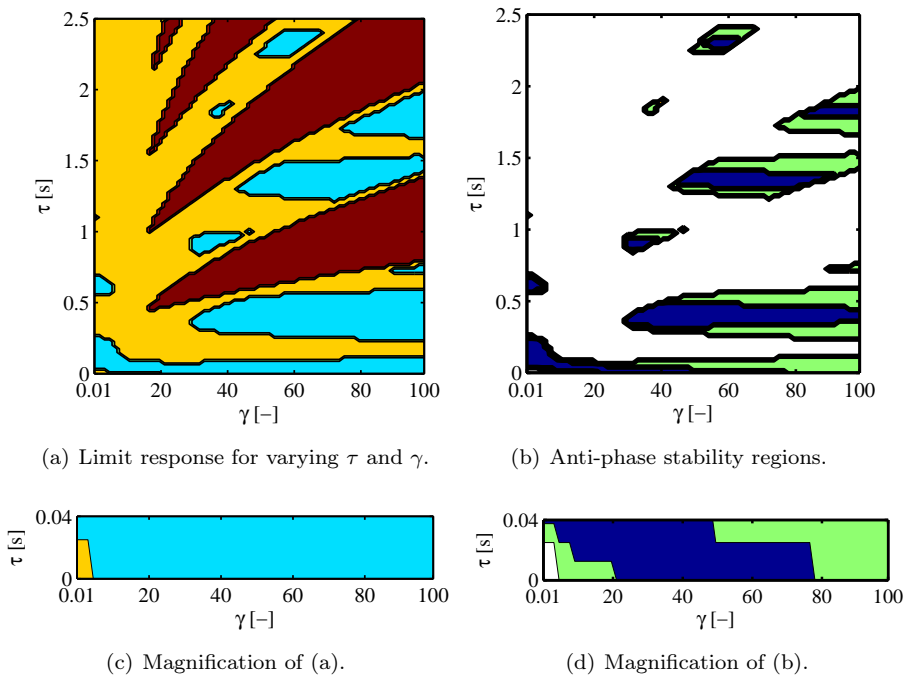


Figure 6.4 Van der Pol escapement. Numerical results for the delayed unidirectional case. In figures (a),(c) cyan: anti-phase synchronization, orange: in-phase synchronization, and brown: unstable behaviour. In figures (b),(d), dark blue: stable anti-phase synchronization calculated by DDE-BIFTOOL, green: stable anti-phase synchronization according to the simulations presented in figure (a).

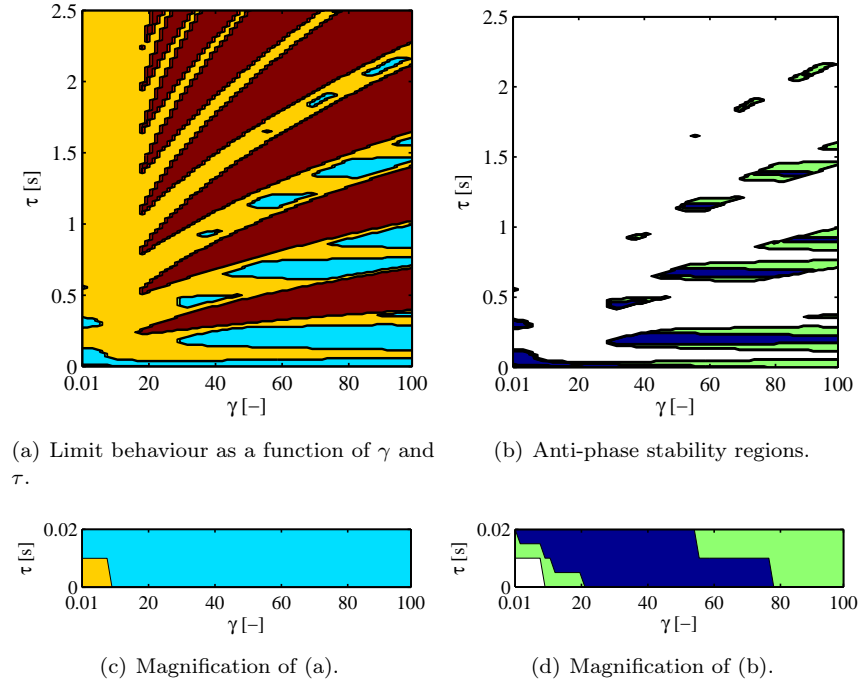


Figure 6.5 Van der Pol escapement. Numerical results for the delayed bidirectional case. In figure (a),(c), cyan: anti-phase synchronization, orange: in-phase synchronization, and brown: unstable behaviour. In figure (b),(d), dark blue: stable anti-phase synchronization calculated by DDE-BIFTOOL, green: stable anti-phase synchronization according to the simulations presented in figure (a).

The stability of the anti-phase synchronized motion can again be studied by assuming small oscillations. This yields a linearized error system that coincides with (6.18) after replacing λH^* by ν in (6.19). Figure 6.4(b) shows the stability regions for the anti-phase motion. The dark blue color denotes a stable region calculated by DDE-BIFTOOL and the green color denotes a stable region according to the simulations presented in Figure 6.4(a).

Finally, a similar analysis is conducted for the delayed bidirectional coupling, where (6.4) is replaced by (6.23). Figure 6.5(a) shows the obtained simulation results with parameter values and initial conditions identical to the unidirectional case. Again, the synchronization regions (in-phase and anti-phase) are considerably reduced. The corresponding stability analysis for anti-phase synchronization is depicted in Figure 6.5(b).

6.5 Oscillators self-driven by a discontinuous force

Consider again system (6.1) and assume that the nonlinear function in the oscillators is given by (4.13), i.e.

$$f(x_i(t), \dot{x}_i(t)) = -\alpha \dot{x}_i(t) \text{sign}(|x_i(t)| - x_{ref}), \quad i = 1, 2, \quad (6.26)$$

where $\alpha \in \mathbb{R}^+$ and the constant $x_{ref} \in \mathbb{R}^+$ represents a threshold displacement value.

Again, the limit behaviour of the coupled system is investigated as a function of the coupling strength γ and the time delay τ . For the case of delayed unidirectional coupling, the limit response of the coupled system (6.1), (6.3)-(6.6), (6.11), (6.26) is as depicted in Figure 6.6(a). In this numerical analysis, the system's response has been simulated for $\alpha = 10.1866$ [1/s] and $x_{ref} = 0.0025$ [m]. Other parameter values and initial conditions for the oscillators are the same as in Subsection 6.3.1.

The obtained results are very close to the results obtained in Figure 6.2(a) and Figure 6.4(a) for the Hamiltonian and van der Pol escapements respectively. Namely, the time delay induces a phase-flip bifurcation and also induces unstable behaviour.

Regarding the delayed bidirectional coupling where (6.4) is replaced by (6.23), the numerical analysis reveals that the regions with in-phase and anti-phase synchronization are considerably smaller, as depicted in Figure 6.6(b). Parameter values and initial conditions are as mentioned above for the unidirectional case.

Note that the stability of the anti-phase motion can not be analyzed by following the assumption of small oscillations, as already mentioned in Section 4.4. For the present case, the stability of the anti-phase motion is demonstrated by means of experiments.

6.6 Experimental validation

The effect of time delay in the synchronized motion of self-driven nonlinear oscillators with delayed Huygens' coupling is experimentally studied by using the electro-mechanical system depicted in Figure 2.3. The original mechanical coupling bar has been mechanically fixed, such that the setup is reduced to two isolated oscillators, which can only interact via their control input,

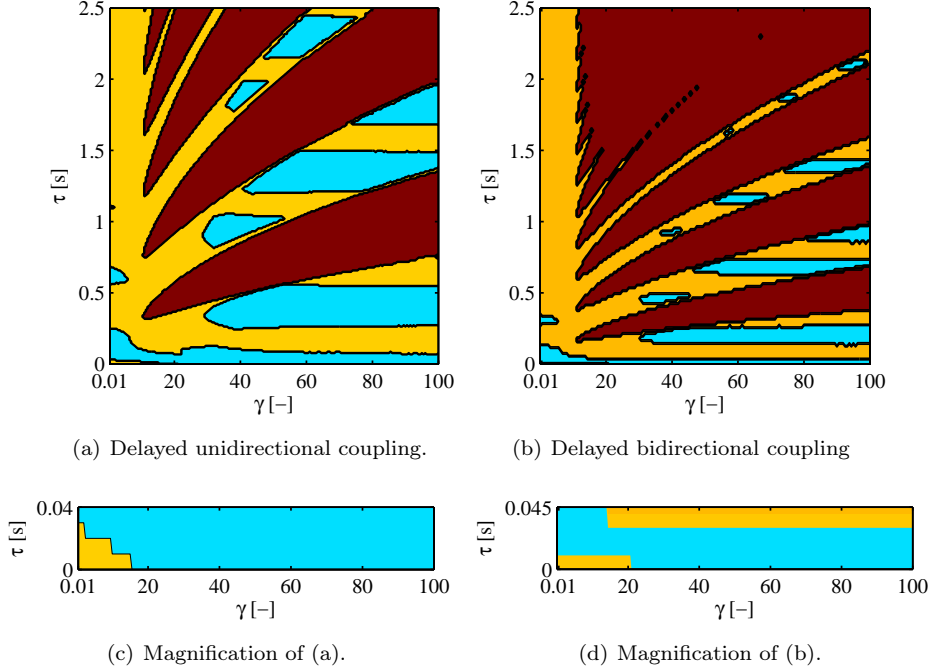


Figure 6.6 Self-driven discontinuous oscillators. Limit response as a function of γ and τ : numerical results. In these figures, cyan: anti-phase synchronization, orange: in-phase synchronization, and brown: unstable behaviour.

In the first experiment, the controllers of the oscillators in the experimental setup are adjusted such that the oscillator's dynamic behaviour is approximately described by (6.12)-(6.13), i.e. the case of delayed unidirectional coupling is considered for the oscillators self-driven by a Hamiltonian escapement discussed in Section 6.3. Obviously, the experimental set-up introduces some uncertainty in the dynamics intended by the model. The dynamical system (6.13) is implemented in software. The parameter values for the oscillators are as given in Table 2.1, the parameter values of (6.11) are assumed to be $\omega = 13.29$ [rad/s], $\zeta = 0.3829$ [-], and the remaining parameter values are $\lambda = 13244$ [s/kg·m²], $m = 0.210$ [kg], $\kappa = 37.108$ [N/m], $H^* = 7.83 \times 10^{-4}$ [Nm], $\alpha_1 = \frac{2204.4095}{\gamma}$ [1/s²], $\alpha_2 = \frac{35.9104}{\gamma}$ [1/s], and initial conditions $x_1(0) = 2.4$ [mm] and $x_2(0) = 2.15$ [mm]. The remaining initial conditions are set to zero. The coupling strength is computed for $\gamma = 60$ [-].

Initially, the interaction between the oscillators and the control input is free of delay³, i.e. $\tau = 0$. Although the oscillators are released from initial conditions close to in-phase, after transient behaviour the oscillators practically synchronize in anti-phase, see Figure 6.7(a). At $t = 250$ [s], a delay $\tau = 0.15$ [s] is induced in the control input to the oscillators, see Figure 6.7(a). As a consequence, the synchronized behaviour switches from anti-phase to in-phase as shown in Figure 6.7(b). Likewise, the synchronization frequency of the oscillators increases as depicted in Figure 6.7(c). Once the oscillators are synchronized in-phase, the control input, see Figure 6.7(d) becomes periodic with constant amplitude. These experimental results are in agreement with the numerical results presented in Figure 6.2(a). Moreover, it should be noted the limit amplitude of the oscillators differs. This is directly related to the differences in the oscillators, see Table (2.1).

A second experiment is conducted for the case of self-driven discontinuous oscillators discussed in Section 6.5. The case of delayed unidirectional coupling is considered. For the nonlinear function (6.26), the parameter values are: $\alpha = 10.1866$ [1/s] and $x_{ref} = 2.5$ [mm]. Other parameter values and initial conditions in the experiment are the same as used in experiment one. The coupling strength is computed for $\gamma = 50$ [-].

Again, in order to better appreciate the influence of the time delay in the synchronized motion of the oscillators, the experiment is started by considering $\tau = 0$ [s]. Figure 6.8(a) shows the time series of the oscillators for this experiment. After a short time interval of transient behaviour, the oscillators synchronize in anti-phase as depicted in Figure 6.8(b). At $t = 35$ [s], a unidirectional time delay of $\tau = 0.155$ [s] is induced and as a consequence the oscillators synchronize in-phase, as illustrated in Figure 6.8(c).

Note that besides the change from anti-phase to in-phase synchronization, the oscillation frequency f (measured from peak to peak) also changes as shown in Figure 6.8(d). This is further explained in Section 6.7. Figure 6.8(e) shows the control input (6.11) applied to the oscillators. It can be seen that the control input (almost) vanishes when anti-phase synchronization is achieved, whereas for the in-phase case, the control input becomes periodic.

The numerical results presented in Section 6.5 are in agreement with these results. Note that for $\gamma = 50$ [-] and $\tau = 0$ [s], the numerical results presented in Figures 6.6(a) and 6.6(c) indicate that anti-phase synchronization is likely to occur, whereas for $\tau = 0.155$ [s], in-phase synchronization is expected to occur.

In a third experiment, the case of self-driven discontinuous oscillators is considered again but now for the case of bidirectional delayed coupling. The parameter values

³The actual time delay in the set-up is negligible.

are the same as used in the second experiment, except for the coupling strength, which now is computed for $\gamma = 10$ [-]. The nonzero initial conditions are chosen as follows: $x_1(0) = 2.45$ [mm] and $x_2(0) = -2.3$ [mm].

Again, at the beginning of the experiment, the time delay is assumed to be zero. The time series corresponding to x_1 and x_2 are depicted in Figure 6.9(a). From Figure 6.9(b) it can be observed that after the transient behaviour the oscillators synchronize in-phase. Then, at $t = 15$ [s], a time delay of $\tau = 0.043$ [s] is induced in the oscillators. As a result, the synchronized motion switches from in-phase to anti-phase as depicted in Figure 6.9(c). Note that now the transition is slower in comparison with the transition observed in the first experiment. This result is in agreement with the numerical results presented in Figure 6.6(b) and 6.6(d). Figure 6.9(d) shows the oscillation frequency f , which increases to the value of the frequency of the individual self-driven oscillators. In theory, the interaction between the oscillators should vanish and consequently the control $u(t)$, see (6.11), should also vanish, but due to the small differences between the oscillators in the experiment, the control input remains oscillating with small amplitude as illustrated in Figure 6.9(e).

Note that in experiment one, the differences in the limit amplitude of the oscillators are larger than in experiments two and three. The reason is due to the fact that in the first experiment, the Hamiltonian escapement only keeps a certain amount of energy in each oscillator without forcing the oscillations to reach a certain reference value. On the other hand, in experiments two and three, the oscillators are forced by the discontinuous escapement mechanism to reach a certain reference amplitude.

The experimental results presented here confirm that the delay can be seen as a bifurcation parameter leading to a phase-flip bifurcation.

6.7 Discussion

In this final section, a discussion of the obtained results is presented.

- The influence of time delay in the appearance of transitions from in-phase to anti-phase synchronization and vice versa, i.e. a phase-flip bifurcation, occurring in delayed coupled oscillators, has already been studied for the case of diffusive couplings, see e.g. [68]. However, to the best of our knowledge, this is the first time that these transitions are studied in the context of Huygens' coupling.

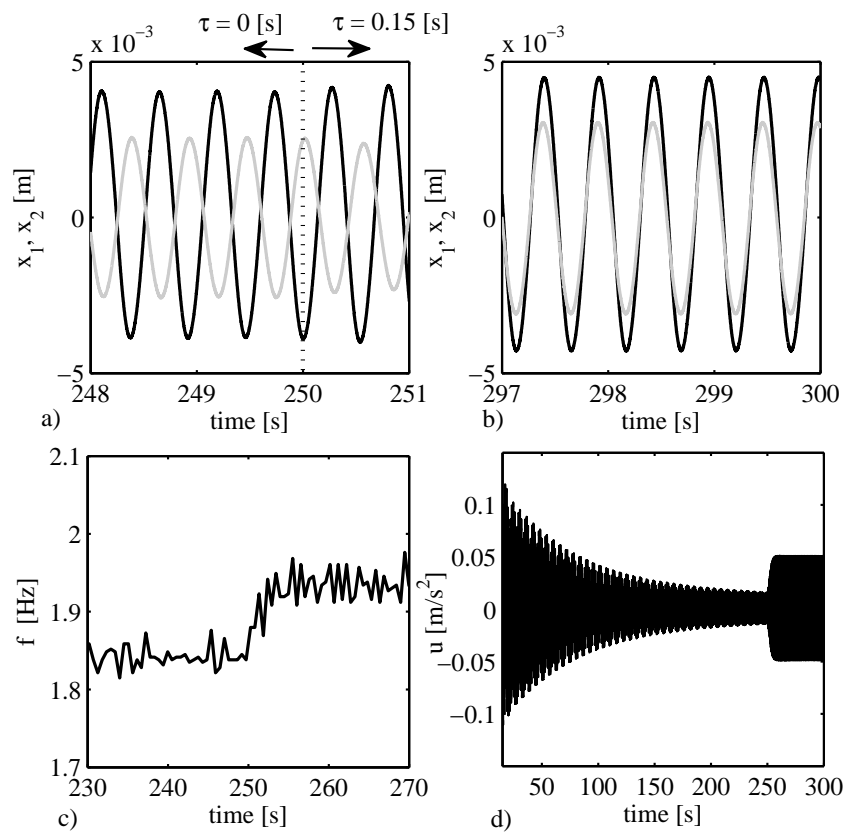


Figure 6.7 Oscillators driven by the Hamiltonian escapement: delayed unidirectional coupling. Experimental results. x_1 (black line) and x_2 (gray line).

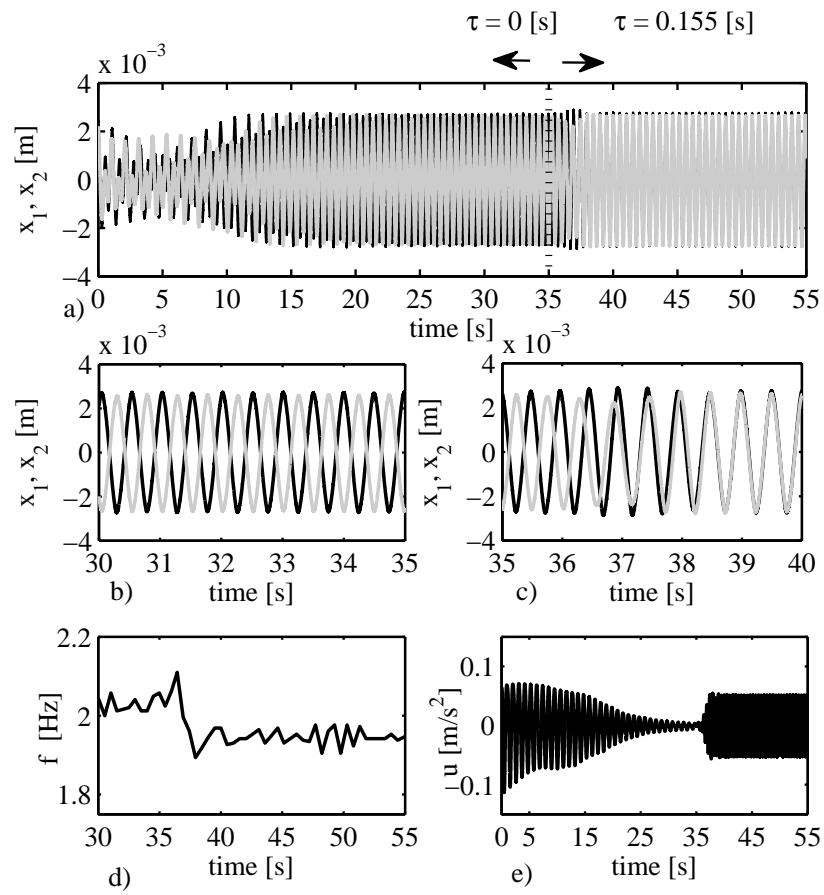


Figure 6.8 Self-driven discontinuous oscillators with delayed unidirectional coupling: experimental results. The oscillators synchronize in-phase. x_1 (black line) and x_2 (gray line).

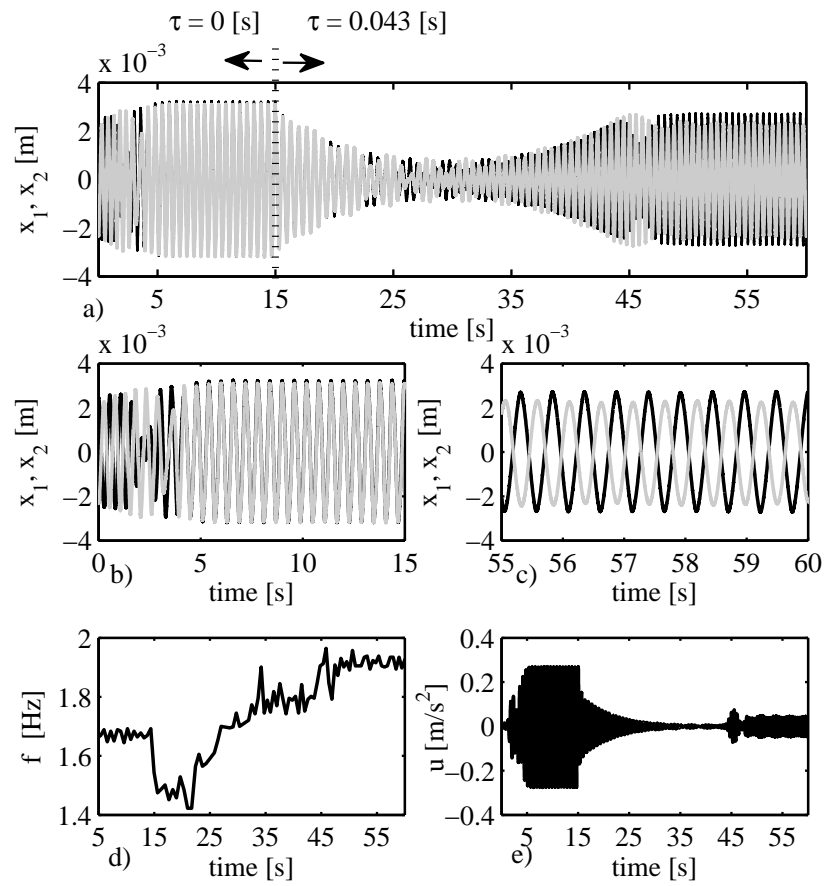


Figure 6.9 Self-driven discontinuous oscillators with delayed bidirectional coupling: experimental results. The oscillators synchronize in anti-phase. x_1 (black line) and x_2 (gray line).

- For the three types of oscillators considered in this section there is a striking similarity in the limit behaviour of the oscillators as shown in Figures 6.2(a), 6.4(a), and 6.6(a) for the unidirectional case and 6.3(a), 6.5(a), and 6.6(b) for the bidirectional case. These results suggest that in a qualitative sense the limit behaviour of the system is independent of the type of escapement used to resupply energy into the system. The behaviour is strongly influenced by the size of time delay and the magnitude of the coupling strength.
- The synchronization problem addressed here may seem artificial, but it may find interesting industrial applications like for example in the control of vibrations during the start-up phase of two generators/industrial motors, cf. [8], which are placed close to each other. Initially, the generators/motors can be forced to synchronize in anti-phase, this will reduce the amount of vibrations in the supporting structure and when the generators/motors are operating at nominal speed, they can be forced to synchronize in-phase in order to reduce the consumption of energy. According to the results presented here, this can be done by using the same control law and just varying one parameter, e.g. the time delay. Moreover, further studies of the proposed delayed Huygens' coupling may lead to understand similar phenomena occurring in other fields. For example in neurosystems, where it has been found that time delay induces transitions from in-phase to anti-phase synchronization in two coupled excitable neurons [73].
- The analysis presented here focused mainly on the in-phase or anti-phase synchronizing limit behaviour of the oscillators. However, it is worthwhile mentioning that for our system, other dynamical limit behaviours exist. For instance, amplitude death [24], where the oscillations of both oscillators decay. This has not only been observed in computer simulations but also in experiments (not included here).
- The experimental results have revealed that when the oscillators synchronize in anti-phase, the oscillation frequency corresponds to the frequency of the uncoupled self-driven oscillators. This results from the fact that in anti-phase, the coupling vanishes (as in the original Huygens' experiment) and, consequently, the oscillators run uncoupled (in the ideal case). When the oscillators synchronize in-phase, it has been found that the oscillation frequency can be tuned by properly choosing parameter α_1 in (6.6). This follows from the fact that α_1 can be seen as a kind of eigenfrequency of the 'virtual' coupling bar (6.5).

Chapter 7

Huygens' coupling: more than a rigid bar

Science is built up of facts, as a house is built of stones; but an accumulation of facts is no more a science than a heap of stones is a house.

Henri Poincaré (1854–1912)

Abstract This chapter presents numerical results related to the “true” infinite dimensional Huygens' coupling of pendulum clocks. The coupling structure, on which the clocks are hanging (a wooden bar on top of two chairs) is assumed to be *flexible*, i.e. the coupling structure is considered as an infinite dimensional system. A linear model is derived for this structure by using the Finite Element method. The pendula are considered as local nonlinearities and consequently the resulting coupled model consists of a finite set of nonlinear ordinary differential equations. Next, this model is used in order to obtain numerical results illustrating the possible limit behaviours of the system, like in-phase and anti-phase synchronization of the pendula. Finally, a discussion of the obtained results is presented.

7.1 Introduction

In order to derive a mathematical model of a real system it is unavoidable to make some simplifications, i.e. to idealize the system under consideration. In the case of the Huygens system of pendulum clocks, depicted in Figure 7.1(a), the model used in Chapter 2 of this thesis and the ones reported in the literature, see e.g. [5, 8, 54, 55, 75], are simplifications of the real situation: the coupling structure has been modelled as a single dof suspended rigid bar, each pendulum clock has been modelled by a driven and damped pendulum, and these pendula are both attached to the rigid coupling bar. However, in the real Huygens experiment, the bar, to which the clocks are attached, is indeed an infinite dimensional system (since the bar is flexible), for which, as far as is known, a rigorous study of the in-phase and anti-phase synchronized motion of the two pendula has never been carried out, although there are some related works where the coupling bar has been considered as a flexible beam, see e.g. [14, 33].

Note that the wooden coupling in Huygens' experiment can be modelled by a partial differential equation (pde) with suitable boundary conditions, whereas for each pendulum a simple ordinary differential equation may suffice. Deriving an analytic or numerical solution for such a model is not a trivial task. This can be circumvented by discretizing the pde by using the Finite Element (FE) method.

This chapter introduces a new model for the original Huygens experiment on synchronization. The model takes into account the flexibility of the coupling structure, on which the pendulums are hanging, and is derived by using the FE method and a component mode synthesis technique in order to reduce the number of dofs of the FE model.

The structure of the chapter is as follows. Section 7.2 presents the modeling of the system. Next, in Section 7.3, a numerical analysis is conducted in order to determine all the possible limit behaviours (like in-phase and anti-phase synchronization) of the coupled system. Then, in Section 7.4, a set of key parameters for the onset of synchronization is identified. Finally, a discussion of the obtained results is presented in Section 7.5.

7.2 Modeling of the system

In this section, a mathematical model for the classical Huygens setup of pendulum clocks, depicted in Figure 7.1(a), is derived. The coupling bar is modelled by a flexible horizontal beam, the chairs are modelled by two flexible vertical beams and

it is assumed that all beams can experience bending and axial stretching. First, in Subsection 7.2.1, a linear FE model is derived for this flexible structure. Secondly, in Subsection 7.2.2, each pendulum clock is modelled as a driven and damped swinging pendulum consisting of a small bob (modelled by a point mass) attached to the bottom side of a massless rigid bar, see Figure 7.1(b). The escapement mechanism that keeps each clock running is replaced by a control input, which is generated by using the angular displacement and angular velocity of each simple pendulum. Then, in Subsection 7.2.3, the pendula are coupled to the flexible structure.

7.2.1 Modeling of the supporting structure

Consider the flexible coupling structure depicted in Figure 7.1(b), i.e. the complete structure without the pendula. The horizontal beam, as well as both vertical beams, are discretized, as depicted in Figure 7.1(c), by using two node Euler beam elements¹. At each node, there are three dofs namely axial displacement, transversal displacement, and rotation. Note that only 2D in-plane deformation of the system is considered. At the two contact points between the horizontal beam and the two vertical beams, the rotational dof corresponding to the horizontal beam is uncoupled from the rotational dof corresponding to the vertical beam similar to the situation of Huygens' experiment. The coupling structure is assumed to have geometrical and material properties as given in Table 7.1. Some of the parameter values (length and thickness of the horizontal beam) have been taken from the details provided by Huygens in his lab notebook cf. [63]. The parameter values for the vertical beams have been estimated based on a standard chair. Furthermore, it has been assumed that all beams are made of (parana) pine wood.

The horizontal beam is discretized by 99 beam elements and the vertical beams by 100 beam elements each. This yields, after assembling all beam elements and after imposing the displacement boundary conditions², a FE model with $n = 896$ dofs given by

$$M\ddot{q} + B\dot{q} + Kq = f \quad (7.1)$$

where $q \in \mathbb{R}^{n \times 1}$ is a column with dofs (labeled as D'_i s in Figure 7.1(c)). Matrices $M \in \mathbb{R}^{n \times n}$, $B \in \mathbb{R}^{n \times n}$, and $K \in \mathbb{R}^{n \times n}$, and column $f \in \mathbb{R}^{n \times 1}$ are the (global) mass, damping, and stiffness matrix, and the column with external loads and coupling loads from both pendula, respectively.

¹The mass and stiffness matrices for a single Euler beam element are provided in Appendix B.

²The vertical beams are fixed to the world at their bottom sides, hence 6 dofs are constrained to be zero.

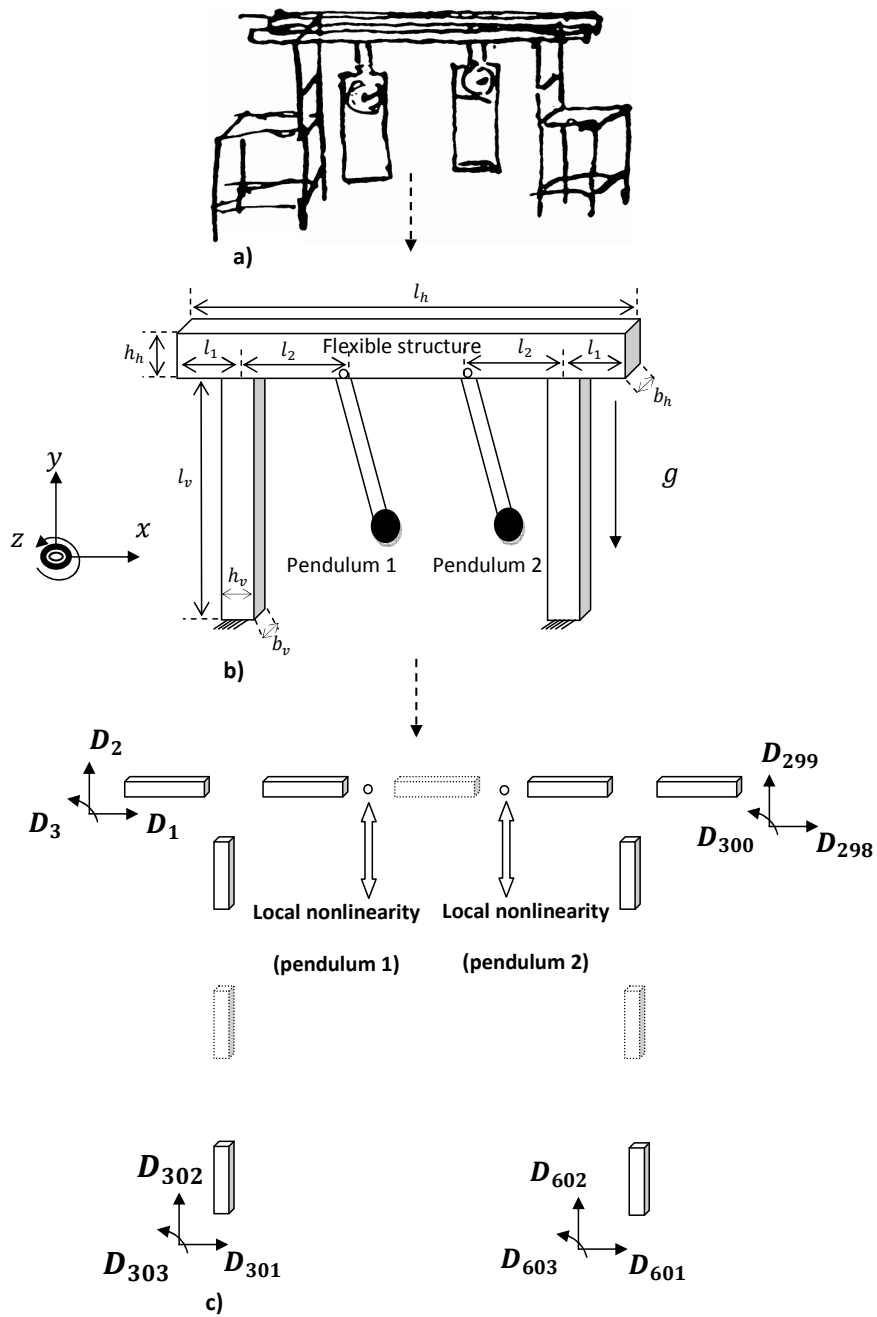


Figure 7.1 (a) Classical Huygens setup. (b) Idealized model. (c) Discretized model.

Table 7.1 Geometrical and material (wood) properties of the coupling structure.

Property	Horizontal beam	Each vertical beam
Length	$l_h = 2.4$ [m]	$l_v = 1$ [m]
Width	$b_h = 0.55$ [m]	$b_v = 0.03$ [m]
Thickness	$h_h = 0.0762$ [m]	$h_v = 0.03$ [m]
Density	$\rho_h = 560$ [kg/m ³]	$\rho_v = \rho_h$ [kg/m ³]
Young's modulus	$E_h = 8.963 \cdot 10^9$ [N/m ²]	$E_v = E_h$ [N/m ²]
Other dimensions, see Figure 7.1b).		
	$l_1 = 0.0242$ [m]	
	$l_2 = 1.0667$ [m]	

Next, a modal analysis is performed in order to determine the undamped eigenfrequencies and corresponding eigenmodes of the coupling structure. This is achieved by solving the eigenvalue problem

$$[K - \omega_i^2 M] \varphi_i = 0, \quad i = 1, \dots, n, \quad (7.2)$$

where $\omega_i = 2\pi f_i$ is the i^{th} undamped angular eigenfrequency in [rad/s] and φ_i is the corresponding mode shape.

Table 7.2 shows the five lowest eigenfrequencies in Hz. Clearly, for the considered geometrical and material properties, see Table 7.1, the eigenfrequency f_1 of the first mode almost coincides with the oscillation frequency of a standard pendulum clock (1 Hz).

Table 7.2 Lowest eigenfrequencies of the coupling structure.

i	f_i [Hz]
1	1.2749
2	24.1724
3	85.0168
4	85.1116
5	86.8341

The corresponding modeshapes are depicted in Figure 7.2. Note that in eigenmodes 1,3, and 4, the vertical beams experience bending, whereas the deformations in the horizontal beam are almost negligible. In contrast, eigenmodes 2 and 5 show bending of the horizontal beam, whereas the deformations in the vertical beams are imperceptible.

The eigenmodes are normalized on the mass matrix, i.e. $\varphi^T M \varphi = I$ where φ contains the eigenmodes φ_i , which are stored columnwise and I is an identity

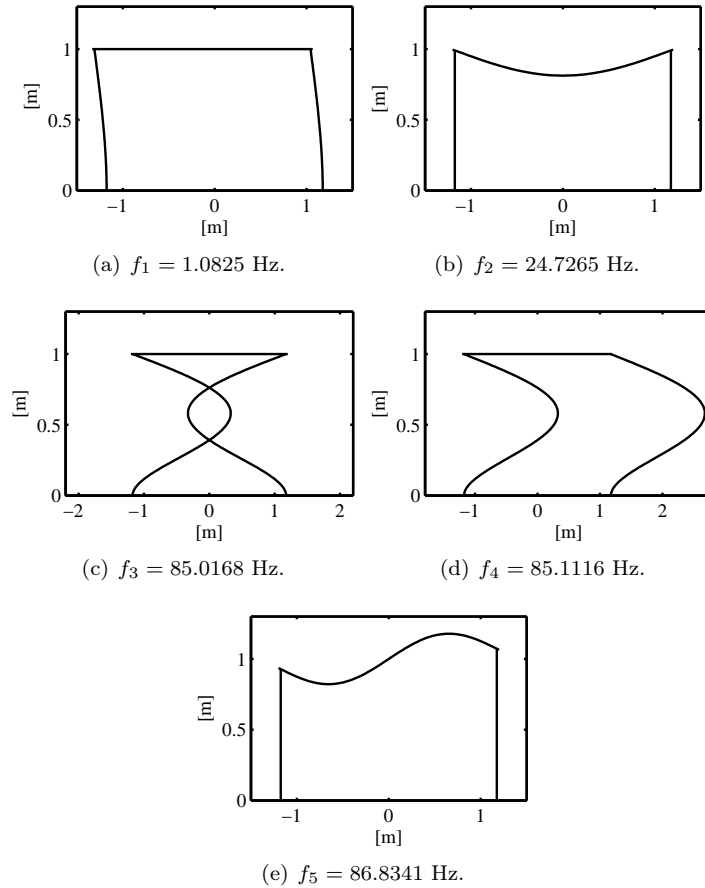


Figure 7.2 Modeshapes corresponding to the five lowest eigenfrequencies.

matrix of appropriate dimensions. When this normalization is combined with the eigenvalue problem (7.2), it can easily be shown that $\varphi^T K \varphi = \Omega$, where Ω is a diagonal matrix containing the angular eigenfrequencies ω_i .

Now, assuming proportional damping, the damping matrix B in (7.1) is computed according to $B = 2\varphi^T Z \Omega \varphi^{-1}$, where Z is a diagonal matrix with dimensionless damping coefficients ζ_i for eigenmode i .

In Appendix C, a static analysis is conducted. It is shown that the influence of the gravity in the coupling structure is negligible and it is demonstrated that the vertical beams are not close to buckling.

Reduction of the model

As seen earlier, in the equations of motion (7.1) describing the linear dynamic behaviour of the wooden coupling structure many hundreds of dofs are involved. It is well-known that numerical solution of this kind of systems (many dofs) may become computationally costly. This is especially true when the final model is nonlinear and parameter studies need to be carried out as is the case in the current study. In order to prevent this, a dynamic model reduction technique for linear systems is used [12, 25]. The technique belonging to the class of component mode synthesis techniques is based on free-interface eigenmodes and residual flexibility modes and allows deriving a reduced model, which is accurate within a certain frequency range of interest. The method is as follows.

First, column q , see (7.1), is partitioned as

$$q = \begin{bmatrix} q_B \\ q_I \end{bmatrix}, \quad (7.3)$$

where $q_B \in \mathbb{R}^{n_B \times 1}$ contains the *boundary dofs* and $q_I \in \mathbb{R}^{n_I \times 1}$ contains the *internal dofs*. The boundary dofs are the dofs that are coupled to the pendula.

Next, a transformation from original (physical) dofs to generalized dofs is performed

$$q = T_1 p_1, \quad T_1 = [\phi_B \quad \phi_K]; \quad p_1 = \begin{bmatrix} p_B \\ p_K \end{bmatrix}, \quad (7.4)$$

where matrix $\phi_K \in \mathbb{R}^{n \times n_K}$ contains the kept elastic eigenmodes, which are the mass normalized solutions φ_i of the undamped eigenproblem (7.2) for $\omega_i \in (0, \omega_c]$ for $i = 1, \dots, n_K$. The angular cut-off frequency ω_c is chosen by the user.

The matrix $\phi_B \in \mathbb{R}^{n \times n_B}$ contains residual flexibility modes (they provide a static correction for the deleted higher frequency eigenmodes) and is defined as follows

$$\phi_B = [K^{-1} - \phi_K \Omega_{KK}^{-2} \phi_K^T] [I_{BB} \quad 0_{BI}]^T, \quad (7.5)$$

where $\Omega_{KK} \in \mathbb{R}^{n_K \times n_K}$ is a diagonal matrix with the kept angular eigenfrequencies lower than or equal to ω_c .

For the sake of easy coupling later in Subsection 7.2.2, the generalized dofs p_1 described in (7.4) are transformed according to

$$p_1 = T_2 p, \quad p = \begin{bmatrix} p_B \\ p_K \end{bmatrix}, \quad (7.6)$$

with

$$T_2 = \begin{bmatrix} \phi_{BB}^{-1} & -\phi_{BB}^{-1} \phi_{BK} \\ O_{KB} & I_{KK} \end{bmatrix}. \quad (7.7)$$

Finally, the total transformation matrix verifies (by combining (7.4) and (7.6))

$$T = T_1 T_2 \quad (7.8)$$

and the reduced equations of motion for the wooden flexible coupling structure become

$$\underbrace{T^T M T}_{M_r} \ddot{p} + \underbrace{T^T B T}_{B_r} \dot{p} + \underbrace{T^T K T}_{K_r} p = \underbrace{T^T f}_{f_r}. \quad (7.9)$$

where $f_r = [f_{x1} \ f_{y1} \ f_{x2} \ f_{y2} \ f_{int}]^T$, f_{xi} , $i = 1, 2$, is the horizontal force exerted by pendulum i at the horizontal boundary dof where pendulum i is attached, f_{yi} , $i = 1, 2$, is the vertical force exerted by pendulum i at the vertical boundary dof where pendulum i is attached and f_{int} is a zero row of appropriate dimensions.

For the present application only the lowest eigenfrequencies are of interest. The reason behind this is that the structure is assumed to only be excited by the pendula, which operate near 1 Hz. Therefore, only the first 5 lowest eigenmodes are kept and, consequently, the resulting reduced model is accurate up to approximately $f_c = 90$ Hz (see Table 7.2). The reduced model (7.9) will have 9 dofs: 4 boundary dofs and 5 dofs corresponding to kept dynamic eigenmodes.

7.2.2 Modeling of the pendula

Each pendulum is modelled by a point mass of mass m_i [kg] attached at the lower end of a massless rigid bar of length l_i [m]. The damping in each pendulum is assumed to be viscous, linear, and concentrated in the revolute joint, which couples the pendulum to the coupling structure. The rotational damping coefficient is d_i [Nms/rad]. The dynamic behaviour of each (uncoupled) pendulum is described by the (idealized) set of equations

$$\ddot{\theta}_i = -\frac{g}{l_i} \sin \theta_i - \frac{d_i}{m_i l_i^2} \dot{\theta}_i + \frac{u_i}{m_i l_i^2}, \quad i = 1, 2, \quad (7.10)$$

where g [m/s²] is the gravitational acceleration, $\theta_i \in \mathcal{S}^1$ is the rotation angle of pendulum i in [rad], and u_i , $i = 1, 2$, represents the so-called escapement mechanism of pendulum i in [Nm].

The modelling of an escapement mechanism is not a trivial task [72]. For this reason, in literature, usually the escapement mechanism is replaced by a (non-linear) function, which depends on the angular displacement and velocity of the pendulum [17, 26]. In the present case, the escapement mechanism is modelled by

the nonlinear function [54]

$$u_i = \begin{cases} -\sigma \left(\frac{1 - \cos\left(\frac{2\pi\theta - \phi}{\Delta\phi}\right)}{2\Delta\phi} \right) & \text{for } (\theta_i \leq \phi) \wedge (\theta_i \geq \phi - \Delta\phi) \wedge (\dot{\theta} < 0) \\ \sigma \left(\frac{1 - \cos\left(\frac{2\pi\theta - \phi}{\Delta\phi}\right)}{2\Delta\phi} \right) & \text{for } (\theta_i \geq -\phi) \wedge (\theta_i \leq -\phi + \Delta\phi) \wedge (\dot{\theta} > 0) \\ 0 & \text{otherwise,} \end{cases} \quad (7.11)$$

where θ_i , $i = 1, 2$, is the rotation angle of pendulum i and $\sigma > 0$, $\phi < 0$, and $\Delta\phi > 0$ are design parameters. The operation of the escapement is depicted in Figure 7.3, where the time series for the exerted torque and angular displacement are shown. Basically, a ‘kick’ is delivered to the pendulum each time that the pendulum reaches a threshold angle³.

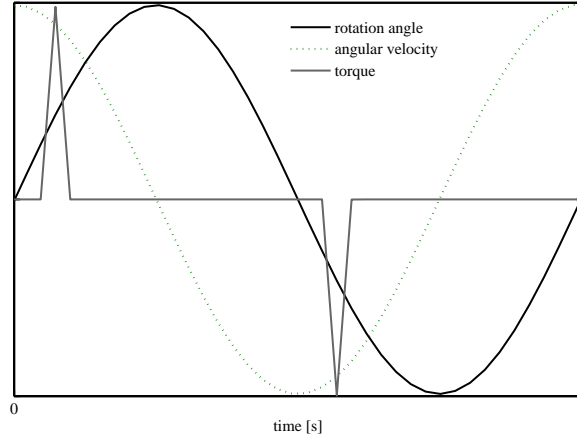


Figure 7.3 The torque on the pendulum exerted by the escapement mechanism. The quantities have been scaled by using their corresponding infinity norm.

7.2.3 Coupling of the pendulums to the structure

In order to derive the coupled model the free body diagram depicted in Figure 7.4 is considered. The horizontal and vertical displacements corresponding to the boundary node i (the node, at which pendulum i is attached to the structure) are

³Note however that other state dependent nonlinear functions can be considered as well, as for example the ones discussed in Chapters 3 and 4.

given by x_i and y_i , respectively. The horizontal motion of the pendulum's bob is

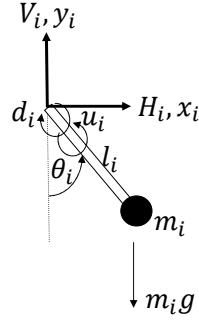


Figure 7.4 Free body diagram at each boundary node.

described by

$$m_i \frac{d^2}{dt^2} (x_i + l_i \sin \theta_i) = H_i, \quad i = 1, 2, \quad (7.12)$$

where $H_i = -f_{x_i}$ is the horizontal force exerted by the structure to the upper side of the pendulum. The vertical motion is described by

$$m_i \frac{d^2}{dt^2} (y_i - l_i \cos \theta_i) = V_i - m_i g \quad i = 1, 2, \quad (7.13)$$

where $V_i = -f_{y_i}$ is the vertical force exerted by the structure to the upper side of the pendulum.

Equilibrium of moments with respect to an axis in z-direction going through point mass m_i results in

$$0 = -H_i l_i \cos \theta_i - V_i l_i \sin \theta_i - d_i \dot{\theta}_i + u_i, \quad i = 1, 2. \quad (7.14)$$

By combining (7.12)-(7.14), the following equation can be determined

$$m_i l_i^2 \ddot{\theta}_i = -m_i l_i \ddot{x}_i \cos \theta_i - m_i \ddot{y}_i l_i \sin \theta_i - m_i g l_i \sin \theta_i - d_i \dot{\theta}_i + u_i \quad i = 1, 2. \quad (7.15)$$

After coupling of the pendula to the structure, the dynamic model of the idealized Huygens setup of synchronization, depicted in Figure 7.1(b), consists of 11 dofs and is described by the following set of equations

$$M_r \ddot{p} = -K_r p - B_r \dot{p} + f_r \quad (7.16)$$

$$m_i l_i^2 \ddot{\theta}_i = -m_i l_i \ddot{x}_i \cos \theta_i - m_i \ddot{y}_i l_i \sin \theta_i - m_i g l_i \sin \theta_i - d_i \dot{\theta}_i + u_i, \quad i = 1, 2 \quad (7.17)$$

where $p = [x_1 \ y_1 \ x_2 \ y_2 \ p_1 \ p_2 \ p_3 \ p_4 \ p_5]^T$ is the column of boundary dofs and modal dofs, $\theta_i \in \mathcal{S}^1$ is the rotation angle of pendulum i , and M_r , B_r , and K_r are matrices as described in (7.9). The force column of the flexible structure is given by $f_r = [-H_1 \ -V_1 \ -H_2 \ -V_2 \ f_{int}]^T$ where H_i , $i = 1, 2$, is as given in (7.12), V_i , $i = 1, 2$, as given in (7.13), and f_{int} is a zero row of appropriate dimensions.

7.3 Numerical analysis

In this section, numerical analyses will be carried out in order to determine all potential synchronizing limit solutions of system (7.16)-(7.17). In particular, the dependence of the synchronized motion of the pendula on system parameters and initial conditions is studied by means of computer simulations.

Since in system (7.16)-(7.17) there are quite a number of parameters, for a manageable parameter study it is necessary to choose those parameters, which dominantly influence the occurrence of and type of synchronized motion. At this point, it is worth to remember that in previous chapters and in the literature, see e.g. [5, 17], it has been shown that (in a simpler model) the “critical parameters” determining the occurrence and type of synchronization are: the ratio of the mass of each pendulum and the mass of the coupling bar, and the amount of damping in the system. Furthermore, the initial conditions also may play a role in the occurring type of synchronized behaviour.

This section presents three numerical parameter studies based on numerical integration of (7.16)-(7.17), in which different (combinations of) parameters are varied.

First, the synchronized motion of the coupled system is studied as a function of the mass of each pendulum and the initial angle of pendulum two. The parameter values of the structure are as given in Table 7.1 with damping coefficients $\zeta_i = 0.01$ [-]. The parameter values for the pendula, see (7.17), are $l_1 = l_2 = 0.2286^4$ [m], $d_1 = d_2 = 0.01$ [Nms/rad], and the mass of each pendulum is (simultaneously) varied from 0.2 to 7 [kg] in steps of 0.05 [kg], i.e. $m_1 = m_2 \in [0.2, 7]$ [kg]. For the escapement mechanism (7.11), the parameter values are $\sigma = 8 \times 10^{-3}$ [Nm], $\phi = -\Delta_\phi = -0.06$ [rad]. The nonzero initial conditions are $\theta_1 = 0.2$ [rad] and θ_2 is varied in the interval $[-0.2, 0.2]$ [rad] in steps of 0.02 [rad].

The obtained results are depicted in Figure 7.5. When the mass of each pendulum is lower than approximately 0.65 [kg], the pendula synchronize in-phase (green area) for most of the initial conditions. Note, however, that there is a region around the origin, denoted by the brown area, where the initial condition of the second pendulum is not large enough to “engage” this pendulum to its escapement mechanism. As a consequence, the second pendulum never gets energy from its escapement mechanism. However, due to the vibrations of pendulum one, the second pendulum shows small oscillations and the phase difference between the pendula remains constant but is neither 0 degrees nor 180 degrees, as depicted in Figure 7.6. When the mass of each pendulum is slightly increased, then the only existing regime is in-phase synchronization, as can be seen in Figure 7.5 for the

⁴This value is taken from Huygens’ laboratory notebook, see [63].

interval $m_1 = m_2 \in [0.65, 0.8]$ [kg]. The anti-phase synchronized motion appears when the mass of each pendulum is further increased (blue area). From Figure 7.5 it is clear that in the interval $m_1 = m_2 \in [0.8, 7]$ [kg], the in-phase region shrinks and the anti-phase region grows. Between the boundaries of the in-phase and anti-phase synchronization regions, there are small areas, denoted by a dark blue color, where the pendula show unsynchronized behaviour (or have not come to a 'steady-state' yet).

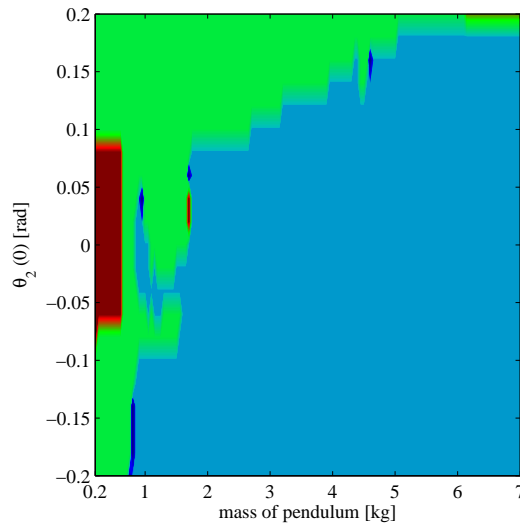


Figure 7.5 Limit response of the coupled system (7.16)-(7.17) as a function of the mass of each pendulum and the initial condition $\theta_2(0)$ [rad]. The colors indicate the type of behaviour the system exhibits after 1500 [s]; blue for anti-phase, green for in-phase, brown for the case where the oscillations of pendulum 2 are due to the influence of pendulum 1 and not due to the escapement (phase difference is constant), and dark blue for unsynchronized behaviour.

In the second parameter study, the limit behaviour of system (7.16)-(7.17) is investigated as a function of the damping in the flexible structure and again the initial angle of pendulum two. The parameter values are almost the same as used in the previous simulation except for the mass of each pendulum, which now is $m_1 = m_2 = 0.8267$ [kg] and the damping coefficient $\zeta = \zeta_i$, which is varied now in the interval $\zeta \in [0.01, 0.4]$ [-] in steps of 0.005 [-]. The initial conditions are also the same as used in the first parameter study.

As can be seen in Figure 7.7, for small damping the pendula may synchronize either in-phase (green area), in anti-phase (blue area) or run unsynchronized (dark blue

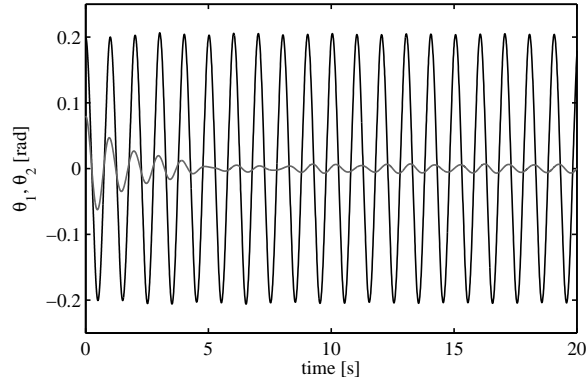


Figure 7.6 The initial condition $\theta_2(0)$ of pendulum two is not enough to engage the pendulum to the escapement mechanism. Nevertheless, pendulum two (grey line) shows small oscillations due to the vibrations of pendulum one (black line).

area). For larger damping, the in-phase synchronized motion disappears. For certain initial conditions around the origin, the escapement of pendulum two will never work. However, the vibrations of pendulum one, transmitted via the flexible structure, will keep pendulum two oscillating, although with small amplitude. Again, there is a constant phase difference between the two oscillators, but they are oscillating neither in-phase nor in anti-phase and have different amplitude, as already shown in Figure 7.6.

Again, the anti-phase synchronized motion is the dominant limit behaviour.

Finally, the influence of the width of the horizontal beam and the initial angle of pendulum two on the synchronized motion of the coupled pendula is studied. It is clear that, by varying the width of the horizontal beam, not only its mass but also its stiffness is modified. The parameter values for the flexible structure are (see Table 7.1 for definition of the parameters): $h_h = 0.1876$ [-], $b_v = b_v = 0.04$ [m], $h_v = h_v = 0.03$ [m] and $\zeta = 0.2$ [-]. For the pendula (7.17) the following is assumed: $m_1 = m_2 = 1.1226$ [kg], $l_1 = l_2 = 0.2286$ [m], $d_1 = d_2 = 0.01$ [Nms/rad]; the parameter values in the escapement mechanism (7.11) are : $\sigma = 6 \times 10^{-3}$ [Nm], $\phi = -0.05$ [rad] and $\Delta_\phi = 0.05$ [rad].

Figure 7.8 shows the obtained results. For a narrow horizontal beam (light beam), the in-phase motion is more dominant than the anti-phase motion. When the width increases (heavier beam) the in-phase motion disappears and the pendula eventually synchronize in anti-phase for all the initial conditions. The results for the latter case are in line with the observations made by Huygens. In his case, the

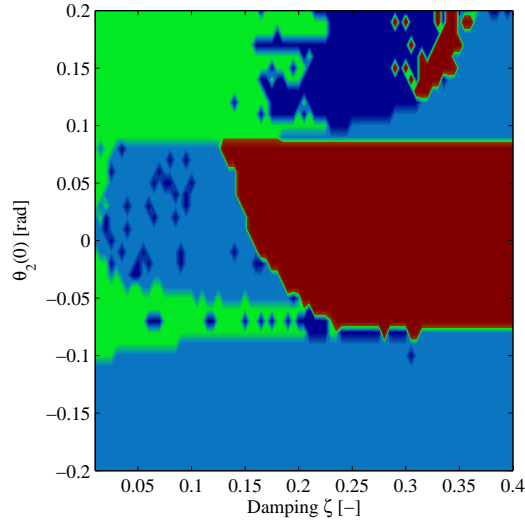


Figure 7.7 Limit response of the coupled system (7.16)-(7.17) as a function of the damping coefficient ζ [-] and the initial condition $\theta_2(0)$ [rad]. The colors indicate the type of behaviour the system exhibits after 1500 [s]; blue for anti-phase, green for in-phase, brown for the case where the oscillations of pendulum 2 are due to the influence of pendulum 1 and not due to the escapement (phase difference is constant), and dark blue for unsynchronized behaviour.

extra mass placed at the bottom of the cases of the pendulum clocks (around 45 [kg]), increased the total mass of the horizontal beam, i.e. Huygens setup had a heavy horizontal beam.

Other limit behaviours

Besides the aforementioned (synchronizing) limit solutions, other limit behaviours can be observed in system (7.16)-(7.17). In particular, three additional ‘stationary’ solutions of the pendula have been observed: quenching (oscillations death), beating death, and seemingly chaotic motion. These limit solutions are explained in what follows. The numerical results are obtained by numerical integration of (7.16)-(7.17) with parameter values: $l_1 = l_2 = 0.2286$ [m], $d_1 = d_2 = 0.0106$ [Nms/rad], $m_1 = m_2 = 0.4226$ [kg], $\sigma = 4 \times 10^{-3}$ [Nm rad], $\phi = -0.06$ [rad] and $\Delta_\phi = 0.06$ [rad]. The parameter values of the coupling structure are given in Table 7.1, except $b_h = 0.25$ [m], $b_v = 0.100$ [m] and $h_v = 0.012$ [m].

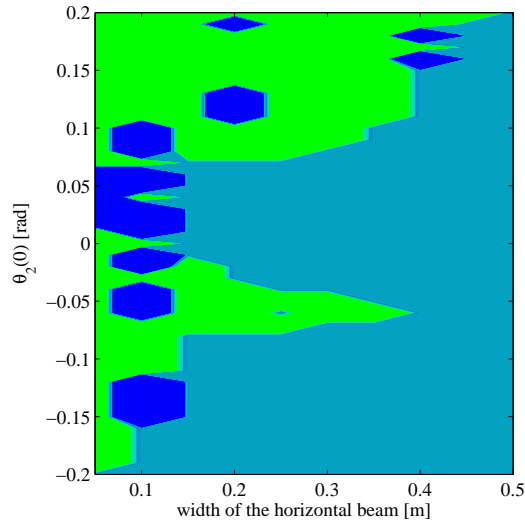


Figure 7.8 Limit response of the coupled system (7.16)-(7.17) as a function of the width b_h [m] of the coupling bar and the initial condition $\theta_2(0)$ [rad]. The colors indicate the type of behaviour the system exhibits after 1500 [s]; blue for anti-phase, green for in-phase, and dark blue for unsynchronized behaviour.

- **Quenching.** Sir John William Strutt, Lord Rayleigh (1842-1919) observed mutual synchronization in two (similar) organ tubes, but also he observed the effect of quenching (oscillation death), i.e. when the coupling results in suppression of oscillations of the interacting systems. The derived model (7.16)-(7.17) also shows this behaviour as depicted in Figure 7.9. The pendula are released from the initial conditions $\theta_1(0) = 0.26$ [rad] and $\theta_2(0) = 0.26$ [rad]. Other initial conditions are zero. The time series of the pendula is depicted in Figure 7.9. The quenching (oscillation death) phenomenon is evident.
- **Beating death.** Figure 7.10 shows a peculiar behaviour: the escapement mechanism of one pendulum stops working. Notwithstanding this, the pendulum remains oscillating (with small amplitude) due to the influence, exerted via the coupling structure, of the other pendulum. The nonzero initial conditions used in this case are $\theta_1(0) = 0.21$ [rad] and $\theta_2(0) = 0$ [rad]. The escapement mechanism of pendulum 2 stops working after $t = 10.71$ [s] as depicted in Figure 7.10(d).
- **Chaotic motion.** When the damping in the pendula is slightly decreased, it is possible to observe chaotic behaviour in the coupled pendula as shown

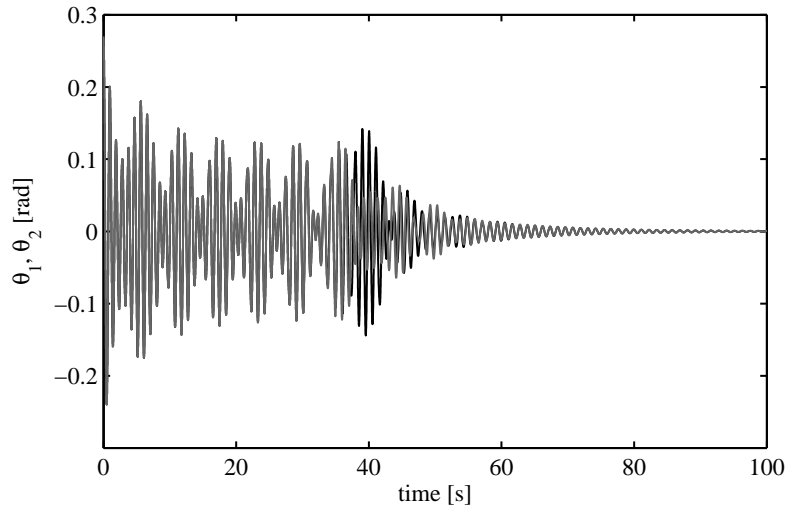


Figure 7.9 Quenching (oscillation death).

in Figure 7.11. The initial conditions of the pendula are the same as the one used in the previous case (beating death) but the damping in the pendula is decreased to $d_1 = d_2 = 0.0106$ [Nms/rad].

7.4 Key parameters for the onset of synchronization

From the numerical study presented in the previous section, it is possible to draw some conclusions regarding key parameters that have a large influence in the limit behaviour of the system. These parameters are listed as follows:

- the ratio of the mass of each pendulum and the coupling beam mass. Given a flexible structure with certain fixed parameters, the onset of in-phase or anti-phase synchronized motion may be triggered by increasing or decreasing the mass of the pendula while keeping the effective mass of the coupling structure constant, or vice versa. In particular, from the results presented in Figure 7.5, it follows that for a slightly damped structure, the pendula synchronize in anti-phase (for almost all initial conditions) when their mass is increased.
- the amount of damping in the system. If damping is neglected in the flexible structure, then synchronization will not occur because transient behaviour

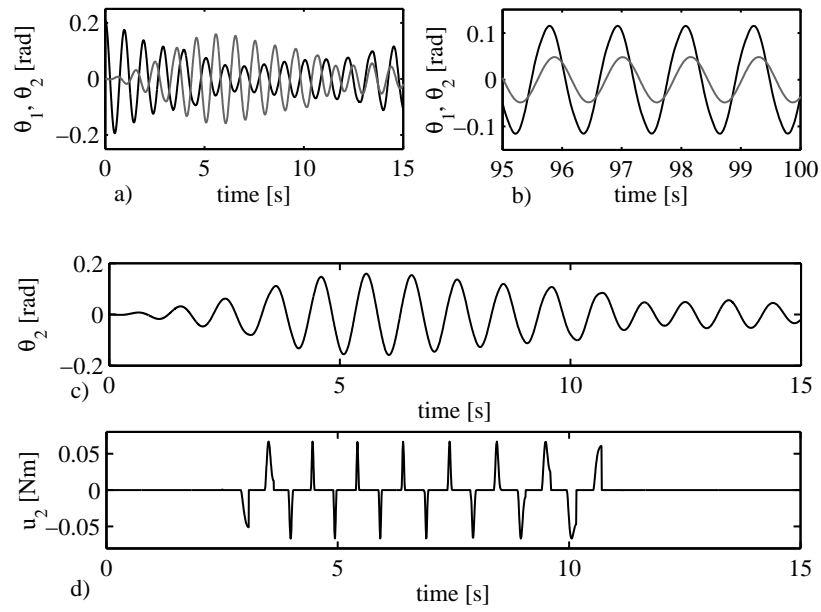


Figure 7.10 Beating death. a) Transient behaviour. b) Limit behaviour. c) Time series for θ_2 in the interval $0 \leq t \leq 15$. d) Time response of the escapement mechanism of pendulum two in the interval $0 \leq t \leq 15$. In figures a) and b), black line: θ_1 , grey line: θ_2 .

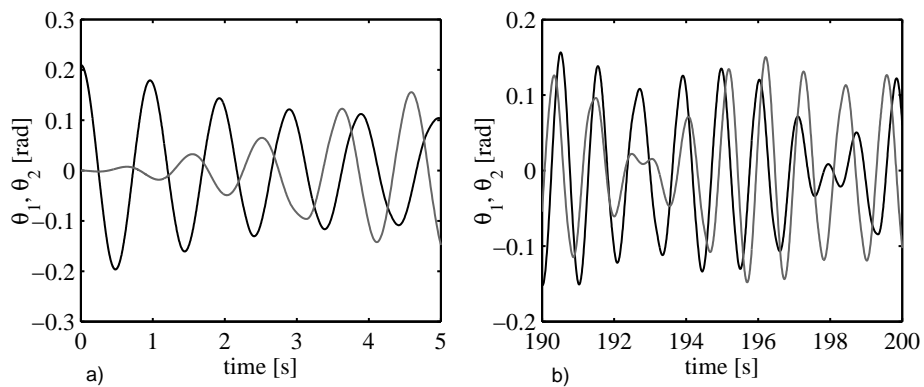


Figure 7.11 Chaotic motion. a) Transient behaviour. b) Limit behaviour. Black line: θ_1 , grey line: θ_2 .

will not disappear. When small damping is included in the model of the structure, both in-phase and anti-phase regimes exist. When the damping in the structure is large, anti-phase synchronized motion seems to be dominant.

- the cross-sectional area ratio between the horizontal beam and the vertical beams. The vertical beams, on which the horizontal beam is placed, should be more flexible than the horizontal beam. With this choice, it is guaranteed that the first eigenmode of the structure corresponds to a horizontal displacement of the horizontal beam. One way of achieving this is by taking vertical beams with relatively small cross-sectional area compared to the cross-sectional area of the horizontal beam. In [15], the authors were not able to carry out successful experiments possibly due to the fact that they used a structure where the horizontal/vertical beam cross-sectional area ratio is nearly one.
- the escapement mechanism. Due to the damping in the flexible structure and in the revolute joints by which the pendula are attached to the structure, initial energy in the system will be partly dissipated. Therefore, in order to have sustained oscillations of the pendula with a certain desired amplitude, an escapement mechanism should be included. Note, however, that the escapement mechanism does not affect directly the occurrence of phase synchronization, but is a necessary element in the system. In this chapter, escapement (7.II) was used. However, other escapement mechanisms can/may be used as for example the ones presented in previous chapters.

7.5 Discussion

This chapter has presented a new model for the original Huygens setup of pendulum clocks. The model incorporates the flexibility of the coupling structure and it has been derived by using the FE method in combination with a component mode synthesis technique. By means of numerical analysis, the possible limit behaviours of the system, for certain combinations of parameter values and initial conditions, have been determined. It has been found that the coupled pendula may show in-phase and anti-phase synchronized motion.

On the one hand, the obtained results are comparable to the results obtained with more simplified models, as the ones considered in previous chapters. For instance, the results for a slightly damped bar, presented in Chapter 3, are in good agreement

with the results presented in Figure 7.5, whereas the results presented in Figure 7.8 for a flexible structure with large damping are in line with the analysis presented in Chapter 4. On the other hand, other limit behaviours have been observed in the coupled pendula, namely quenching (oscillation death), beating death, and seemingly chaotic motion. As far as is known, these ‘stationary’ solutions were not reported by Huygens.

Hence, it should be clear that the derived model for the Huygens setup of coupled pendulum clocks is more complete, not only in the sense that it takes into account more properties of the coupling structure, but also because it reveals that there are more limit solutions besides in-phase and anti-phase synchronization.

Finally, note that there is still a challenge: a study of the stability of the ‘stationary’ or limit solutions presented in the previous section. However, this stability study turns out to be complicated, in part, due to the impulsive nature of the escapement mechanism. A recommendation for addressing this issue is provided in the next chapter.

Chapter 8

Conclusions and Recommendations

I think and think for months and years. Ninety-nine times, the conclusion is false. The hundredth time I am right.

Albert Einstein (1879 - 1955)

Abstract In this chapter, conclusions of this thesis are given. In addition, recommendations for future research directions are provided.

8.1 Conclusions

In this thesis, the occurrence of synchronization in pairs of nonlinear oscillators interacting via Huygens' coupling has been investigated. By means of analytic results, computer simulations, and experimental results it has been demonstrated that the "sympathy" observed by Huygens more than 3 centuries ago in a pair of pendulum clocks, can also be observed even if the pendulums are replaced by other nonlinear oscillators. Although Huygens' experiment has been revisited several times, in literature, the analysis always centers on a specific type of oscillators, namely metronomes. Consequently, the objective of this thesis is to extend the study of Huygens' experiment on synchronization to other second order self-driven oscillators with Huygens' coupling.

In the first part of this thesis, the problem of *natural*, i.e. unforced synchronization of coupled second order nonlinear oscillators has been addressed. It has been shown that two self-sustained nonlinear oscillators linked via Huygens' coupling, i.e. a single dof suspended rigid bar, may synchronize in-phase or in anti-phase

depending on the amount of coupling strength, i.e. the ratio between the oscillators' mass and the mass of the coupling bar. Two cases have been considered, namely oscillators with small coupling strength, small damping, weak excitation forces, and weak nonlinearities and oscillators without these limitations.

The first case has been studied in Chapter 3. Sufficient conditions for the existence and stability of synchronous solutions in the coupled oscillators have been derived by using the Poincaré perturbation method based on a small parameter. This small parameter appears naturally in the system and corresponds to the coupling strength. The theoretical results are supported by means of computer simulations and experimental results. It has been found that when the coupling strength is increased (but still weak), i.e. by decreasing the mass of the coupling bar, anti-phase synchronization is the only expected stable synchronous mode, whereas when the coupling strength is decreased, i.e. by increasing the mass of the coupling bar, it is possible to have two stable synchronous solutions, namely in-phase and anti-phase synchronized motion, depending on the initial conditions. Once the oscillators have synchronized in anti-phase, the coupling bar no longer influences the oscillators because it has come to rest and, consequently, the oscillation frequency will be determined by the uncoupled oscillators. However, when the oscillators have synchronized in-phase, the coupling bar converges to an oscillatory motion, which will influence the oscillation frequency of the oscillators.

The second case, i.e. coupled oscillators without the above mentioned limitations has been studied in Chapter 4. Since it is much more difficult to study this case analytically, the synchronized motion in these oscillators has been largely illustrated by means of experiments. In addition, some conditions related to the stability of the anti-phase synchronous motion have been derived. These conditions are in good agreement with computer simulations and with the experiments. Similar to the case studied in Chapter 3, it has been found that the synchronized limit behaviour in the oscillators is influenced by the mass of the coupling bar, i.e. by the coupling strength. Furthermore, from a comparison of the obtained results in Chapter 3 and Chapter 4, it has been concluded that the limit synchronizing behaviour of the coupled oscillators not only depends on the magnitude of the coupling strength but also the amount of damping in the system has an important influence on the type of synchronized behaviour.

The second part of the thesis has presented a study of *controlled* synchronization of oscillators with Huygens' coupling.

First, in Chapter 5, the problem of (controlled) synchronization of chaotic oscillators has been considered. It has been shown that by driving the coupling bar with an external periodic excitation, it is possible to trigger the onset of chaos in the oscillators. The mass of the coupling bar has been considered as the bi-

furcation parameter. When the oscillators behave chaotically, the synchronization phenomenon does not occur naturally. Consequently, it has been demonstrated that by using a master/slave configuration, it is possible to achieve (controlled) synchronization in the chaotic oscillators. Additionally, it has been shown that the chaotic behaviour may disappear when the oscillators are synchronized in anti-phase.

Secondly, the effect of time delay in the synchronized motion of possibly remote oscillators with Huygens' coupling has been investigated in Chapter 6. It has been assumed that the oscillators are not physically connected via the coupling bar. Rather, a suitable control input is created and applied to each oscillator, such that, in closed loop, the oscillators resemble a pair of oscillators with Huygens' coupling. In this approach, the oscillators do not need to be at the same location and moreover, the mechanism generating the control input should be implemented separately, using for instance a computer. Consequently, the possibility of having communication time-delays (either in the oscillators or in the applied control input) comes into play. The onset of in-phase and anti-phase synchronization in the coupled/controlled oscillators has been studied as a function of the coupling strength and the time delay. It has been found that the synchronized motion of the oscillators with delayed coupling may experience a phase-flip bifurcation, i.e. an abrupt change from in-phase to antiphase synchronization and vice versa due to a variation in the time delay and/or due to a variation in the magnitude of coupling strength. For the three types of oscillators considered there is a striking similarity in the limit behaviour of the oscillators. These results suggest that the limit behaviour of the system is independent of the type of controller used to resupply energy into the system.

In the third part of this thesis, a new model for the original Huygens setup of pendulum clocks has been derived and presented in Chapter 7. The model of the classical Huygens experiment on synchronization used in Chapters 2 to 6, and the ones reported in the literature are simplifications of the real setup of coupled pendulum clocks used by Huygens: the coupling bar has been considered as a single dof rigid body. However, in the real Huygens experiment, the coupling structure, to which the clocks are attached, is indeed an infinite dimensional system, since the structure is flexible.

In the derived model, the coupling bar is considered as a horizontal flexible beam and the chairs are replaced by two flexible vertical beams. It has been assumed that all three beams can experience bending and axial stretching. The model of the coupling structure has been derived by using the FE method and a component mode synthesis technique in order to reduce the number of dofs in the FE model. Each pendulum clock has been modelled as a self-driven, damped pendulum consisting of a small bob attached to the bottom of a massless rigid bar. Suitable

control inputs for both pendula have been included in order to mimic the escapement mechanism that keeps a pendulum clock running. By means of a numerical analysis, the possible limit behaviours of the system, for certain combinations of parameters and initial conditions, have been determined. It has been found that important parameters that influence the limit behaviour are the mass of each pendulum, the mass of the horizontal coupling bar, the damping in the system, and the cross sectional area of the vertical supports, on which the horizontal coupling bar is placed. The numerical analysis has revealed that in many situations the coupled pendula show in-phase and anti-phase synchronized motion. However, there exist other limit behaviours not reported by Huygens, like quenching (oscillation death), beating death, seemingly chaotic motion, and unsynchronized behaviour.

8.2 Recommendations

Based on the results of this thesis, some recommendations and directions for future research are given below.

- In Chapter 3, analytical conditions for existence and stability of in-phase and anti-phase synchronized motion in a pair of nonlinear oscillators have been derived under the assumption that the oscillators are *identical*. However, in the experimental analysis it has been shown that the oscillators show synchronized behaviour even when there are unavoidable differences between them. Hence, a natural extension of the analytic results presented in Chapter 3 is to derive existence and stability conditions for the case of nonidentical oscillators. The machinery of the Poincaré method may not be helpful in this case and consequently, a different mathematical tool should be used in the analysis.
- The analytic stability conditions (only for the case of anti-phase synchronization) presented in Chapter 4 have been derived under the assumption of small oscillations. Consequently, further research is needed in order to prove the global stability of the in-phase and anti-phase synchronized motion of the oscillators. At this point it is worth to note that in a pair of oscillators interacting via Huygens' coupling, both oscillators receive the same "input" (the influence of the bar on them is the same). Hence, in order to study the in-phase motion, some kind of converge criterion cf. [65], may be used.
- The nonlinear controllers used in Chapter 5, require inclusion of a compensation term in order to deal with the nonlinearities and/or to cancel the influence of the coupling bar. Sometimes, however, it is desired to have a

controller that on the one hand is as simple as possible, but on the other hand should be robust enough to guarantee that the stability is not compromised. Hence, it would be interesting to perform a stability analysis of the (in-phase and/or anti-phase) synchronization error dynamics when the simple controller presented at the end of the chapter is used. Note that this control law has the advantage that it does not require knowledge of the parameters of the oscillators to be controlled.

- The analysis presented in Chapter 6 has focused mainly on determining the influence of the time delay and the magnitude of the coupling strength in the limit behaviour of a pair of coupled oscillators. However, it has been assumed that the time delay is constant and is the same for all communication channels. Hence, future work may focus on considering different time delays in the communication channels. Additionally, the analysis of the phase-flip bifurcation for the case of n oscillators with Huygens' coupling seems to be the next step.
- In Chapter 7, a new model for the classical Huygens' experiment on synchronization has been derived and numerical results illustrating the limit behaviour of the system, including in-phase and anti-phase synchronized motion of the pendula, have been presented. Future research may focus on performing a rigorous stability study of these limit solutions. This of course requires having a suitable model consisting of a partial differential equation, describing the behaviour of the flexible structure, plus two ordinary differential equations, describing the motion of the pendula. Furthermore, it is interesting to investigate the influence of the distance that exists between the connection points of pendula in the limit behaviour of the coupled pendula. In other words, to determine how the synchronized behaviour is affected when the pendula are close each other and when they are further apart. Note that the FE model presented in Chapter 7 allows to perform such an analysis.
- In general, this thesis focuses on *pairs* of self-sustained nonlinear oscillators. A direction for future research is to extend the analysis to the case of n arbitrary oscillators interacting via Huygens coupling, cf. [16]. One can distinguish two challenges in this case. One challenge is the issue of determining all the limit synchronous solutions in the system of n oscillators. Furthermore, there is the problem of determining the global stability of these solutions.
- Another extension of the results of this research is related to the class of oscillators used in the analysis. Here, only second order oscillators have been considered. This is in part due to the fact that each pendulum clock in Huygens' classical experiment on synchronization may be casted into this

class of oscillators. However, there are several interesting oscillatory systems that do not belong to the class of second order oscillators. For example the Lorenz system, the Chua circuit, and neural models like the Hindmarsh-Rose model. Consequently, future work on synchronization of these kinds of systems by using the Huygens' coupling may form the next step. This may require to consider Huygens' coupling not as a physical coupling but rather as a suitable control input.

This thesis has focused on the *analysis* of oscillatory systems interacting via Huygens' coupling. Next to the recommendations given above, it is interesting to continue this research from a control point of view, i.e. to *synthesize* controllers based on Huygens coupling. In order to motivate the reader, three potential examples are discussed.

- **Control of humanoid robots** Consider the problem of controlling and stabilizing a humanoid robot. Controlling the walking motion may require to force the two legs of the robot to move synchronously in opposite directions, i.e. in anti-phase, see for instance [89]. Furthermore, in [23], it has been suggested that the head of a humanoid may be stabilized during locomotion by 'synchronizing' the head pitch rotation and the trunk pitch rotation in anti-phase. In general, in a humanoid robot one can distinguish both in-phase and anti-phase correlations in the motions of its components (arms, legs, knees, hips, antiphase rotation of upper and lower body, etc.). Hence the problem to be considered for future research is how to synthesize a controller (based on Huygens' coupling) such that synchronized locomotion of a humanoid robot is achieved.
- **Control of parametric roll** As a second example consider the case of stabilization of parametric roll. Parametric roll - heavy roll motion in a ship - is an undesired phenomenon because it may produce cargo damage or loss, delay or even suspension of the activities performed by the crew, seasickness of passengers and crew, and in the worst case it can lead to the capsizing of the ship. In order to prevent the onset of parametric roll and/or to reduce the effects of this phenomenon, some ships are equipped with active U-tanks. When the ship is experiencing heavy roll motion, the water in the U-tank is forced to move in anti-phase (via a pump) with respect to the roll motion. As a result, the weight of the water provides a counteracting force to the force exerted by the waves. The challenge in this example is again to synthesize a suitable controller (inspired by Huygens coupling), such that the pump is controlled to force the water in the U-tank to move in anti-phase with respect to the roll motion.

- **Controlled transmission in a wireless sensor network** Consider the problem of reliable data transmission (collision-free messages) in a wireless sensor network. In [47], it has been found that this can be achieved by anti-phase synchronization of the transmission scheduling of the nodes. Moreover, given two neighboring nodes in the network, by using anti-phase synchronization it may be possible to organize sleep cycles for the nodes, such that while one node is transmitting (awake), its neighbor is sleep and therefore the latter will consume less energy. Obviously, a possible mechanism for realizing anti-phase synchronization at the nodes is again the Huygens coupling. Hence, future work should focus on determining the conditions, under which a controller or algorithm, based on Huygens' coupling, may lead to robust wireless transmission and at the same time reduction in the consumption of energy at the nodes.

Summarizing, the results presented in this thesis confirm that the observations made by Huygens extend beyond pendulum clocks. Further research of this exciting topic is required but it is the belief of the author that the results presented here have provided new insight in understanding the synchronized motion of coupled oscillators.

When one looks at the intriguing order that exists in the cosmos, one can easily reach the conclusion that

synchronization

is one of the most pervasive behaviours in the universe.

Appendix **A**

Proof of Theorem 1.1

Proof. Denote by β_s , $s = 1, \dots, l$, the deviations from the initial values between solution of system (1.10) and the solution of the generating system (1.11), i.e.

$$\beta_s = y_s(0) - y_s^0(0), \quad s = 1, \dots, l. \quad (\text{A.1})$$

The Poincaré method searches for solutions $y_s(t, \beta_1, \dots, \beta_l, \mu)$, $s = 1, \dots, l$, of (1.10) in the form of power series in μ and β_s , $s = 1, \dots, l$, i.e.

$$\begin{aligned} y_s(t, \beta_1, \dots, \beta_l, \mu) &= \underbrace{y_s(t, 0, \dots, 0, 0)}_{y_s^0(t)} + \sum_{i=1}^l \frac{\partial y_s(t, 0, \dots, 0, 0)}{\partial \beta_i} \beta_i \\ &+ \frac{\partial y_s(t, 0, \dots, 0, 0)}{\partial \mu} \mu + \frac{1}{2} \sum_{i=1}^l \sum_{j=1}^l \frac{\partial^2 y_s(t, 0, \dots, 0, 0)}{\partial \beta_i \partial \beta_j} \beta_i \beta_j \\ &+ \frac{1}{2} \frac{\partial^2 y_s(t, 0, \dots, 0, 0)}{\partial \mu^2} \mu^2 + \frac{1}{2} \sum_{i=1}^l \frac{\partial^2 y_s(t, 0, \dots, 0, 0)}{\partial \beta_i \partial \mu} \beta_i \mu + \dots \end{aligned} \quad (\text{A.2})$$

This solution can be rewritten in the form

$$y_s(t, \beta_1, \dots, \beta_l, \mu) = y_s^0(t) + \sum_{i=1}^l A_{si} \beta_i + B_s \mu + \sum_{i=1}^l \sum_{j=1}^l C_{sij} \beta_i \beta_j + \sum_{i=1}^l D_{si} \beta_i \mu + E_s \mu^2 + \dots, \quad (\text{A.3})$$

where $s = 1, \dots, l$, $y_s^0(t)$ is as given in (1.14) and A_{si} , B_s , C_{sij} , D_{si} , and E_s are so far unknown functions of time (if one compares (A.2) with (A.3) then it is easy to see that $A_{si} = \frac{\partial y_s(t, 0, \dots, 0, 0)}{\partial \beta_i}$, $B_s = \frac{\partial y_s(t, 0, \dots, 0, 0)}{\partial \mu}$, and so on).

Likewise, functions $f_s(y_1, \dots, y_l)$, $s = 1, \dots, l$ in equation (1.10) are expanded as

a Taylor series around y_s^0 , $s = 1, \dots, l$. This yields

$$\begin{aligned} f_s(y_1, \dots, y_l) &= f_s(y_1^0, \dots, y_l^0) + \sum_{p=1}^l \frac{\partial f_s(y_1^0, \dots, y_l^0)}{\partial y_p} (y_p - y_p^0) \\ &+ \frac{1}{2} \sum_{p=1}^l \sum_{q=1}^l \frac{\partial^2 f_s(y_1^0, \dots, y_l^0)}{\partial y_p \partial y_q} (y_p - y_p^0)(y_q - y_q^0) + \dots \end{aligned} \quad (\text{A.4})$$

By using (1.14), (A.1), and (A.3), expression (A.4) is rewritten as

$$\begin{aligned} f_s(y_1, \dots, y_l) &= f_s(\alpha_1 e^{\lambda_1 t}, \dots, \alpha_k e^{\lambda_k t}, 0, \dots, 0) \\ &+ \sum_{p=1}^l \frac{\partial f_s(\alpha_1 e^{\lambda_1 t}, \dots, \alpha_k e^{\lambda_k t}, 0, \dots, 0)}{\partial y_p} a \\ &+ \frac{1}{2} \sum_{p=1}^l \sum_{q=1}^l \frac{\partial^2 f_s(\alpha_1 e^{\lambda_1 t}, \dots, \alpha_k e^{\lambda_k t}, 0, \dots, 0)}{\partial y_p \partial y_q} ab + \dots, \end{aligned} \quad (\text{A.5})$$

where $a = \left[\sum_{i=1}^l A_{pi} \beta_i + B_p \mu + \sum_{i=1}^l \sum_{j=1}^l C_{pij} \beta_i \beta_j + \sum_{i=1}^l D_{pi} \beta_i \mu + E_p \mu^2 \right]$
and $b = \left[\sum_{i=1}^l A_{qi} \beta_i + B_q \mu + \sum_{i=1}^l \sum_{j=1}^l C_{qij} \beta_i \beta_j + \sum_{i=1}^l D_{qi} \beta_i \mu + E_q \mu^2 \right]$.

The unknown functions A_{si} , B_s , C_{sij} , D_{si} , and E_s in (A.3) can be obtained by substitution of the expressions for y_s and f_s in the original equation (1.10) and equating the coefficients of similar terms in β_s and μ . This is done as follows. First, (A.3) and (A.5) are substituted in (1.10). This yields (after neglecting terms in μ and β_i of order greater than two)

$$\begin{aligned} \dot{y}_s^0 + \sum_{i=1}^l \dot{A}_{si} \beta_i + \dot{B}_s \mu + \sum_{i=1}^l \sum_{j=1}^l \dot{C}_{sij} \beta_i \beta_j + \sum_{i=1}^l \dot{D}_{si} \beta_i \mu + \dot{E}_s \mu^2 &= \lambda_s y_s^0 \\ + \lambda_s \sum_{i=1}^l A_{si} \beta_i + \lambda_s B_s \mu + \lambda_s \sum_{i=1}^l \sum_{j=1}^l C_{sij} \beta_i \beta_j + \lambda_s \sum_{i=1}^l D_{si} \beta_i \mu + \lambda_s E_s \mu^2 \\ &+ \mu f_s(\alpha_1 e^{\lambda_1 t}, \dots, \alpha_k e^{\lambda_k t}, 0, \dots, 0) \\ &+ \sum_{p=1}^l \sum_{i=1}^l \frac{\partial f_s(\alpha_1 e^{\lambda_1 t}, \dots, \alpha_k e^{\lambda_k t}, 0, \dots, 0)}{\partial y_p} A_{pi} \beta_i \mu \\ &+ \sum_{p=1}^l \frac{\partial f_s(\alpha_1 e^{\lambda_1 t}, \dots, \alpha_k e^{\lambda_k t}, 0, \dots, 0)}{\partial y_p} B_p \mu^2, \quad s = 1, \dots, l. \end{aligned} \quad (\text{A.6})$$

Next, by equating terms depending on β_s , $s = 1, \dots, l$, and μ yields the following

set of first order linear equations

$$\dot{A}_{si} - \lambda_s A_{si} = 0, \quad s = 1, \dots, l \quad (\text{A.7})$$

$$\dot{B}_s - \lambda_s B_s = f_s(\alpha_1 e^{\lambda_1 t}, \dots, \alpha_k e^{\lambda_k t}, 0, \dots, 0), \quad s = 1, \dots, l. \quad (\text{A.8})$$

$$\dot{C}_{sij} - \lambda_s C_{sij} = 0, \quad s, i, j = 1, \dots, l. \quad (\text{A.9})$$

$$\dot{D}_{si} - \lambda_s D_{si} = \sum_{p=1}^l \frac{\partial f_s(\alpha_1 e^{\lambda_1 t}, \dots, \alpha_k e^{\lambda_k t}, 0, \dots, 0)}{\partial y_p} A_{pi}, \quad s, i = 1, \dots, l. \quad (\text{A.10})$$

$$\dot{E}_s - \lambda_s E_s = \sum_{p=1}^l \frac{\partial f_s(\alpha_1 e^{\lambda_1 t}, \dots, \alpha_k e^{\lambda_k t}, 0, \dots, 0)}{\partial y_p} B_p, \quad s = 1, \dots, l. \quad (\text{A.11})$$

The values at $t = 0$ for the above set of equations can be obtained from (A.1) and (A.3) and it follows that

$$A_{si}(0) = \delta_{si}, \quad B_s(0) = C_{sij}(0) = D_{si}(0) = E_s(0) = 0, \quad (\text{A.12})$$

where δ_{si} is the Kronecker delta as defined in (1.18).

Integration of (A.7) to (A.11) and considering (A.12) yields the solutions

$$A_{si}(t) = \delta_{si} e^{\lambda_s t}, \quad s = 1, \dots, l. \quad (\text{A.13})$$

$$B_s(t) = e^{\lambda_s t} \int_0^t f_s(\alpha_1 e^{\lambda_1 u}, \dots, \alpha_k e^{\lambda_k u}, 0, \dots, 0) e^{-\lambda_s u} du, \quad s = 1, \dots, l. \quad (\text{A.14})$$

$$C_{sij}(t) = 0, \quad s, i, j = 1, \dots, l. \quad (\text{A.15})$$

Functions D_{si} and E_s do not play a significant role in the upcoming analysis (this is shown later in the proof) and therefore, their explicit solution is not computed. Expressions (A.13)-(A.15) can now be substituted in (A.3).

At this point, it is worth to remember that we are looking for periodic solutions among the solutions (A.3) of (1.10) when μ is a small parameter. Then, let the period of a certain periodic solution be equal to $\tilde{T} = T + \tau_c(\mu)$ with $\tau_c \rightarrow 0$ when $\mu \rightarrow 0$. A solution of (1.10) will be called periodic (of period \tilde{T}) if the following condition is satisfied

$$y_s(t + \tilde{T}) - y_s(t) = 0, \quad s = 1, \dots, k. \quad (\text{A.16})$$

or by considering the initial value of (A.16) at $t = 0$

$$y_s(\tilde{T}) - y_s(0) = 0, \quad s = 1, \dots, k. \quad (\text{A.17})$$

Note that subindex k is used instead of subindex l because for $s = k + 1, \dots, l$ condition (A.17) is trivially satisfied. Actually, (A.17) provides necessary and sufficient conditions for the periodicity of the solution $y_s(t)$ of (1.10). For a theorem on this, the reader is referred to [13] and [41].

Next, since $\tau_c(\mu)$ is assumed to be a small parameter ($\tau_c(\mu) = 0$ for $\mu = 0$), it is possible to expand $y_s(\tilde{T})$ around $\tau_c(\mu) = 0$. This yields

$$y_s(\tilde{T}) = y_s(T + \tau_c(\mu)) = y_s(T) + \tau_c(\mu)\dot{y}_s(T) + \frac{\tau_c^2(\mu)}{2}\ddot{y}_s(T) + \dots, \quad s = 1, \dots, k. \quad (\text{A.18})$$

The values $y_s(T)$, $\dot{y}_s(T)$, etc, can be determined from (A.3) by replacing the functions A_{si} , B_s , C_{sij} , etc by their respective values at $t = T$.

Just before doing this, it is convenient to remember that

$$\lambda_s = in_s\omega = in_s\frac{2\pi}{T}, \quad s = 1, \dots, k, \quad (\text{A.19})$$

and consequently

$$\lambda_s T = 2\pi n_s i, \quad s = 1, \dots, k. \quad (\text{A.20})$$

Taking this into account in (A.13) to (A.15), yields the following expressions

$$A_{si}(T) = \delta_{si}, \quad s, i = 1, \dots, k, \quad (\text{A.21})$$

$$B_s(T) = \int_0^T f_s(\alpha_1 e^{\lambda_1 t}, \dots, \alpha_k e^{\lambda_k t}, 0, \dots, 0) e^{-\lambda_s t} dt, \quad s = 1, \dots, k. \quad (\text{A.22})$$

Substitution of these expressions in (A.3) up to second order yields

$$y_s(T) = y_s^0(T) + \beta_s + \mu \int_0^T f_s(\alpha_1 e^{\lambda_1 t}, \dots, \alpha_k e^{\lambda_k t}, 0, \dots, 0) e^{-\lambda_s t} dt + \sum_{i=1}^l D_{si}(T)\beta_i \mu + E_s \mu^2 \quad (\text{A.23})$$

and the time derivative of (A.3) up to second order verifies¹

$$\dot{y}_s(T) = \dot{y}_s^0(T) + \sum_{i=1}^l \dot{A}_{si}(T)\beta_i + \dot{B}_s(T)\mu + \sum_{i=1}^l \sum_{j=1}^l \dot{C}_{sij}(T)\beta_i \beta_j + \sum_{i=1}^l \dot{D}_{si}(T)\beta_i \mu + \dot{E}_s \mu^2. \quad (\text{A.24})$$

Then, the first order approximation of (A.18) is written as

$$\begin{aligned} y_s(\tilde{T}) &= y_s^0(T) + \beta_s + \mu \int_0^T f_s(\alpha_1 e^{\lambda_1 t}, \dots, \alpha_k e^{\lambda_k t}, 0, \dots, 0) e^{-\lambda_s t} dt \\ &+ \sum_{i=1}^l D_{si}(T)\beta_i \mu + E_s \mu^2 + \tau_c(\mu)\dot{y}_s^0(T) + \tau_c(\mu) \sum_{i=1}^l \dot{A}_{si}(T)\beta_i + \tau_c(\mu)\dot{B}_s(T)\mu \\ &+ \tau_c(\mu) \sum_{i=1}^l \sum_{j=1}^l \dot{C}_{sij}(T)\beta_i \beta_j + \tau_c(\mu) \sum_{i=1}^l \dot{D}_{si}(T)\beta_i \mu + \tau_c(\mu)\dot{E}_s(T)\mu^2, \quad s = 1, \dots, k. \end{aligned} \quad (\text{A.25})$$

¹Note that for convenience the explicit expressions for \dot{A}_{si} , \dot{B}_s , and so on, have not been included. Actually, these expressions will be irrelevant as will be shown later in this proof.

From equation (1.12) and (A.20) it follows that

$$y_s^0(T) = \alpha_s e^{\lambda_s T} = \alpha_s \quad \text{and} \quad \dot{y}_s^0(T) = \lambda_s \alpha_s e^{\lambda_s T} = \lambda_s \alpha_s, \quad s = 1, \dots, k. \quad (\text{A.26})$$

At this point, it should be noted that for $\mu \rightarrow 0$, it should hold that $\tau_c(\mu) \rightarrow 0$ and $\beta_s \rightarrow 0$. Hence, τ and β_s are now written as power series in μ . Note that in the expansions of $\tau_c(\mu)$ and β_s the zero order terms must be absent. The expansion of τ and β_s verify

$$\tau_c(\mu) = \mu\tau_1 + \mu^2\tau_2 + \dots \quad (\text{A.27})$$

$$\beta_s = \mu\beta_{s1} + \mu^2\beta_{s2} + \dots, \quad s = 1, \dots, k. \quad (\text{A.28})$$

Then, by substitution of (A.26-A.28) in (A.25) the following is obtained

$$\begin{aligned} y_s(\tilde{T}) &= \alpha_s + \beta_s + \mu \int_0^T f_s(\alpha_1 e^{\lambda_1 u}, \dots, \alpha_k e^{\lambda_k u}, 0) e^{-\lambda_s t} dt \\ &\quad + \sum_{i=1}^l D_{si}(T) [\mu\beta_{i1} + \mu^2\beta_{i2}] \mu + E_s \mu^2 + \lambda_s \alpha_s [\mu\tau_1 + \mu^2\tau_2] \\ &\quad + [\mu\tau_1 + \mu^2\tau_2] \sum_{i=1}^l \dot{A}_{si}(T) [\mu\beta_{i1} + \mu^2\beta_{i2}] + [\mu\tau_1 + \mu^2\tau_2] \dot{B}_s(T) \mu \\ &\quad + [\mu\tau_1 + \mu^2\tau_2] \sum_{i=1}^l \sum_{j=1}^l \dot{C}_{sij}(T) [\mu\beta_{i1} + \mu^2\beta_{i2}] [\mu\beta_{j1} + \mu^2\beta_{j2}] \\ &\quad + [\mu\tau_1 + \mu^2\tau_2] \sum_{i=1}^l \dot{D}_{si}(T) [\mu\beta_{i1} + \mu^2\beta_{i2}] \mu + [\mu\tau_1 + \mu^2\tau_2] \dot{E}_s(T) \mu^2, \quad s = 1, \dots, k. \end{aligned} \quad (\text{A.29})$$

Neglecting terms of order ≥ 2 in μ yields

$$y_s(\tilde{T}) = \alpha_s + \beta_s + \mu \int_0^T f_s(\alpha_1 e^{\lambda_1 t}, \dots, \alpha_k e^{\lambda_k t}, 0, \dots, 0) e^{-\lambda_s t} dt + \lambda_s \alpha_s \tau_1 \mu. \quad (\text{A.30})$$

Consequently, the periodicity condition (A.17) can be written as

$$y_s(\tilde{T}) - y_s(0) = \alpha_s + \beta_s + \mu \int_0^T f_s(\alpha_1 e^{\lambda_1 t}, \dots, \alpha_k e^{\lambda_k t}, 0, \dots, 0) e^{-\lambda_s t} dt + \lambda_s \alpha_s \tau_1 \mu - y_s(0) = 0. \quad (\text{A.31})$$

Finally, by using (A.1) in the above equation it follows that

$$y_s(\tilde{T}) - y_s(0) = \mu \int_0^T f_s(\alpha_1 e^{\lambda_1 t}, \dots, \alpha_k e^{\lambda_k t}, 0, \dots, 0) e^{-\lambda_s t} dt + \lambda_s \alpha_s \tau_1 \mu = 0. \quad (\text{A.32})$$

According to (1.14), there will be k equations like (A.32), i.e.

$$\begin{aligned} y_1(\tilde{T}) - y_1(0) &= \mu \int_0^T f_1(\alpha_1 e^{\lambda_1 t}, \dots, \alpha_k e^{\lambda_k t}, 0, \dots, 0) e^{-\lambda_1 t} dt + \lambda_1 \alpha_1 \tau_1 \mu = 0, \\ &\vdots \\ y_k(\tilde{T}) - y_k(0) &= \mu \int_0^T f_k(\alpha_1 e^{\lambda_1 t}, \dots, \alpha_k e^{\lambda_k t}, 0, \dots, 0) e^{-\lambda_k t} dt + \lambda_k \alpha_k \tau_1 \mu = 0. \end{aligned} \quad (\text{A.33})$$

The value of τ_1 can (for example) be obtained from the last equation of (A.33)

$$\tau_1 = -\frac{1}{\lambda_k \alpha_k} \int_0^T f_k(\alpha_1 e^{\lambda_1 t}, \dots, \alpha_k e^{\lambda_k t}, 0, \dots, 0) e^{-\lambda_k t} dt. \quad (\text{A.34})$$

This value is then used in the first $k-1$ equations of (A.33).

$$\begin{aligned} y_1(\tilde{T}) - y_1(0) &= \mu \int_0^T f_1(\alpha_1 e^{\lambda_1 t}, \dots, \alpha_k e^{\lambda_k t}, 0, \dots, 0) e^{-\lambda_1 t} dt \\ &\quad - \mu \frac{\lambda_1 \alpha_1}{\lambda_k \alpha_k} \int_0^T f_k(\alpha_1 e^{\lambda_1 t}, \dots, \alpha_k e^{\lambda_k t}, 0, \dots, 0) e^{-\lambda_k t} dt = 0, \\ &\vdots \\ y_{k-1}(\tilde{T}) - y_{k-1}(0) &= \mu \int_0^T f_{k-1}(\alpha_1 e^{\lambda_1 t}, \dots, \alpha_k e^{\lambda_k t}, 0, \dots, 0) e^{-\lambda_{k-1} t} dt \\ &\quad - \mu \frac{\lambda_{k-1} \alpha_{k-1}}{\lambda_k \alpha_k} \int_0^T f_k(\alpha_1 e^{\lambda_1 t}, \dots, \alpha_k e^{\lambda_k t}, 0, \dots, 0) e^{-\lambda_k t} dt = 0. \end{aligned} \quad (\text{A.35})$$

Define

$$\psi_s := y_s(\tilde{T}) - y_s(0) = 0 \quad \text{and} \quad (\text{A.36})$$

$$P_s := \int_0^T f_s(\alpha_1 e^{\lambda_1 t}, \dots, \alpha_k e^{\lambda_k t}, 0, \dots, 0) e^{-\lambda_s t} dt, \quad s = 1, \dots, k-1.$$

Then, (A.35) is rewritten as

$$\psi_s = \mu P_s - \mu \frac{\lambda_s \alpha_s}{\lambda_k \alpha_k} = 0, \quad s = 1, \dots, k-1, \quad (\text{A.37})$$

and multiplying both sides of (A.37) by $\frac{\lambda_k \alpha_k}{\mu}$ yields

$$\bar{\psi}_s = \lambda_k \alpha_k P_s - \lambda_s \alpha_s P_k = 0, \quad s = 1, \dots, k-1. \quad (\text{A.38})$$

Finally, by using (1.13) and dividing both sides of (A.38) by $i\omega$ it follows that

$$Q_s = \frac{\bar{\psi}_s}{i\omega} = n_k \alpha_k P_s - n_s \alpha_s P_k = 0, \quad s = 1, \dots, k-1. \quad (\text{A.39})$$

Note that in (A.39), the number of unknowns $\alpha_1, \dots, \alpha_k$ is one larger than the number of equations. Therefore, one of the α 's can be chosen arbitrarily and according to the conditions of Theorem 1,

$$\alpha_{k-1} = \alpha_k. \quad (\text{A.40})$$

Thus, the question about the existence of periodic solutions of system (1.10) reduces to the question of solvability of (A.39)-(A.40) with respect to $\alpha_1, \dots, \alpha_k$.

On the basis of the well-known theorem on the existence of implicit functions, see for instance [39], equation (A.39) will have, for sufficiently small μ , one and only one solution α_s , $s = 1, \dots, k$, if and only if the Jacobian matrix associated to (A.39) is invertible, i.e.

$$\det \left(\left[\begin{array}{ccc} \frac{\partial Q_1}{\partial \alpha_1} & \cdots & \frac{\partial Q_1}{\partial \alpha_{k-1}} \\ \vdots & \ddots & \vdots \\ \frac{\partial Q_{k-1}}{\partial \alpha_1} & \cdots & \frac{\partial Q_{k-1}}{\partial \alpha_{k-1}} \end{array} \right] \Big|_{\alpha_1 = \alpha_1^*, \dots, \alpha_{k-1} = \alpha_{k-1}^*} \right) \neq 0, \quad (\text{A.41})$$

where the set of constants α_s^* , $s = 1, \dots, k-1$ satisfy (A.39).

The partial derivatives of the function Q_s are computed according to (A.39). This yields

$$\frac{\partial Q_s(\alpha_1, \dots, \alpha_k)}{\partial \alpha_j} = n_k \alpha_k \frac{\partial P_s}{\partial \alpha_j} - n_s \alpha_s \frac{\partial P_k}{\partial \alpha_j} - \delta_{sj} n_s P_k \quad s, j = 1, \dots, k-1. \quad (\text{A.42})$$

From this equation, it is clear that the rows/columns of the Jacobian matrix are linearly independent and consequently (A.41) holds and the computed solution will be unique.

Finally, a proof for the stability condition/criteria presented in equation (1.18) is presented.

In virtue of (1.14) it follows that the system only has k periodic solutions. For investigating the stability of these periodic solutions it is convenient to obtain the so called *equations in variations* [40].

It is possible to show that the characteristic equation, obtained when writing

system (1.10) as a set of equations in variations, is given by

$$\begin{vmatrix} y_{11}(\tilde{T}) - \rho & y_{12}(\tilde{T}) & \cdots & y_{1k}(\tilde{T}) \\ y_{21}(\tilde{T}) & y_{22}(\tilde{T}) - \rho & \cdots & y_{2k}(\tilde{T}) \\ \vdots & \vdots & \vdots & \vdots \\ y_{k1}(\tilde{T}) & y_{k2}(\tilde{T}) & \cdots & y_{kk}(\tilde{T}) - \rho(\tilde{T}) \end{vmatrix} = 0. \quad (\text{A.43})$$

The values of y_{sj} , $s, j = 1, \dots, k$ can be determined by using a property of the equations in variations presented in [41]. It should be noticed that in the present case, the periodic solution $\varphi_s(\tilde{T}) = y_s(\tilde{T})$, $s = 1, \dots, k$, can be obtained from (A.36), i.e.

$$\varphi_s(\tilde{T}) = \psi_s(\tilde{T}) + y_s(0). \quad (\text{A.44})$$

By using (A.1) it follows that

$$\varphi_s(\tilde{T}) = \psi_s(\tilde{T}) + \beta_s + y_s^0(0) = \psi_s(\tilde{T}) + \beta_s + \alpha_s, \quad s = 1, \dots, k, \quad (\text{A.45})$$

where β_s is a constant. Then, the elements y_{sj} of (A.43) are given by [41]

$$y_{sj} = \frac{\partial \psi_s(\tilde{T})}{\partial \alpha_j} + \delta_{sj}, \quad s, j = 1, \dots, k, \quad (\text{A.46})$$

where δ_{sj} denotes the Kronecker delta. Consequently, (A.43) is rewritten as

$$\begin{vmatrix} \frac{\partial \psi_1(\tilde{T})}{\partial \alpha_1} + 1 - \rho & \frac{\partial \psi_1(\tilde{T})}{\partial \alpha_2} & \cdots & \frac{\partial \psi_1(\tilde{T})}{\partial \alpha_k} \\ \frac{\partial \psi_2(\tilde{T})}{\partial \alpha_1} & \frac{\partial \psi_2(\tilde{T})}{\partial \alpha_2} + 1 - \rho & \cdots & \frac{\partial \psi_2(\tilde{T})}{\partial \alpha_k} \\ \vdots & \vdots & \vdots & \vdots \\ \frac{\partial \psi_k(\tilde{T})}{\partial \alpha_1} & \frac{\partial \psi_k(\tilde{T})}{\partial \alpha_2} & \cdots & \frac{\partial \psi_k(\tilde{T})}{\partial \alpha_k} + 1 - \rho \end{vmatrix} = 0. \quad (\text{A.47})$$

It should be noted that equations (A.37) only hold under the assumption that $\psi_k = 0$ (see last equation of (A.33)). Using this fact in (A.47), it follows that the characteristic equation becomes

$$\begin{vmatrix} \frac{\partial \psi_1(\tilde{T})}{\partial \alpha_1} + 1 - \rho & \frac{\partial \psi_1(\tilde{T})}{\partial \alpha_2} & \cdots & \frac{\partial \psi_1(\tilde{T})}{\partial \alpha_k} \\ \frac{\partial \psi_2(\tilde{T})}{\partial \alpha_1} & \frac{\partial \psi_2(\tilde{T})}{\partial \alpha_2} + 1 - \rho & \cdots & \frac{\partial \psi_2(\tilde{T})}{\partial \alpha_k} \\ \vdots & \vdots & \vdots & \vdots \\ \frac{\partial \psi_{k-1}(\tilde{T})}{\partial \alpha_1} & \cdots & \frac{\partial \psi_{k-1}(\tilde{T})}{\partial \alpha_{k-1}} + 1 - \rho & \frac{\partial \psi_{k-1}(\tilde{T})}{\partial \alpha_k} \\ 0 & 0 & \cdots & 1 - \rho \end{vmatrix} = 0. \quad (\text{A.48})$$

Therefore, one of the roots is $\rho = 1$. From the stability criteria for periodic motion, cf. [40], it follows that the stability of the periodic solutions will be determined

by the remaining roots of (A.48), which are determined from

$$\begin{vmatrix} \frac{\partial \psi_1(\tilde{T})}{\partial \alpha_1} + 1 - \rho & \frac{\partial \psi_1(\tilde{T})}{\partial \alpha_2} & \cdots & \frac{\partial \psi_1(\tilde{T})}{\partial \alpha_{k-1}} \\ \frac{\partial \psi_2(\tilde{T})}{\partial \alpha_1} & \frac{\partial \psi_2(\tilde{T})}{\partial \alpha_2} + 1 - \rho & \cdots & \frac{\partial \psi_2(\tilde{T})}{\partial \alpha_{k-1}} \\ \vdots & \vdots & \vdots & \vdots \\ \frac{\partial \psi_{k-1}(\tilde{T})}{\partial \alpha_1} & \frac{\partial \psi_{k-1}(\tilde{T})}{\partial \alpha_2} & \cdots & \frac{\partial \psi_{k-1}(\tilde{T})}{\partial \alpha_{k-1}} + 1 - \rho \end{vmatrix} = 0. \quad (\text{A.49})$$

In order to continue, it should be noted that for $\mu = 0$, it follows that $\rho_s = e^{\lambda_s T}$. In (A.27), it has been assumed that the period when μ is small becomes $\tilde{T} = T + \tau = T + \mu\tau_1$. Therefore, we can look for the roots of (A.49) in the form

$$\rho_s(\mu) = e^{\lambda_s \tilde{T}} = e^{\lambda_s T} e^{\mu \lambda_s \tau_1} = e^{\lambda_s T} (1 + \chi \mu + h.o.t.) \quad s = 1, \dots, k. \quad (\text{A.50})$$

By using this expression and the fact that $e^{\lambda_s T} = 1$ for $s = 1, \dots, k-1$ it follows that

$$\begin{vmatrix} \frac{\partial \psi_1(\tilde{T})}{\partial \alpha_1} - \mu \chi & \frac{\partial \psi_1(\tilde{T})}{\partial \alpha_2} & \cdots & \frac{\partial \psi_1(\tilde{T})}{\partial \alpha_{k-1}} \\ \frac{\partial \psi_2(\tilde{T})}{\partial \alpha_1} & \frac{\partial \psi_2(\tilde{T})}{\partial \alpha_2} - \mu \chi & \cdots & \frac{\partial \psi_2(\tilde{T})}{\partial \alpha_{k-1}} \\ \vdots & \vdots & \vdots & \vdots \\ \frac{\partial \psi_{k-1}(\tilde{T})}{\partial \alpha_1} & \frac{\partial \psi_{k-1}(\tilde{T})}{\partial \alpha_2} & \cdots & \frac{\partial \psi_{k-1}(\tilde{T})}{\partial \alpha_{k-1}} - \mu \chi \end{vmatrix} = 0. \quad (\text{A.51})$$

Now the condition of having all the roots of (A.49) satisfying $|\rho_i| < 0$, $i = 1, \dots, k-1$ is satisfied if $\text{Re}\{\chi\} < 0$. Finally, by factorizing the term $\frac{\mu}{\lambda_k \alpha_k}$ from the above equation (see (A.38)-(A.39)), it follows that the characteristic equation determining the stability of the periodic solutions is given by:

$$\frac{i\omega\mu}{\lambda_k \alpha_k} \begin{vmatrix} \frac{\partial Q_1}{\partial \alpha_1} - n_k \alpha_k \chi & \frac{\partial Q_1}{\partial \alpha_2} & \cdots & \frac{\partial Q_1}{\partial \alpha_{k-1}} \\ \frac{\partial Q_2}{\partial \alpha_1} & \frac{\partial Q_2}{\partial \alpha_2} - n_k \alpha_k \chi & \cdots & \frac{\partial Q_2}{\partial \alpha_{k-1}} \\ \vdots & \vdots & \vdots & \vdots \\ \frac{\partial Q_{k-1}}{\partial \alpha_1} & \frac{\partial Q_{k-1}}{\partial \alpha_2} & \cdots & \frac{\partial Q_{k-1}}{\partial \alpha_{k-1}} - n_k \alpha_k \chi \end{vmatrix} = 0. \quad (\text{A.52})$$

□

Appendix B

Euler beam element matrices

The Euler element stiffness matrix is given by

$$k_e = \frac{EI}{l^3} \begin{bmatrix} \frac{AI^2}{I} & 0 & 0 & -\frac{AI^2}{I} & 0 & 0 \\ 0 & 12 & 6l & 0 & -12 & 6l \\ 0 & 6l & 4l^2 & 0 & -6l & 2l^2 \\ -\frac{AI^2}{I} & 0 & 0 & \frac{AI^2}{I} & 0 & 0 \\ 0 & -12 & -6l & 0 & 12 & -6l \\ 0 & 6l & 2l^2 & 0 & -6l & 4l^2 \end{bmatrix}, \quad (\text{B.1})$$

where A is the area of the cross-section of the beam element in $[\text{m}^2]$, I is the second moment of area in $[\text{m}^4]$, E is the Young's modulus in $[\text{N}/\text{m}^2]$, and l is the length of the beam element in $[\text{m}]$. The Euler beam element consistent mass matrix is given by

$$m_e = \frac{\rho Al}{420} \begin{bmatrix} 140 & 0 & 0 & 70 & 0 & 0 \\ 0 & 156 & 22l & 0 & 54 & -13l \\ 0 & 22l & 4l^2 & 0 & 13l & -3l^2 \\ 70 & 0 & 0 & 140 & 0 & 0 \\ 0 & 54 & 13l & 0 & 156 & -22l \\ 0 & -13l & -3l^2 & -22l & 4l^2 & \end{bmatrix}, \quad (\text{B.2})$$

where ρ is the mass density of the beam material in $[\text{kg}/\text{m}^3]$.

Appendix C

Static analysis for the flexible coupling structure

In this Appendix, a static analysis for the coupling structure depicted in Figure 7.1 is conducted.

First, the influence of gravity on the structural deformation of the coupling structure is investigated. This requires to solve the following equation for q

$$Kq = f_g = -M\bar{g} \quad (\text{C.1})$$

where $\bar{g} = g [0 \ 1 \ 0 \ 0 \ 1 \ 0 \ \dots]^T$ and $g = 9.81 \text{ [m/s}^2\text{]}$ is the gravitational acceleration. Non-zero entries of column \bar{g} refer to dofs representing displacements in vertical direction. The resulting static mode (magnified by a factor 1000) $q = \varphi_g$ is depicted in Figure C.1. The maximum transversal displacement is $5.38 \times 10^{-4} \text{ [m]}$. It is verified that the influence of the gravity in the coupling structure is negligible in the upcoming analysis, namely in the results presented in Section 7.3 and consequently, this effect is not taken into account.

Secondly, since the vertical beams must carry the weight of the horizontal beam and the pendula, these may be prone to experience buckling. Hence, a buckling analysis is performed. For this analysis it is assumed that each vertical beam has its lower end fixed and its upper end pinned. For a beam of this type the critical

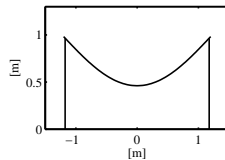


Figure C.1 Static mode due to gravity.

load (or Euler load) P_c , for which static buckling occurs is given by [81]

$$P_c = \frac{20.187 EI}{l^2}. \quad (\text{C.2})$$

Each vertical beam is at its upper end vertically loaded with half the weight of the horizontal beam and the weight of one pendulum. Then, the total vertical load applied to each vertical beam is given by

$$P = \frac{1}{2}m_b g + m_p g, \quad (\text{C.3})$$

where $m_b = 56.3$ [kg] is the mass of the horizontal beam (see Table 7.1) and the mass of one pendulum is assumed to be at most $m_p = 10$ [kg]. Hence,

$$P = 3.743 \times 10^2 \text{ [N]}. \quad (\text{C.4})$$

The critical load is obtained by substituting the parameter values given in Table 7.1 into equation (C.2). This yields

$$P_c = 1.221 \times 10^4 \text{ [N]}. \quad (\text{C.5})$$

Since $P \ll P_c$, it is concluded that the vertical beams are not close to buckling.

Bibliography

- [1] *Oxford advanced learner's dictionary*. Oxford University Press, Oxford, 1997.
- [2] V. S. Afraimovich, N. N. Verichev, and M. I. Rabinovich. Stochastic synchronization of oscillation in dissipative systems. *Radiophysics and Quantum Electronics*, 29(9):795–803, 1986.
- [3] A. Alvarez-Aguirre. *Remote control and motion coordination of mobile robots*. PhD thesis, Eindhoven University of Technology, 2011.
- [4] A. A. Andronov, A. A. Vitt, and S. E. Khaikin. *Theory of oscillators*. Dover Publications, New York, 1987.
- [5] M. Bennett, M. Schatz, H. Rockwood, and K. Wiesenfeld. Huygens's clocks. *Proceedings of the Royal Society of London A: Mathematical, Physical and Engineering Sciences*, 458(2019):563–579, 2002.
- [6] H. Berghuis and H. Nijmeijer. Robust control of robots via linear estimated state feedback. *IEEE Transactions on Automatic Control*, 39(10):2159–2162, 1994.
- [7] I. I. Blekhman. *Synchronization of dynamic systems*. Nauka, Moscow, 1971.
- [8] I. I. Blekhman. *Synchronization in science and technology*. ASME Press, New York, 1988.
- [9] I. I. Blekhman, Fradkov, A. L., Nijmeijer, H., and Pogromsky, A. Yu. On self-synchronization and controlled synchronization. *Systems and Control Letters*, 31(5):299–305, 1997.
- [10] S. Boccaletti, J. Kurths, G. Osipov, D. L. Valladares, and C. S. Zhou. The synchronization of chaotic systems. *Physics Reports*, 366(1-2):1–101, 2002.

-
- [11] G. Chen and X. Dong. On feedback control of chaotic continuous-time systems. *IEEE Transactions on Circuits and Systems I: Fundamental Theory and Applications*, 40(9):591–601, 1993.
- [12] R. Craig and A. Kurdila. *Fundamentals of structural dynamics*. John Wiley & Sons, Hoboken, New Jersey, 2006.
- [13] J. Cronin. *Fixed points and topological degree in nonlinear analysis*. Number 11 in Mathematical Surveys and Monographs. American Mathematical Society, 1964.
- [14] K. Czolczyński, T. Kapitaniak, P. Perlikowski, and A. Stefański. Periodization of Duffing oscillators suspended on elastic structure: mechanical explanation. *Chaos, Solitons & Fractals*, 32(3):920–926, 2007.
- [15] K. Czolczyński, P. Perlikowski, A. Stefański, and T. Kapitaniak. Huygens’ odd sympathy experiment revisited. *International Journal of Bifurcations and Chaos*, 21(7):2047–2056, 2011.
- [16] K. Czolczyński, A. Stefański, P. Perlikowski, and T. Kapitaniak. Clustering and synchronization of n Huygens’ clocks. *Physica A*, 388(24):5013–5023, 2009.
- [17] R. Dilão. Antiphase and in-phase synchronization of nonlinear oscillators: The Huygens’s clocks system. *Chaos: An Interdisciplinary Journal of Nonlinear Science*, 19(2):023118, 2009.
- [18] J. Ellicott. An account of the influence which two pendulum clocks were observed to have upon each other. *Philosophical Transactions*, 41(452-461):126–128, 1739.
- [19] J. Ellicott. Further observations and experiments concerning the two clocks above mentioned. *Philosophical Transactions*, 41:128–135, 1753.
- [20] W. Ellis. On sympathetic influence between clocks. *Monthly Notices of the Royal Astronomical Society*, 33:480–484, 1873.
- [21] K. Engelborghs, T. Luzyanina, and D. Roose. Numerical bifurcation analysis of delay differential equations using DDE-BIFTOOL. *ACM Transactions on Mathematical Software*, 28(1):1–21, 2002.
- [22] H. J. Estrada-García, L. A. Márquez-Martínez, and C. H. Moog. Master-slave synchronization for two inverted pendulums with communication time-delay. In J. Loiseau, W. Michiels, S. Niculescu, and R. Sipahi, editors, *Topics in Time Delay Systems*, Lecture Notes in Control and Information Sciences. Springer, Berlin, 2009.

- [23] E. Falotico, C. Laschi, P. Dario, D. Bernardin, and A. Berthoz. Using trunk compensation to model head stabilization during locomotion. In *11th IEEE-RAS International Conference on Humanoid Robots*. October 26–28, 2011. Bled, Slovenia, 2011.
- [24] A. Fatihcan. Synchronization and amplitude death in coupled limit cycle oscillators with time delays. In J. Loiseau, W. Michiels, S. Niculescu, and R. Sipahi, editors, *Topics in Time Delay Systems*, Lecture Notes in Control and Information Sciences, pages 403–413. Springer, Berlin, 2009.
- [25] R. H. B. Fey, D. H. van Campen, and A. de Kraker. Long term structural dynamics of mechanical systems with local nonlinearities. *Journal of Vibration and Acoustics*, 118:147–153, 1996.
- [26] A. Fradkov and B. Andrievsky. Synchronization and phase relations in the motion of two-pendulum system. *International Journal of Nonlinear Mechanics*, 42(6):895–901, 2007.
- [27] H. Fujisaka and T. Yamada. Stability theory of synchronized motion in coupled-oscillator systems. *Progress of Theoretical Physics*, 69(1):32–37, 1983.
- [28] J. Guckenheimer and P. Holmes. *Nonlinear oscillations, dynamical systems, and bifurcations of vector fields*. Springer-Verlag, New York, 1983.
- [29] D. Hurley and M. Vandyck. An observation about the Huygens clock problem. In K. Williams, editor, *Two Cultures*, pages 59–70. Birkhäuser, Basel, 2006.
- [30] C. Huygens. In Martinus Nijhoff, editor, *Oeuvres completes de Christiaan Huygens*, volume 17, pages 156–189. 1660.
- [31] Y. Il Gu, K. L. Hyun, H. J. Sung, and J. K. Beom. Antiphase synchronization of two nonidentical pendulums. *International Journal of Bifurcation and Chaos*, 20(7):2179–2184, 2010.
- [32] V. Jovanovic and S. Koshkin. Synchronization of Huygens’ clocks and the Poincaré method. *Journal of Sound and Vibration*, 331(12):2887–2900, 2012.
- [33] A. Y. Kanunnikov and R. E. Lamper. Synchronization of pendulum clocks suspended on an elastic beam. *Journal of Applied Mechanics and Technical Physics*, 44(5):748–752, 2003.
- [34] M. Kapitaniak, K. Czolczyński, P. Perlikowski, A. Stefański, and T. Kapitaniak. Synchronization of clocks. *Physics Reports*, 517(1–2):1–69, 2012.
- [35] H. Khalil. *Nonlinear Systems*. Prentice Hall, New Jersey, third edition, 2002.
- [36] J. R. Kim, D. Shin, S. H. Jung, P. Heslop-Harrison, and K. H. Cho. A design principle underlying the synchronization of oscillations in cellular systems. *Journal of Cell Science*, 123(4):537–543, 2010.

- [37] D. J. Korteweg. Les horloges sympathiques de Huygens. In Martinus Nijhoff, editor, *Archives Neerlandaises des Sciences Exactes et Naturelles*, volume XI, pages 273–295. La Societe Hollandaise des Sciences A Harlem, The Hague, 1906.
- [38] I Kovacic and M. J. Brennan. *The Duffing equation. Nonlinear oscillators and their behaviour*. John Wiley & Sons, United Kingdom, 2011.
- [39] S. G. Krantz and H. R. Parks. *The implicit function theorem: history, theory and applications*. Birkhäuser, Boston, 2002.
- [40] A. M. Lyapunov. *The general problem of the stability of motion*. Taylor and Francis, London, 1992.
- [41] I. G. Malkin. *Some problems in the theory of nonlinear oscillations*. State Publishing House of Technical and Theoretical Literature, Moscow, 1956.
- [42] W. Michiels and S. Niculescu. *Stability and Stabilization of Time-Delay Systems*. (Advances in Design & Control). Society for Industrial and Applied Mathematics, Philadelphia, 2007.
- [43] F. C. Moon. Chaotic clocks: a paradigm for the evolution of noise in machines. In G. Rega and F. Vestroni, editors, *IUTAM Symposium*. Springer, London, 2005.
- [44] F. Mormann, T. Kreuz, R. G. Andrzejak, P. David, K. Lehnertz, and C. E. Elger. Epileptic seizures are preceded by a decrease in synchronization. *Epilepsy Research*, 53(3):173–185, 2003.
- [45] M. Moser, M. Fruhwirth, and T. Kenner. The symphony of life. *Engineering in Medicine and Biology Magazine, IEEE*, 27(1):29–37, 2008.
- [46] K. Murali and M. Lakshmanan. Drive-response scenario of chaos synchronization in identical nonlinear systems. *Physical Review E*, 49(6):4882–4885, 1994.
- [47] A. Mutazono, M. Sugano, and M. Murata. Frog call-inspired self-organizing anti-phase synchronization for wireless sensor networks. In *Proceedings of the 2nd International Workshop on Nonlinear Dynamics and Synchronization (INDS'09)*, July 20- July 21, 2009, Carinthia, Austria, 2009.
- [48] A. H. Nayfeh and D. T. Mook. *Nonlinear Oscillations*. John Wiley & Sons, New York, 1979.
- [49] H. Nijmeijer. A dynamical control view on synchronization. *Physica D*, 154(3):219–228, 2001.
- [50] H. Nijmeijer and H. Berghuis. On Lyapunov control of the Duffing equation. *IEEE Transactions on Circuits and Systems I: Fundamental Theory and Applications*, 42(8):473–477, 1995.

- [51] H. Nijmeijer, I. I. Blekhman, A. L. Fradkov, and A. Yu Pogromski. Self-synchronization and controlled synchronization. In *Proceedings of the first International Conference on Control of Oscillations and Chaos*, 1997.
- [52] H. Nijmeijer and A. Yu Pogromski. Huygens' synchronization: a challenge. In G. Leonov, H. Nijmeijer, A. Yu Pogromski, and A. Fradkov, editors, *Dynamics and Control of Hybrid Mechanical Systems*, pages 1–6. World Scientific Publishing Company, Singapore, 2010.
- [53] T. Oguchi and H. Nijmeijer. A synchronization condition for coupled nonlinear systems with time-delay: a frequency domain approach. *International Journal of Bifurcation and Chaos*, 21(9):2525–2538, 2011.
- [54] W. T. Oud, Nijmeijer, H., and Pogromsky, A. Yu. A study of Huygens' synchronization: experimental results. In K. Pettersen, J. Grasdahl, and H. Nijmeijer, editors, *Group Coordination and Cooperative Control*, volume 336 of *Lecture Notes in Control and Information Sciences*, pages 191–203. Springer, Berlin, 2006.
- [55] J. Pantaleone. Synchronization of metronomes. *American Journal of Physics*, 70(10):992–1000, 2002.
- [56] L. M. Pecora and T. L. Carroll. Synchronization in chaotic systems. *Physical Review Letters*, 64(8):821–824, 1990.
- [57] J. Pena-Ramirez, A. Alvarez-Aguirre, R. H. B. Fey, and H. Nijmeijer. Effects of time delay in the synchronized motion of oscillators with Huygens' coupling. In *Proceedings of the 3rd IFAC Conference on Analysis and Control of Chaotic Systems.*, 2012.
- [58] J. Pena-Ramirez, R. H. B. Fey, and H. Nijmeijer. On phase synchronization of oscillators mounted on a movable support. In *Proceedings of the 7th EUROMECH Nonlinear Dynamics Conference (ENOC 2011)*, July 24 - July 29, 2011, Rome, Italy, 2011.
- [59] J. Pena-Ramirez, R. H. B. Fey, and H. Nijmeijer. An experimental study on synchronization of nonlinear oscillators with Huygens' coupling. *Nonlinear Theory and its Applications, IEICE*, 3(2):128–142, 2012.
- [60] J. Pena-Ramirez, R. H. B. Fey, and H. Nijmeijer. In-phase and anti-phase synchronization of oscillators with Huygens' coupling. *Cybernetics and Physics*, 1(1):58–66, 2012.
- [61] J. Pena-Ramirez, R. H. B. Fey, and H. Nijmeijer. An introduction to parametric resonance. In T. I. Fossen and H. Nijmeijer, editors, *Parametric resonance in dynamical systems*. Springer, New York, 2012.

- [62] J. Pena-Ramirez and H. Nijmeijer. A study of the onset and stabilization of parametric roll by using an electro-mechanical device. In T. I. Fossen and H. Nijmeijer, editors, *Parametric resonance in dynamical systems*. Springer, New York, 2012.
- [63] A. Pikovsky, M. Rosenblum, and J. Kurths. *Synchronization. A universal concept in nonlinear sciences*. Cambridge University Press, Cambridge, 2001.
- [64] R. L. Pitman and S. J. Chivers. Terror in black and white. Naturalist at large. *Natural History*, pages 26–29, December, 1999.
- [65] A. Yu. Pogromsky. Passivity based design of synchronizing systems. *International Journal of Bifurcation and Chaos*, 8(2):295–319, 1998.
- [66] A. Yu. Pogromsky, V. N. Belykh, and H. Nijmeijer. Controlled synchronization of pendula. In *Proceedings 42nd IEEE International Conference on Decision and Control*, pages 4381–4386, December 9-12, Maui, Hawaii, USA., 2003.
- [67] A. Prasad, S. K. Dana, R. Karnatak, J. Kurths, B. Blasius, and R. Ramaswamy. Universal occurrence of the phase-flip bifurcation in time-delay coupled systems. *Chaos*, 18:023111–(1–8), 2008.
- [68] A. Prasad, J. Kurths, S. K. Dana, and R. Ramaswamy. Phase-flip bifurcation induced by time delay. *Physical Review E*, 74(3):035204(1–4), 2006.
- [69] D. Rijlaarsdam. Huygens synchronization in various dynamical systems. Master’s thesis, Eindhoven University of Technology, 2008.
- [70] Rijlaarsdam, D., A. Yu. Pogromsky, and H. Nijmeijer. Synchronization between coupled oscillators : an experimental approach. In G. Leonov, H. Nijmeijer, A. Yu Pogromsky and A. Fradkov, editors, *Dynamics and control of hybrid dynamical systems*, volume 14 of *B*, pages 153–165. World Scientific Publishing Company, Singapore, 2010.
- [71] D. Rosas, J. Alvarez, and L. Fridman. Robust observation and identification of nDOF Lagrangian systems. *International Journal of Robust and Nonlinear Control*, 17:842–861, 2006.
- [72] A. V. Roup, D. S. Bernstein, S. G. Nersesov, W. S. Haddad, and V. Chellaboina. Limit cycle analysis of the verge and foliot clock escapement using impulsive differential equations and Poincaré maps. *International Journal of Control*, 76:1685–1698, 2003.
- [73] E. Scholl, G. Hiller, P. Hovel, and M. Dahlem. Time-delayed feedback in neurosystems. *Philosophical Transactions of the Royal Society A*, 367:1079–1096, 2009.

- [74] C. H. Scholz. Large earthquake triggering, clustering, and the synchronization of faults. *Bulletin of the Seismological Society of America*, 100(3):901–909, 2010.
- [75] M. Senator. Synchronization of two coupled escapement-driven pendulum clocks. *Journal of Sound and Vibration*, 291(3–5):566–603, 2006.
- [76] P. S. Spoor and G. W. Swift. The Huygens entrainment phenomenon and thermoacoustic engines. *Acoustical Society of America*, 108(2):588–599, 2000.
- [77] E. Steur and H. Nijmeijer. Synchronization in networks of diffusively time-delay coupled (semi-)passive systems. *IEEE Transactions on Circuits and Systems*, (6):1358–1371, 2011.
- [78] S. Strogatz. *Sync. The emerging science of spontaneous order*. Hyperon, New York, 2003.
- [79] S. Strogatz and I. Steward. Coupled oscillators and biological synchronization. *Scientific American*, 269(6):102–109, 1993.
- [80] C. S. Teoh and L. E. Davis. A coupled pendula system as an analogy to coupled transmission lines. *IEEE Transactions on Education*, 39(4):548–557, 1996.
- [81] S. P. Timoshenko and J. M. Gere. *Theory of elastic stability*. McGraw-Hill, New York, 1961.
- [82] H. Ulrichs, A. Mann, and U. Parlitz. Synchronization and chaotic dynamics of coupled mechanical metronomes. *Chaos*, 19(4):043120(1)–043120(6), 2009.
- [83] M. H. L. M. van den Tillaart. Design of a mechanical synchronizing system for research and demonstration purposes for D & C. Master’s thesis, Eindhoven University of Technology, 2006.
- [84] B. van der Pol. On oscillation hysteresis in a simple triode generator. *Philosophical Magazine*, 43:700–719, 1922.
- [85] B. van der Pol. On relaxation-oscillations. *Philosophical Magazine Series 7*, 2(11):978–992, 1926.
- [86] K. Wiesenfeld and D. Borrero-Echeverry. Huygens (and others) revisited. *Chaos: An interdisciplinary Journal of Nonlinear Science*, 21:047515, 2011.
- [87] B. J. Wolf, H. B. Russell, and K. Wang. Synchronizing transmission schedules of partitioned ad hoc networks. In *Military Communications Conference. MILCOM 2007 IEEE*, pages 1–7, October 29 - October 31, Orlando, FL, USA, 2007.

-
- [88] M. Yoshimoto, K. Yoshikawa, and Y. Mori. Coupling among three chemical oscillators: Synchronization, phase death, and frustration. *Phys. Rev. E*, 47(2):864-874, 1993.
- [89] L. Zhenze, T. Yantao, and Z. Changjiu. Controlled anti-phase synchronization of passive gait. In *Proceedings of the 2006 IEEE International Conference on Robotics and Biomimetics*, December 17 - 20, 2006, Kunming, China, 2006.

Samenvatting

Synchronisatie is één van de meest diep gewortelde en alomtegenwoordige fenomenen in de natuur. Het kan worden waargenomen bij mensen en andere levende wezens, maar ook bij onbewuste entiteiten. Een aantal bekende voorbeelden zijn de synchrone beweging van een school vissen, het synchroon oplichten van vuurvliegjes, een danspaar dat samen danst op het ritme van de muziek, synchrone activering van neuronen en pacemakercellen en de synchrone beweging van pendule klokken. Op het eerste gezicht lijkt het bestaan van synchronisatie in de natuur wonderbaarlijk. Het belangrijkste "geheim" achter dit fenomeen is echter dat er communicatie (dit wordt aangeduid met koppeling) is tussen de entiteiten/systemen, waardoor deze elkaar beïnvloeden. Deze koppeling kan bijvoorbeeld worden gerealiseerd via een fysische verbinding of een chemisch proces.

Hoewel synchronisatie een veel voorkomend fenomeen is bij gekoppelde oscillerende systemen, ligt de verklaring waarom synchronisatie optreedt niet altijd voor de hand. Dit geeft aanleiding tot de volgende vragen: hoe synchroniseren gekoppelde oscillatoren precies en onder welke voorwaarden? In sommige gevallen is het zeer uitdagend om antwoorden te formuleren op deze vragen. Beschouw bijvoorbeeld het fameuze voorbeeld van Christiaan Huygens, waarbij twee pendule klokken gesynchroniseerde beweging vertonen, die in fase, maar ook in tegenfase kan zijn. Huygens nam waar dat er een "medium" is, dat verantwoordelijk is voor de het optreden van gesynchroniseerde beweging, namelijk de verbindingsbalk, waarmee de twee pendule klokken gekoppeld zijn. Ondanks deze opmerkelijk correcte observatie ontbreekt echter tot op de dag van vandaag een volledige mathematische verklaring (gebaseerd op geschikte modellen voor de pendules en de flexibele verbindingsbalk) van dit fenomeen.

De doelstelling van dit proefschrift is om de mechanismen achter het optreden van gesynchroniseerde beweging verder te onderzoeken. Het eerste deel van het proefschrift richt zich op de analyse van natuurlijke synchronisatie van willekeurige,

identieke oscillatoren met Huygens koppeling. De originele experimentele set-up van Huygens is hierbij enigszins aangepast, doordat iedere pendule klok wordt vervangen door een (willekeurige) niet-lineaire oscillator. Bovendien wordt de flexibele balk (de originele Huygens koppeling) vereenvoudigd tot een massa-demper-veer system met één graad van vrijheid. De identieke oscillatoren worden beide aan de massa gekoppeld. Iedere oscillator wordt aangestuurd door een kracht om steady-state oscillaties te garanderen. De noodzaak van deze regelkracht komt voort uit het feit dat beide pendule klokken, die Huygens gebruikte, voorzien waren van een zogenaamd escapement mechanisme, dat periodiek een kortdurende kracht leverde om iedere klok te laten lopen. Getoond wordt dat het optreden van synchronisatie van de oscillatoren onafhankelijk is van het type regelkracht/energiebron. De sleutel tot het optreden van synchronisatie wordt eerder gevonden in de Huygens koppeling. Meer specifiek wordt aangetoond dat de massa van de koppeling in hoge mate de uiteindelijke vorm van gesynchroniseerd gedrag, namelijk in fase synchronisatie of tegenfase synchronisatie, bepaalt. De methode van Poincaré wordt gebruikt om het bestaan van deze gesynchroniseerde bewegingen aan te tonen en de lokale stabiliteit ervan te bepalen. Deze analytische methode kan worden toegepast omdat het systeem een natuurlijke kleine parameter bevat, namelijk de sterkte van de koppeling, die wordt bepaald door de ratio van de massa van een oscillator en de massa van de koppeling.

Vervolgens wordt het synchronisatie probleem vanuit regeltechnisch oogpunt bekeken. Allereerst wordt het synchronisatie probleem van twee oscillatoren die chaotisch gedrag vertonen besproken. Het optreden van chaotisch gedrag in beide oscillatoren wordt geïnitieerd door de koppeling periodiek te exciteren. De massa van de koppeling wordt beschouwd als de bifurcatie parameter. Als de oscillatoren chaotisch gedrag vertonen zal synchronisatie niet op een natuurlijke manier optreden. Geregelde synchronisatie van chaotisch gedrag is echter wel mogelijk door toepassing van een master-slave configuratie of een wederzijds synchronisatie schema. Hierna wordt het effect van tijdsvertraging op de synchronisatie van de oscillatoren met Huygens koppeling onderzocht. In dit geval wordt de mechanische koppeling vervangen door een representatief dynamisch systeem. Dit dynamische systeem genereert dusdanige regelsignalen voor de oscillatoren, zodat het totale systeem in gesloten lus een paar oscillatoren met Huygens koppeling representeert. De beide oscillatoren hoeven zich nu niet fysiek op dezelfde plaats te bevinden. Het dynamische systeem dat de regelkrachten genereert wordt afzonderlijk op een computer geïmplementeerd. Het moge duidelijk zijn dat bij deze opzet tijdsvertraging in de communicatie tussen oscillatoren en koppeling/regelsysteem relevant kan worden. Het ontstaan van in fase en tegenfase synchronisatie in de gekoppelde/geregelde oscillatoren wordt vervolgens bestudeerd als een functie van de sterkte van de koppeling en de tijdsvertraging.

In aanvulling op theoretische en numerieke analyse wordt natuurlijke en geregelde synchronisatie van de oscillatoren gevalideerd door middel van experimenten, die

worden uitgevoerd met behulp van een experimentele opstelling. Deze bestaat uit een elastisch ondersteunde starre balk, die de Huygens koppeling representeert, en twee daaraan bevestigde oscillatoren (massa-demper-veer systemen met één graad van vrijheid), die de pendule klokken representeren. Zowel de starre balk als de twee oscillatoren kunnen onafhankelijk worden geactueerd door regelkrachten. Een belangrijke eigenschap van de opstelling is dat het dynamisch gedrag van zowel de starre balk als de beide oscillatoren kan worden gemodificeerd door gebruik te maken van terugkoppeling. Deze eigenschap is erg nuttig, omdat het hierdoor mogelijk is om synchronisatie experimenten uit te voeren voor een brede klasse van dynamische systemen.

Het laatste onderwerp van dit proefschrift behelst de modelvorming en analyse van het originele experiment van Huygens. De modellen die in het eerste deel van het proefschrift en in de literatuur gebruikt worden zijn sterke vereenvoudigingen van de werkelijkheid: de koppeling wordt hier beschouwd als een elastisch ondersteund star lichaam met één graad van vrijheid. In het originele experiment van Huygens was de verbindings balk (de koppeling), waaraan de twee pendule klokken waren bevestigd, in principe een elastisch continuüm. Resultaten van een rigoureuze studie van in fase en tegenfase synchronisatie van de twee pendules gebaseerd op een koppeling via een elastisch continuüm zijn, voor zover bekend nooit in de literatuur besproken. Van de koppeling is een Eindige Elementen model gemaakt dat na reductie geassembleerd is met de modellen van de twee pendules, resulterend in een model bestaande uit een stelsel gekoppelde gewone differentiaalvergelijkingen. Numerieke resultaten worden getoond, die mogelijke steady-state oplossingen van het "werkelijke" Huygens experiment illustreren.

Samenvattend kan worden gesteld dat de resultaten van dit proefschrift laten zien dat de gesynchroniseerde beweging geobserveerd door Huygens niet alleen optreedt bij gekoppelde pendule klokken maar in veel algemenere zin.

Resumen

Sincronización tipo Huygens de sistemas dinámicos: más allá de los relojes de péndulo

La sincronización es uno de los comportamientos más dominantes en la naturaleza. Este comportamiento puede ser observado en los seres vivos y en objetos inanimados. Algunos ejemplos de sincronización que pueden ser conocidos para el lector son: el fascinante movimiento de un cardumen o banco de peces, la emisión simultánea de luz en enjambres de luciérnagas, una pareja bailando en sincronía con el ritmo de la música, neuronas y células del corazón produciendo impulsos nerviosos sincronizados o el movimiento sincronizado de relojes de péndulo. A primera vista, estos ejemplos sugieren que la existencia de sincronización en la naturaleza es algo milagroso. Sin embargo, el principal “secreto” detrás del fenómeno de sincronización es que existe un canal de comunicación, llamado acoplamiento, el cual permite la interacción de los seres, sistemas u objetos. Algunos ejemplos de acoplamientos son: una interconexión física, un proceso químico.

Si bien es cierto que el fenómeno de sincronización es omnipresente, su origen no siempre es perceptible. Debido a esto, es natural que surjan las siguientes preguntas: ¿cómo es que sistemas (osciladores) acoplados pueden sincronizarse? ¿bajo qué condiciones? Las respuestas a estas preguntas en la mayoría de los casos no son sencillas de obtener y representan un reto científico. Considere por ejemplo el famoso ejemplo de Christiaan Huygens de dos relojes de péndulo colgando de una tabla de madera, la cual estaba colocada sobre dos sillas. Huygens observó que a

partir de cierto instante, los péndulos de los relojes oscilaban en sincronía, ya fuese en la misma dirección (en fase) o en direcciones opuestas (anti-fase). Basado en sus observaciones, Huygens concluyó que hay un “medio” responsable del movimiento sincronizado observado en sus relojes. Dicho medio es la tabla de madera de la cual colgaban los relojes. A pesar de la simple –pero exacta– explicación dada por Huygens, hoy en día no existe una explicación matemática y bien fundamentada de este fenómeno. Puede decirse que esta carencia de una explicación formal se debe a la falta de un modelo matemático adecuado del sistema de relojes de péndulo de Huygens.

El propósito de esta tesis es continuar con la investigación del origen del movimiento sincronizado que ocurre en sistemas, específicamente osciladores, que están acoplados. La primera parte de la tesis considera el problema de sincronización natural de osciladores que *per se* generan oscilaciones y que están acoplados a través de un acoplamiento tipo Huygens. Esto significa que en el análisis aquí presentado, el experimento realizado por Huygens es ligeramente modificado en el sentido que cada reloj de péndulo es reemplazado por un oscilador (arbitrario) de segundo orden y que tiene una respuesta no lineal. La tabla (flexible) de madera usada por Huygens (esta tabla de madera es lo que en esta tesis se llama acoplamiento de Huygens) es reemplazada por una barra rígida de un grado de libertad. Cada oscilador es provisto con una entrada de control, la cual garantiza que las oscilaciones no se amortiguan. De hecho, esta entrada de control tiene la misma función que el mecanismo de escape en los relojes de péndulo (este mecanismo produce el peculiar sonido *tic tac*), el cual mantiene el péndulo del reloj oscilando. Los resultados presentados en esta tesis muestran que el movimiento sincronizado de los osciladores es independiente del tipo de mecanismo de escape usado para mantener las oscilaciones. Mas bien, la barra rígida que acopla a los osciladores es considerada como el elemento clave que influye en la aparición de movimiento sincronizado en los osciladores. En particular, la masa de la barra de acoplamiento determina el tipo de sincronización que puede llegarse a observar en los osciladores, ya sea sincronización en fase o sincronización en anti-phase. El método de Poincaré es usado como herramienta matemática para determinar la existencia y estabilidad del movimiento sincronizado. El uso de este método es factible debido a que en el sistema de osciladores con acoplamiento de Huygens aparece de manera natural un parámetro pequeño. Este parámetro es la fuerza de acoplamiento, la cual está determinada por la masa de la barra que acopla los osciladores.

En la segunda parte de esta tesis se estudia el problema de sincronización controlada. Primero se considera el problema de sincronizar dos osciladores caóticos con acoplamiento de Huygens. Se muestra que el comportamiento caótico en los osciladores es iniciado al aplicar una excitación periódica a la barra de acoplamiento. La masa de la barra se considera como parámetro de bifurcación. Cuando los osciladores se comportan de manera caótica, el fenómeno de sincronización no

aparecerá de manera natural. Por lo tanto es demostrado que al usar una configuración de maestro-esclavo es posible forzar a los osciladores a que se sincronicen. Después se investiga el efecto que un retardo en tiempo tiene en la aparición del fenómeno de sincronización. En este caso la tabla de madera es reemplazada por un modelo dinámico. Este sistema dinámico genera una entrada de control para los osciladores de tal manera que en lazo cerrado el sistema se asemeja a un par de osciladores con acoplamiento de Huygens. Se debe recalcar que bajo este enfoque no es necesario que los osciladores estén ubicados en el mismo lugar y más aún, el sistema dinámico que genera la señal de control para los osciladores debe ser implementado de manera separada usando por ejemplo una computadora. En consecuencia, existe la posibilidad de tener retardos en la comunicación (ya sea en las señales de los osciladores o en la señal de control). La aparición del comportamiento sincronizado en los osciladores acoplados es analizada tomando como parámetros de estudio la fuerza de acoplamiento y la magnitud del retardo.

El movimiento sincronizado (ya sea natural o controlado) de los osciladores es validado por medio de simulaciones en computadora y por medio de experimentos. Los experimentos son ejecutados en una plataforma experimental la cual consiste de dos osciladores (controlables) del tipo masa-resorte-amortiguador (en lugar de los relojes de péndulo usados por Huygens) que están acoplados por medio de una barra rígida controlable que esta soportada en los extremos por medio resortes (esta representa la tabla de madera en el caso del experimento de Huygens). Una característica esencial de esta plataforma experimental es que su comportamiento dinámico puede ser ajustado. Esto es posible ya que los osciladores y la barra de acoplamiento pueden ser actuados/controlados de manera independiente. Entonces, por medio de realimentación es posible imponer un comportamiento dinámico deseado en los osciladores y de la misma manera es posible modificar el comportamiento dinámico de la barra de acoplamiento. Gracias a esta característica ha sido posible realizar un estudio experimental para una variedad amplia de sistemas dinámicos.

En la tercer parte de esta tesis se considera una cuestión relacionada con el modelaje del experimento original de Huygens. Los modelos usados en la primeras dos partes de esta tesis y los modelos reportados en la literatura son simplificaciones del modelo real porque la tabla de madera que acopla a los relojes de péndulo ha sido modelada como un objeto rígido de un grado de libertad. Sin embargo, en el experimento real realizado por Huygens, la tabla de la cual cuelgan los relojes debe ser modelada como un sistema de dimensión infinita. Hasta ahora y de acuerdo con la investigación realizada por el autor, no existe un estudio riguroso que considere esto. Por lo tanto, la tercera parte de la tesis considera este problema. Una técnica del método del Elemento Finito es usada para obtener un modelo el cual consiste de un conjunto (finito) de ecuaciones diferenciales ordinarias. Resultados numéricos ilustrando todas las posibles soluciones límite del “verdadero” experimento de Huygens (dimensión infinita).

En resumen, los resultados contenidos en esta tesis revelan que el fenómeno de sincronización observado por Huygens se extiende más allá de los relojes de péndulo.

Acknowledgements

In order to achieve a challenging task, as is the case of getting a PhD degree, one should have a ‘backup team’, i.e. a group of people providing guidance, advices, and encouragement. In my case, this team was composed by professors, colleagues, friends, and family. I will try to briefly express my gratitude to each of them. Let me start by expressing my deepest gratitude to my parents. Among other things, they ‘shape’ my soul, my mind, and my spirit in such way that for me, everything is possible and achievable. I would not be able to pursue a PhD without their encouragement and support. Mom and dad, thank you for everything, you are my heroes.

Next, I want to thank my supervisor during the PhD, Professor Nijmeijer. Dear Henk, it has been a privilege to be guided by such a brilliant mind. I did enjoy all our discussions and all our countless meetings. Thanks for introducing me in the exciting field of synchronization. I can never repay you for everything you have taught me, for all the scientific fun we have had together, and for always being there whenever I needed your advice and support.

I extend my gratitude to my co-supervisor Rob Fey. Dear Rob, I am glad that, around 3 years ago, you did accept the invitation to be part of this project. Thanks for your guidance, for your valuable suggestions and advices, for always being open for a ‘short’ discussion, and for your real interest in helping me with my research. I did learn a lot from you. Thanks for carefully reading the early drafts of this thesis. I hope one day I will become as ‘sharp’ as you are.

I would like to thank the professors that participated in the core committee, Rodolphe Sepulchre, Kees Grimbergen, Gert-Jan van Heijst, and Joaquin Alvarez for their willing participation in reading and evaluating this thesis. In fact, for Professor Alvarez I have an additional acknowledgement since he provided me a lot of (essential) help during the application process to the PhD program.

My gratitude is further extended to the Mexican Council for Science and Technology (CONACYT) for the financial help to conduct my PhD studies.

Regarding the experimental setup used during my experiments, I want to thank the help of David Rijlaarsdam who, among other things, developed a model for the setup and help

me to get familiarized with the operation of the setup. Likewise, I am grateful to Ben van den Elshout who did perform key adjustments in the experimental platform and obtained one of the first successful experiments. I also acknowledge the interesting experimental study conducted by Amir Firooznia and the work done by Roy Cobbenhagen. Finally, I acknowledge the collaboration with Jop de Wit and Joep de Beer.

Since my arrival to the Netherlands, I did have the invaluable help of Alejandro Alvarez. Dear Alex, thanks for always being a source of answers and solutions to my (academic and daily life) concerns/inquietudes. Above all, thanks for your selfless friendship. I am in debt to you.

Regarding administrative matters I want to express my gratitude to Thea Weijers and Hetty van Neerven for their help in getting my residence permit. Likewise, I would like to thank Geertje Janssen-Dols and Petra Aspers for always solving my administrative problems in a very friendly way.

I want to thank my colleagues. Specially to Benjamin Biemond, for his friendship and for the good times that we spend at conferences and/or practicing sports. Likewise, I extend this gratitude to Erik Steur, Rob van Gils, Sinan Oncu, Nick Bauer, Menno Lauret, Robbert van Herpen, Roel Pieters, Zhenyu, and America Morales. Other colleague, or rather friend, to whom I am grateful is Sisdarmanto Adinandra. Dear Nandra, thanks for the stimulating conversations, for your sincere friendship, and for all the fun we had at concerts and sports. Next in line are my roommates, who also are my friends. Dear Carlos and Alper, thanks for our many discussions, thanks for your help whenever I was 'stuck' with a concept or idea. This also applies to my former roommates and friends, Toshiaki Oguchi and Leonardo de Novellis.

Spending 'too much' time doing research may cause madness. Hence, I am grateful to all the persons who share their friendship with me beyond the scientific environment. In this regard, I am grateful to my housemates Kashif Kamran and Mindaugas Kirkus for all the fun we had. Furthermore, during my stay in Eindhoven, I had the gift of having a friend, almost a brother, named Eric van den Hoven. Dear Eric, thanks for all the precious time that we spent together. Also, I had the privilege of having the selfless friendship of Joseph and Colette Douven to whom I am in debt for their infinite many attentions and care and for their invaluable teaching about 'the real happiness'. Likewise, I express my gratitude to Edissa Hellman.

No doubt that my family played an important role by providing me encouragement to always keep the eyes 'in the target'. In this regard, I am grateful to my grandmas Evangelina and Lourdes. To my aunts: Lucia, Andrea, Estela, Adriana, and Natalia. To my uncles: Paco, Pedro, Oswald, and Ricardo. Not to forget, I want to acknowledge the constant encouragement of my close friends Enrique Licon, Ángel Martínez, Valdemar Olvera, Dennise Boyas, Edgar Mejía, and Raúl Arzate and the frequent cheer received from Rocío Espino, Octavia Hernández, Moisés Varela, and Arturo Jiménez.

Finally, in a personal note, I want to thank my girlfriend Ana Alemán for 'cheering me up' especially during the last part of the PhD. Dear Ana, thanks for being my 'escapement mechanism' whenever my energy levels were reduced.

*Jonatán Peña Ramírez
Eindhoven, The Netherlands
February 6, 2013.*

Curriculum Vitae

Jonatán Peña Ramírez was born on May 13, 1982 in Tulancingo de Bravo, Hidalgo, Mexico. He completed his upper-secondary education at CONALEP, Tulancingo, in 2000, where he obtained a diploma as electromechanical technician. In January 2001 he started his undergraduate education at Universidad Autonoma del Estado de Hidalgo, Mexico, where he obtained a bachelor's degree in Electronics and Telecommunications. He continued his education at the Center for Scientific Research and Higher Education (CICESE), Baja California, Mexico, where he obtained a master's degree in Electronics and Telecommunications, majoring in control and instrumentation. His master's thesis was entitled "Control structure with disturbance identification for Lagrangian systems: performance analysis", which was awarded the APACICESE award 2007.

In November 2008, Jonatan started his PhD research in the Dynamics and control group at the Department of Mechanical Engineering of Eindhoven University of Technology, working on synchronization of coupled dynamical systems. The main results of his PhD research are presented in this thesis.

